JAERI-Research
94-043

BULK SHIELDING EXPERIMENTS ON LARGE SS316 ASSEMBLIES BOMBARDED BY D-T NEUTRONS
VOLUME I: EXPERIMENT

December 1994

Chikara KONNO, Fujio MAEKAWA, Yukio OYAMA
Yujiro IKEDA, Kazuaki KOSAKO* and Hiroshi MAEKAWA

日本原子力研究所
Japan Atomic Energy Research Institute

本レポートは，日本原子力研究所が不定期に公刊している研究報告書です。

入手の問合わせは，日本原子力研究所技術情報部情報資料課（〒319-11 茨城県那珂郡東海村）あて，お申し越しください。なお，このほかに財団法人原子力弘済会資料センター（〒319-11 茨城県那珂郡東海村日本原子力研究所内）で複写による実費頒布をおこなっております。

This report is issued irregularly.

Inquiries about availability of the reports should be addressed to Information Division, Department of Technical Information, Japan Atomic Energy Research Institute, Tokai-mura, Naka-gun, Ibaraki-ken 319-11, Japan.

編集兼発行　日本原子力研究所
印　　刷　いばらき印刷㈱

JAERI-Research 94-043

Bulk Shielding Experiments on Large SS316 Assemblies Bombarded by D-T Neutrons
Volume I : Experiment

Chikara KONNO, Fujio MAEKAWA, Yukio OYAMA
Yujiro IKEDA, Kazuaki KOSAKO* and Hiroshi MAEKAWA

Department of Reactor Engineering
Tokai Research Establishment
Japan Atomic Energy Research Institute
Tokai-mura, Naka-gun, Ibaraki-ken

(Received November 15, 1994)

SS316 is one of the most promising candidates for the shielding and structural material of next fusion devices such as ITER. Benchmark experiments to examine the bulk shielding performance of SS316 for D-T neutrons, particularly deep penetration, were performed by using the D-T neutron source FNS in Japan Atomic Energy Research Institute as the '94 ITER/EDA task (T-16). This report compiles the experimental system, measuring procedures and the measured data. The analysis of the experiment is described separately in the Volume II. The test region of the experimental assembly was a cylindrical SS316 of 1200 mm in diameter and 1118 mm in thickness which was located at 300 mm from the D-T neutron source (Assembly #1). A source reflector of 200 mm-thick SS316 surrounding the D-T neutron source was added to the assembly #1 to simulate a neutron field of a fusion reactor (Assembly #2). The measured data for i) neutron spectra in energy regions of MeV, keV and eV, ii) neutron activation reaction rates, iii) fission rates, iv) gamma-ray spectra and v) gamma-ray heating rates were obtained from the test region surface to the depth of 914 mm in the test region. The consistency of the measured data and the effect of the source reflector were examined from the comparison among the measured data.

This report was submitted to the Joint Central Team (JCT) of ITER.
* Sumitomo Atomic Energy Industries, Ltd.

Keywords: SS316, Benchmark Experiment, Bulk Shielding, D-T Neutron, Deep Penetration, ITER/EDA, Source Reflector, Neutron Spectrum, Neutron Activation Reaction Rate, Fission Rate, Gamma-ray Spectrum, Gamma-ray Heating Rate

JAERI-Research 94-043

Ｄ－Ｔ中性子照射された大型ＳＳ３１６体系におけるバルク遮蔽実験
第１部：実験

日本原子力研究所東海研究所原子炉工学部
今野　力・前川　藤夫・大山　幸夫
池田裕二郎・小迫　和明*・前川　洋

（1994年11月15日受理）

ＳＳ３１６は、ＩＴＥＲ等の核融合炉次期装置の遮蔽材・構造材の最有力候補の一つである。'94ＩＴＥＲ／ＥＤＡのタスク（Ｔ－16）として、Ｄ－Ｔ中性子に対するＳＳ３１６のバルク遮蔽性能、特に深層透過を調べるベンチマーク実験を日本原子力研究所ＦＮＳのＤ－Ｔ中性子源を使用して行った。この報告書は、実験システム、測定手法及び実験結果をまとめたものである。実験解析は、別に第２部で述べられている。実験体系は、直径1200mm、厚さ1118mmのＳＳ３１６製円筒体系（テスト領域）で、Ｄ－Ｔ中性子源から300mmの位置に設置した（体系１）。また、核融合炉の中性子場を模擬するため、Ｄ－Ｔ中性子源の周りを厚さ200mmのＳＳ３１６で囲んだ体系（体系２）も用いた。測定項目は、ｉ）MeV、keV、eVエネルギー領域の中性子スペクトル、ii）中性子放射化反応率、iii）核分裂率、iv）γ線スペクトル、ｖ）γ線発熱率で、体系表面から体系内914mmまで測定を行った。得られたデータを相互比較し、実験データの整合性、中性子反射体の効果を調べた。

このレポートはＩＴＥＲ／ＪＣＴに提出したものである。
東海研究所：〒319－11　茨城県那珂郡東海村白方字白根２－４
＊ ㈱住友原子力工業

Contents

1. Introduction 1
2. Experimental Arrangement 3
2.1 Target Room and Neutron Source 3
2.2 Experimental Assemblies 4
3. Measurements and Results 6
3.1 Neutron Spectrum 6
3.1.1 Neutron Spectrum in Energy Region of MeV 6
3.1.2 Neutron Spectrum in Energy Region of keV 9
3.1.3 Neutron Spectrum in Energy Region of eV 12
3.2 Neutron Spectrum Index 16
3.2.1 Neutron Activation Reaction Rate 16
3.2.2 Fission Rate 18
3.3 Gamma-ray Spectrum 19
3.4 Gamma-ray Heating Rate 23
4. Discussions 26
4.1 Comparison among the Measured Data 26
4.2 Comparison of Measured Data between the Assemblies #1 and #2 26
5. Concluding Remarks 28
Acknowledgment 28
References 29

目　　次

1. はじめに …… 1
2. 実験配置 …… 3
2.1 ターゲット室と中性子源 …… 3
2.2 実験体系 …… 4
3. 測定と結果 …… 6
3.1 中性子スペクトル …… 6
3.1.1 MeV エネルギー領域の中性子スペクトル …… 6
3.1.2 keV エネルギー領域の中性子スペクトル …… 9
3.1.3 eV エネルギー領域の中性子スペクトル …… 12
3.2 中性子スペクトルインデックス …… 16
3.2.1 中性子放射化反応率 …… 16
3.2.2 核分裂率 …… 18
3.3 γ線スペクトル …… 19
3.4 γ線発熱率 …… 23
4. 検　討 …… 26
4.1 測定データ間の比較 …… 26
4.2 体系＃1と＃2の実験データの比較 …… 26
5. 結　語 …… 28
謝　辞 …… 28
参考文献 …… 29

1. Introduction

In next fusion devices such as International Thermonuclear Experimental Reactor (ITER), one of the principal functions of the blanket-shield is to protect the vacuum vessel and the troidal field coils from neutron- and gamma-radiation. Many shielding design calculations[1)-14)] have been performed using various calculation codes and nuclear data libraries under ITER/CDA ("Conceptual Design Activities") and /EDA ("Engineering Design Activities"). The shielding design limits[1)] were addressed under ITER/CDA as shown in Table 1.1. The results of shielding design calculations have to be compared with the design limits considering design margins, since there is ambiguity in shielding design calculations. The design margins were estimated in ITER/CDA[2)] as shown in Table 1.2 based on the previous experimental data[15)-24)]. They are, however, questionable since the experimental assemblies of the previous experiments were small compared to a realistic thickness of shield for fusion devices and few neutron data for lower energy than 1 MeV and few gamma-ray data were measured. The effects on shielding performance by coolant such as water, void, auxiliary shielding material such as B_4C/Pb, gap and duct have not been also examined enough. Although larger design margins allow rough shielding design, it is required that the design margin is as small as possible, to reduce the construction cost of ITER.

In order to provide the shielding design margin with reasonable precision, a series of fusion reactor shielding experiments using the strong D-T neutron source FNS (Fusion Neutronics Source)[25)] in Japan Atomic Energy Research Institute was planned for ITER/EDA. Two blanket/shield options are proposed in ITER/EDA[14)]. One is a blanket shielding design which is made of type 316 stainless steel (SS316) as a structural material and water as a coolant. The other is an advanced blanket concept which is made of vanadium alloy (V5Cr5Ti) as a structural material and liquid lithium as a coolant and breeder. The most promising candidate for the shield/coolant for the Basic Performance Phase of ITER is a configuration with SS316 and water, while the advanced blanket concept is being considered for the Extended Performance Phase of ITER. Therefore the examination of the shielding performance on SS316 and water is required urgently. As the first step of the fusion reactor shielding experiments, bulk shielding experiments on SS316[26)] were performed under one (T-16 : "Preparation of neutronic experiments and measuring technique") of the '94 ITER/EDA R & D tasks in order to examine the bulk shielding performance of SS316 for D-T neutrons, particularly deep penetration.

The experimental assembly of SS316 had a cylindrical shape of 1200 mm in diameter and 1118 mm in thickness (Assembly #1), which is large comparably to the inboard shield of ITER. The experimental assembly with a source reflector of 200 mm thick SS316 (Assembly #2) which surrounded the D-T neutron source was also used to make an incident neutron

spectrum into the assembly close to that expected in ITER due to neutron reflection in the source reflector. The configuration of the experimental assembly was determined based on the pre-analysis[27]. Measurements were carried out inside the assembly up to the depth of 914 mm. Neutron spectra were measured not only in MeV region but also in keV and eV regions, which were scarcely measured in the previous experiments and play an important role for the nuclear heating in troidal coils. Various neutron activation reaction rates and fission rates of ^{235}U and ^{238}U were measured as the neutron spectrum index. The measurements of gamma-ray spectra and gamma-ray heating rates were also performed, which made direct estimation of nuclear heating in troidal coils possible. These various neutron and gamma-ray data can be used as the most effective benchmark data to validate calculation codes and nuclear data libraries and to estimate the design margins.

This report focuses on the experimental procedures and the measured data of the bulk shielding experiments on SS316. Chapter 2 describes the experimental arrangement. The measuring procedures and measured data are given in Chapter 3. The mutual comparison among the measured data and the comparison between the assemblies #1 and #2 are performed in Chapter 4. The detailed analyses of the experiments are described in the Volume II[28].

2. Experimental Arrangement

2.1 Target Room and Neutron Source

The experiments were performed in the first target room of the Fusion Neutronics Source (FNS) facility[25] of the Japan Atomic Energy Research Institute. The first target room is 15 m x 15 m wide and 9.1 m high surrounded by the ordinary concrete wall of 1.5 m - 2 m in thickness. In order to decrease the neutron reflection, the floor of the target room has a grating structure and the distance to the basement floor is 3 m. The water cooling tritiated-titanium target is located at the point of 5.5 m from the nearest concrete walls (west and south) and 1.8 m high from the grating floor. Figure 2.1.1 shows the layout of the target room.

About 3.7×10^{11} Bq (10 Ci) tritiums were absorbed to a titanium layer of 2 mg/cm^2 in thickness and 14 mm in diameter on a 1 mm thick copper backing. The copper backing had a cap shape and was mounted on the end of the 80 degree beam line. It was covered by a coolant water jacket of 0.5 mm thick stainless steel, which was modified in order to be inserted to the source reflector through a hole of 80 mm x 160 mm. Cooling water was flowed in the 1 mm gap between the copper backing and stainless steel jacket. The tritiated-titanium target and coolant structure are shown in Fig. 2.1.2.

Single charged deuteron ions, separated by a 90-degree analyzing magnet, were accelerated by 350 keV. This deuteron ion beam was bombarded to the tritiated-titanium target to generate D-T neutrons. The beam current was adjusted from 30 nA to 2 mA corresponding to measuring techniques and positions. A deuteron beam pulsing of 2 ns width (FWHM) was performed using divertor, post-acceleration deflector and buncher to measure neutron spectra in eV region. Long-pulsed deuteron beam of about 1 ms in width and duty ratio of about 1/3 was also produced by switching arc voltage in the duoplasmatron ion source periodically for the measurement of prompt gamma-ray spectra. A beam divertor was used to cut off spilled d^+ ions.

Alpha-particles associated with D-T reactions were measured by two small silicon surface barrier solid state detectors (α-monitors)[29], which were set in the beam drift tube at the distance of 1580 mm from the tritiated-titanium target. The total neutron source yields were absolutely determined with an accuracy within ± 2 % based on the count of the alpha-particle, the solid angle of the detector and the anisotropic factor of emitted alpha-particles. A long counter and ^{232}Th fission counter were placed at the basement and under the beam drift tube, respectively, as the secondary neutron monitors, which were calibrated by the α-monitors if necessary. In the case that the counts of these monitors were not enough, the neutron yields were determined by neutron counts of a small NE213 scintillation counter

which was placed on the front surface of the assemblies. The small NE213 counter was about 40 times more sensitive than the α-monitors. It was calibrated to the α-monitors during high beam current runs. The neutron source spectrum emitting from the target was calculated by MORSE-DD[30] as described in the Volume II[28]. All measured data in this report are normalized to a D-T neutron source.

2.2 Experimental Assemblies

The size and configuration of the experimental assembly were determined based on the pre-analysis[27]. The test region was a cylindrical SS316 assembly of 1200 mm in diameter and 1118 mm in thickness, which was constructed by sandwiching SS316 disks of 1200 mm in diameter and 50.8 or 101.6 mm in thickness. This test region was located at 300 mm from the tritium target as shown in Fig. 2.2.1 (Assembly #1). The atomic number densities of SS316 in the test region are listed in Table 2.1. All the SS316 disks had two brims in order to be placed stably on a supporting frame and some disks of SS316 also had an experimental hole of 50 mm ϕ or 36 mm ϕ x 727 mm from the circumference to the center of the disk as shown in Fig. 2.2.2. The experimental holes were located at the depths of 102, 229, 356, 553, 711 and 914 mm from the front surface of the test region. Measuring detectors were inserted to the experimental holes using SS316 detector adapters as shown in Fig. 2.2.3 by which detectors were able to be set on the central axis of the test region. As for the activation foil and TLD, SS316 plates from 1 mm to 4 mm in thickness were inserted to excessive space of the hole of 100 mm x 10 mm. Experimental holes unused were filled with SS316 rods.

In a fusion reactor, neutrons entering the first wall and blanket/shielding region are composed of not only direct D-T neutrons but also lower energy neutrons reflected at the opposite first wall and so on. A source reflector of 200 mm thick SS316 was added to the assembly #1 as shown in Fig. 2.2.4 (Assembly #2), in order to adjust neutron energy spectrum incident to the test region to that of a fusion reactor. The source reflector consisted of a side wall (800 mm in inner diameter, 1200 mm in outer diameter and 609 mm in thickness) and a back wall (1200 mm in diameter and 203 mm in thickness). Since the tritium target assembly had to be inserted to the cavity of the source reflector, a hole of 80 mm x 160 mm was made in the center of the back wall. The side wall had a hole of 22.5 mm x 22.5 mm on the surface contacting the test region, through which detectors were inserted to the center of the test region surface by using a detector support of 1 mm thick aluminum. This hole was filled up with a SS316 plug, when detectors were not inserted to it. The atomic number densities of SS316 in the source reflector are also listed in Table 2.1.

These experimental assemblies were mounted on a movable deck by a supporting frame as shown in Fig. 2.2.5. The deck and frame were constructed with a quantity of iron as

small as possible in order to decrease neutron reflection. Two decks were used; one was 3440 mm x 1500 mm for the test region, the other was 3440 mm x 850 mm for the source reflector. One deck of 3440 mm x 1500 mm was used in the assembly #1 and two decks were jointed in the assembly #2. These decks were moved manually on the four rails. The frame had several grooves for brims of SS316 disks to support SS316 disks stably. Figure 2.2.6 shows the overview of the assembly #2 and supporting frame.

3. Measurements and Results

3.1 Neutron Spectrum

3.1.1 Neutron Spectrum in Energy Region of MeV

Detector and Electronics Setup

Neutron spectra above 2 MeV were measured by a 14 mm-diameter spherical liquid scintillator[31] which contained NE213 liquid of 1.38 x 10^3 mm^3 in a spherical cell of Pyrex glass of 1 mm in thickness. Figure 3.1.1.1 shows a cross sectional view of this detector. The glass cell was sealed by melting glass in a nitrogen atmosphere since oxygen degrades the scintillator properties. The scintillator was mounted on a photomultiplier tube through a quartz light guide of 11 mm in diameter and 5 mm in length. The scintillator side of the light guide was cut in a spherical shape so as to fit to the surface of the glass cell. The glass cell and the light guide were coated with the NE560 reflector paint made of MgO and covered with an aluminum cap.

The R647-02 photomultiplier tube (Hamamatsu Photonics) was attached and the output signals from the anode were terminated by a 100 kΩ register at the input of the pre-amplifier with 50 Ω output impedance. The signals were fed to a rise time discrimination circuit through the delay line amplifier. The rise time discrimination technique (JAERI model 154A[32]) was used for the neutron and gamma-ray separation. The rise time and pulse height data were accumulated in a two-dimensional array (64 channel x 512 channel) using a PC/AT compatible computer system. The schematic diagram for the electronic circuit is shown in Fig. 3.1.1.2.

The gain drift of the system frequently occurs due to the counting rate variation or temperature change. We applied a gain-stabilizer for a stable measurement. The overall gain of the system was monitored by a peak produced by light emission of LED, which was connected to the detector through a 4 m glass fiber light guide. The difference between the expected position of the peak and observed one was fed back to a high voltage power supply.

Measurement and Data Reduction

The measurements were carried out at the front surface of the SS316 test region and at the depths of 102, 228, 356, 553, 711 and 914 mm from the SS316 test region front surface of the assemblies #1 and #2 using experimental holes and a detector adapter. The measuring time for each experimental run was 2000 seconds. The deuteron beam current was adjusted for the counting rate not to exceed 2000 cps because of dead time loss.

The two dimensional data of rise time and pulse height were stored into the PC/AT

compatible computer system. Recoil proton data (neutron events) were selected from the two dimensional data using the rise time information. The recoil proton spectrum was unfolded to neutron spectrum by the FORIST code[33] using the neutron response matrix previously determined.[34] The response matrix was calculated by Monte Carlo method[30] The responses in specially important energy regions, i.e., 13.6 to 14.8 MeV, were directly measured and replaced for the calculated response. The FORIST code provides the appropriate energy resolution function by internal iterations. The resolution function, defined as the window function W(E) in the code, is given together with the unfolded results for each run. The spectrum observed, $\Phi_{obs}(E)$, in this system is expressed as follows:

$$\Phi_{obs}(E) = \int_0^{\infty} \frac{1}{\sqrt{2\pi}\,\sigma(E)} \cdot \exp\left\{ -\frac{(E-E')^2}{2\sigma^2(E)} \right\} \cdot \Phi_{true}(E')dE' , \qquad (3.1.1.1)$$

where $\Phi_{true}(E)$: true neutron spectrum without any deformation, and

$$\sigma(E') = \frac{W(E') \cdot E'}{235} , \qquad (3.1.1.2)$$

and the denominator 235 is the conversion factor.[33]

Error Assessment and Results

Table 3.1.1.1 shows the systematic errors which were estimated from the measurement for mono-energetic neutrons of 14.8 MeV. The fraction in the table denotes the ratio of the error in the interested energy range due to the response error to the peak flux around 14 MeV. Here the energy dependent error is represented as follows:

$$Error\ (\%) \text{ for } \Phi\,(En) = (\text{fraction}) \times \frac{\Phi_{peak}}{\Phi\,(En)} \times 100 . \qquad (3.1.1.3)$$

If the peak flux around 14 MeV is, for example, ten times larger than the flux below 10 MeV, the proton spectra in the range of 6 to 10 MeV might be distorted by -10 to -20 % , at maximum.

The energy calibration error also affects the unfolded results. The effects of variation in the energy axis are about 3 % above 10 MeV and less than 2 % for 1 to 10 MeV range, respectively. Lastly, the common error of 2 % is from the neutron source intensity which is a basis for all measurements in this experiment. The overall error comes to be 4 % for the flux above 10 MeV and 10 - 20 % below 10 MeV depending on the spectrum shape.

The measured neutron spectra are shown in Figs. 3.1.1.3 - 3.1.1.9 and Figs. 3.1.1.10 - 3.1.1.16 for the assembly #1 and #2, respectively, together with those measured by the proton recoil gas proportional counter and the slowing down time method described in Secs. 3.1.1.2

and 3.1.1.3. Tables 3.1.1.2 and 3.1.1.3 summarize the numerical data of the measured spectra with window functions described above.

The obtained spectrum at the front surface of the test region is deformed in the energy region below 10 MeV since a small error of the response for 14.8 MeV neutrons affects the neutron spectra below the peak energy fairly in the case that 14 MeV neutrons are dominant. In the positions deeper than 700 mm, it is seen that there are some broad oscillations below 10 MeV. This is partly due to the incompleteness of neutron and gamma-ray separation since a fraction of gamma-rays increases with the depth. Therefore, the neutron spectra less than 10 MeV at the front surface of the test region and at the depths of 711 and 914 mm should be considered as tentative data.

3.1.2 Neutron Spectrum in Energy Region of keV

Neutron spectra from a few keV to 1 MeV were measured by a small proton recoil gas proportional counter (PRC). This measuring system was developed by Dr. E. F. Bennett at Argonne National Laboratory in order to measure the neutron spectrum inside the experimental assembly in the frame of the JAERI/USDOE collaboration program on fusion blanket neutronics [35-37].

Counter

The counter head of PRC had a cylindrical shape as shown in Fig. 3.1.2.1. It was made of 0.41 mm thick SS-304 alloy. The outer diameter of the counter was 19 mm so as to achieve a better position resolution, while the effective length of the counter was rather long (127 mm) in order to obtain better counting statistics. The thickness of the anode wire was 20 μm and field tubes were used to define the active counter volume. This counter was inserted with the pre-amplifier into a hole of 21 mm x 21 mm in the detector adapter for PRC.

Two identical counter heads filled with different gases were prepared in order to measure the neutron spectrum from a few keV to 1 MeV. One counter was filled with hydrogen gas at 0.496 MPa (5.06 kgf/cm^2) with 1 percent methane for the lower energy component (from a few keV to 150 keV) and the other at 0.610 MPa (6.22 kgf/cm^2), 50-50 mixture of hydrogen and argon gases with 1.8 percent nitrogen for the higher energy component (from 150 keV to 1 MeV). Argon gas reduces range of recoiled proton since it has larger stopping power. The iron resonance at 27 keV and the peak at 626 keV due to $^{14}N(n,p)^{14}C$ reaction by thermal neutrons were utilized for the energy calibration.

Electronics and Data Acquisition system

A special size preamplifier of 20 mm x 20 mm x 200 mm fabricated based on an original ANL design was inserted into an experimental hole of 21 mm x 21 mm with the counter. The preamplifier was redesigned to operate at +45 V / -15 V to mitigate overload events due to higher energy neutrons by a sufficient margin.

Since the gas multiplication of a gas proportional counter is determined by an supplied high voltage to the counter, the conventional method requires separate runs with several fixed voltages to cover wider energy range measurement. A new data acquisition technique[38] was developed to reduce time of measurement and data process. This new technique makes it possible to take the same data as measured with the conventional method at single run by changing supplied voltage with a ramp shape during acquisition. The block diagram of the data acquisition system is shown in Fig. 3.1.2.2.

An analog programmable high-voltage DC/DC converter supplied the high voltage for the counter. An analog function generator, which produced time dependent analog profile (sawtooth), served as a driver to the DC/DC converter to alter the high voltage. As a result, output high voltage slowly changed with the period of 165 seconds between the upper and lower voltages during the acquisition. The generated high voltage was monitored using a dividing resistance, which scaled down high voltage by about 1/500. Test pulses of about 500 Hz with the rise time shorter than that of any pulse from ionizing events were fed to the preamplifier for normalization and dead time correction. The pulse height of the test pulse also changed like sawtooth with the period of a few seconds.

Two analog pulse amplifiers were devised for pulse shape discrimination against gamma ray events. One was an integration amplifier (Y-amplifier) with output proportional to input pulse height, i. e. the energy of recoiled proton. This amplifier had an R-C filtering[39] in order to reduce the effects by overload signals. The other amplifier, called X-amplifier, had much shorter shaping time constant than the Y-amplifier. Its output was proportional to the input pulse height and the reciprocal of the rise time of input pulse.

The outputs of Y-amplifier, X-amplifier and the dividing resistor were digitized to 4096 channel by one analog digital converter using a multiplexer and logical circuits. The digitized data were taken to an EPSON-PC286V personal computer (CPU: 80286, 80287) through an interface board of LSI 8255A. The data acquisition program calculated on-line 1) the ratio of the X-amplifier output to the Y-amplifier, which is proportional to the reciprocal of the rise time of the event, 2) a gas multiplication corresponding to the applied high voltage and 3) the energy (in log-scale) of recoiled proton using the output of Y-amplifier and the gas multiplication. The X/Y and the energy (in log-scale) were stored to a two dimensional array (32 channel x 512 channel).

Measurement and Data Processing

The measurement was performed at the front surface of the SS316 test region and at the depths of 102, 229, 356, 553, 711 and 914 mm from the front surface of the SS316 test region of both assemblies. The high voltage was changed from 3000 to 4200 V and from 2400 to 3000 V in hydrogen and hydrogen/argon counters, respectively.

In off-line data processing, the recoil proton events and test pulse events were selected by using the rise time information for each proton recoil energy. The test pulse events were used in order to estimate dead time loss and to normalize recoil proton events. Neutron spectra $\Phi(E)$ was derived from the following equation,

$$\Phi(E) = \frac{1}{N \cdot S \cdot \sigma(E)} \cdot \frac{E}{\sigma(E)} \cdot \frac{dD(E)}{dE} , \qquad (3.1.2.1)$$

where N : number of hydrogen atoms,
S : neutron source yield,
$\sigma(E)$: n-p scattering cross-section,
D(E) : recoil proton spectrum.

Error Assessment and Results

Possible error sources of this technique were in gas pressure (number of hydrogen atom), neutron source yield, n-p scattering cross section, fitting process for differentiation of recoil proton spectrum and calibration of recoil energy. The fitting process error was the largest, ranging ± 3 - 10 % above 10 keV. The uncertainty of neutron source yield was estimated to be ± 2 %. The other errors were expected to be less than 1%. Neutron fluxes below 10 keV tend to become smaller due to the uncertainty of the W-value, which is the average energy lost by the incident particle per ion pair formed. The uncertainty due to W-value was not included in the experimental errors.

The measured neutron spectra are also shown in Figs. 3.1.1.3 - 3.1.1.9 and Figs. 3.1.1.10 - 3.1.1.16 for the assembly #1 and #2, respectively, with those measured by the NE213 and the slowing down time method described in Secs. 3.1.1.1 and 3.1.1.3. The numerical data of the measured spectra are given in Tables 3.1.2.1 and 3.1.2.2. The fine structures due to iron resonances around 10, 30, 100, 150, 200, 400 and 800 keV clearly appear in these spectra.

3.1.3 Neutron Spectrum in Energy Region of eV

Slowing Down Time Method

The slowing down time method[40,41] was applied to measure neutron spectra in eV energy region. The principle of the method is as follows : When pulsed mono-energy neutrons are injected into a large experimental assembly, the neutrons slow down with progress of time and the neutron energy spectrum changes from the initial source spectrum to thermal one. If elastic scattering cross section of the material is constant without any resonance structures and the other reaction cross sections are much smaller than the elastic one, a neutron spectrum at each moment has the Gaussian shape with a certain energy resolution determined by the following equation.

$$\mathrm{FWHM}(\%) = 235.5\sqrt{\frac{8}{3A}}\ , \qquad A : \text{Mass number.} \qquad (3.1.3.1)$$

In this situation, the mean energy of neutrons at each moment and the slowing down time are in one to one correspondence. Measured time-dependent neutron fluxes can be converted to neutron energy spectra by utilizing the relation between the slowing down time and the mean energy.

Measurement

The spectra were measured only in the experimental assembly #2. According to a pre-analysis of the experiment by a Monte Carlo transport calculation with the MCNP code[42], it was found that energy resolution of the spectra in a shallower part of the assembly was worse than that in a deeper part as shown in Fig. 3.1.3.1. At shallower positions, not only higher energy neutrons from the cavity but also lower energy ones which slowed down in the test region existed at the same time, and it resulted in the worse energy resolution. In order to obtain neutron spectra with better energy resolution, four measurement points were chosen from deeper part of the assembly; 356, 533, 711 and 914 mm from the front surface. Typical energy resolution of the measured spectra at the four positions was expected to be about 50 ~ 60 %.

A BF_3 gas proportional counter, 14 mm in diameter, 99 mm in effective length and 0.39 MPa (900 mmHg) in pressure, was adopted as the detector. As shown in Table 3.1.3.1, two modes of measurement were selected in order to cover wide neutron energy range from 0.1 eV to 10 keV. Time-dependent $^{10}B(n,\alpha)$ reaction rates in the two modes were measured. Electronic circuit used in the measurement is shown in Fig. 3.1.3.2.

Energy Calibration

The correspondence between the slowing down time and the mean energy, in other words, the calibration curve was calculated by the MCNP code. The resonance filter technique was applied for validation of the calculated calibration curve. The BF_3 counter was covered with resonance filters listed in Table 3.1.3.2, and time-dependent $^{10}B(n,\alpha)$ reaction rates were measured. The time when a difference between the measured time-dependent reaction rates with and without the resonance filters was observed corresponded to the energy of the sharp resonance peak of the filter cross section. The experimentally obtained correspondence between the slowing down time and the mean energy at all the measuring positions is shown in Fig. 3.1.3.3 with the calculated calibration curve at the 711 mm position. Numerical comparisons of the experimental and calculated ones are presented in Table 3.1.3.3. Since the experiment and the calculation agreed within about 5 %, validity of the calculated calibration curve was confirmed.

Data Processing

The calibration curve, that is, neutron mean energy $\bar{E}$ at time t, is expressed as

$$\bar{E} = f(t), \tag{3.1.3.2}$$

and

$$\frac{d\bar{E}}{dt} = \frac{df(t)}{dt}. \tag{3.1.3.3}$$

By using the calculated calibration curve, the measured time-dependent reaction rates C(t) were converted into energy-dependent reaction rates $C(\bar{E})$, and neutron energy spectra were obtained by the following equations;

$$C(\bar{E}) = C(t) \times \frac{dt}{d\bar{E}}, \tag{3.1.3.4}$$

$$\phi(\bar{E}) = \frac{C(\bar{E})}{\sigma(\bar{E}) \cdot N \cdot Yn \cdot f_{ss}(\bar{E}) \cdot f_{\sigma}(\bar{E})}, \tag{3.1.3.5}$$

where,

$C(\bar{E})$: Counts / MeV,

C(t) : Counts / μs,

$\phi(\bar{E})$: Energy spectrum [n / MeV / Source Neutron],

$\sigma(\bar{E})$: Cross section of the $^{10}B(n,\alpha)$ reaction taken from JENDL-3.1 nuclear data library,

N : Number of effective B-10 atoms in the BF_3 counter,

Yn : Neutron source yield,

$f_{ss}(\bar{E})$: Self-shielding correction factor of the counter,

$f_{\sigma}(\bar{E})$: Correction factor for effective $^{10}B(n,\alpha)$ cross section.

The number of effective ^{10}B atoms in the BF_3 counter was determined with accuracy of 3% by irradiating the BF_3 counter in a calibrated thermal neutron field. The self-shielding correction factor of the counter, $f_{ss}(\bar{E})$, was calculated based on the chord length probability function in the cylindrical detector and an assumption of isotropic neutron flux. The maximum self-shielding effect was 6.8 % for thermal neutrons.

Since a neutron spectrum at a certain moment has a broad energy distribution, spectrum weighted $^{10}B(n,\alpha)$ cross section differs from cross section at $\bar{E}$. Hence the correction factor for the cross section, $f_{\sigma}(\bar{E})$, was introduced. The correction factor is expressed as

$$f_{\sigma}(\bar{E}) = \frac{\int \sigma(E') \cdot \phi(E',t) \cdot dE' \Big/ \int \phi(E',t) \cdot dE'}{\sigma(\bar{E})}, \qquad (3.1.3.6)$$

where,

$\phi(E',t)$: Neutron energy spectrum at time t.

The variable t in Eq. (3.1.3.6) could be converted to $\bar{E}$ by using Eq. (3.1.3.2). The correction factors were typically 2 ~ 5 % below 1 keV.

Energy Resolution

The measured spectra by the slowing down time method have the inherent energy resolution. The resolution given by Eq. (3.1.3.1) is 51 % in the case of the ideal material. But the real energy resolution is worse than that by Eq. (3.1.3.1) as seen in Fig. 3.1.3.1.

Time resolution in the measurement was another cause to broaden the energy resolution. There were three main components in the time resolution; (i) fluctuation of timing signal from the BF_3 counter; 0.13 μs, (ii) neutron pulse width; 0.5 μs and 0.005 μs for the modes #1 and #2, respectively, and (iii) time width per channel of the multichannel analyzer; 0.191 μs and 0.0478 μs for the modes #1 and #2, respectively. The time resolution could be converted to energy resolution by multiplying $d\bar{E}/dt$.

Overall energy resolution is sum of all the energy resolutions. The estimated overall resolution is given in Table 3.1.3.4.

Error Estimation and Results

Errors of the measured spectrum are estimated as follows.

1.	Statistical error of counts	2 ~ 7 %
2.	Neutron source yield	2 %
3.	Number of effective ^{10}B atoms	3 %

4.	Self-shielding correction factor	negligible
5.	Correction factor for neutron energy broadening	0.5 ~ 5 %
6.	Error comes from energy calibration	2 ~ 8 %

The overall errors range between 6 and 10 %

The measured neutron spectra are presented in Table 3.1.3.4. Figures 3.1.1.13 - 3.1.1.16 show the measured neutron spectra with those measured by the NE213 and the proton recoil gas proportional counter described in Secs. 3.1.1.1 and 3.1.1.2. In the spectra, detailed structures due to large resonance cross sections, i.e., small dips around 45 eV by molybdenum and 336 eV by manganese, are observed.

3.2 Neutron Spectrum Index

3.2.1 Neutron Activation Reaction Rate

Several activation reaction rates shown in Table 3.2.1.1 were measured by the activation foil technique in order to obtain neutron spectrum indices for wide energy range. The common dosimetry reactions, e.g., $^{27}Al(n,\alpha)^{24}Na$, $^{56}Fe(n,p)^{56}Mn$, $^{58}Ni(n,p)^{58}Co$, $^{58}Ni(n,2n)^{57}Ni$, $^{90}Zr(n,2n)^{89}Zr$, $^{93}Nb(n,2n)^{92m}Nb$, $^{115}In(n,n')^{115m}In$, $^{197}Au(n,\gamma)^{198}Au$ and so forth, were very useful for the comparative study of shielding performance on different material configurations.

Activation Foils and Irradiation

Aluminum, titanium, iron, cobalt, nickel, zinc, zirconium, niobium, indium and gold foils were placed at the front surface of the SS316 test region and at the depths of 102, 229, 356, 533, 711 and 914 mm from the front surface of the SS316 test region of the assemblies #1 and #2. Indium foils had a dimension of 10 x 10 x 1 mm^3. Gold foils with a size of 10 mm x 10 mm x 0.001 mm or 25 mm x 25 mm x 0.001 mm made the self-shielding effect for the $^{197}Au(n,\gamma)^{198}Au$ reaction negligibly small. As for other samples, foils of 10 mm-diam. x 1 mm were used in the positions up to 0.5 m in depth, 20 mm-diam. x 1 mm at 0.53 m and 20 mm-diam. x 2 mm at 0.71 m. Two foils of 20 mm-diam. x 4 mm were set at 0.91 m.

In the assembly #1 the foils were irradiated for 10 hours with D-T neutrons and total neutron yield at the target was 7.5×10^{15} n. The irradiation time and the total neuron yield were 11 hours and 8.2×10^{15} for the measurement with the assemble #2, respectively. The neutron yield fluctuation was monitored every 10 seconds by using the multi-channel scaling (MCS) for the decay correction during irradiation.

Reaction Rate Determination

After the irradiation and appropriate cooling, γ-rays emitted from foils were measured with four germanium detectors. One germanium detector was used as a standard detector, the absolute efficiency of which was determined by using standard gamma-ray sources. Foils were placed at a distance of 77 mm from this standard detector to reduce gamma-ray sum peak and the sample size effects. The other detectors were used as relative detectors. Foils were set at the front surface of these detectors to achieve a higher detector efficiency. The absolute efficiencies for the relative detectors were calibrated to the standard detector by using the same sample which was irradiated at the experiment. This method made the whole counting time shorter.

Reaction rate, **RR**, was derived from the γ-ray counts with necessary corrections. The **RR** is given as,

$$\mathbf{RR} = \frac{\lambda \cdot C \cdot A}{\varepsilon \cdot W \cdot N_a \cdot a \cdot b \cdot Y \cdot S_a \cdot \mu \cdot (1-\exp(-\lambda \cdot t_i)) \cdot \exp(-\lambda \cdot t_c) \cdot (1-\exp(-\lambda \cdot t_m))}, \qquad (3.2.1.1)$$

where,

- λ: decay constant (/sec),
- C: γ-ray peak counts,
- A: atomic mass,
- ε: detector efficiency,
- W: sample weight,
- N_a: Avogadro's number,
- a: natural abundance of the target element,
- b: γ-ray branching ratio,
- Y: neutron source yield,
- S_a: correction factor for the decay during irradiation,
- μ: γ-ray self absorption correction factor,
- t_i: irradiation time,
- t_c: cooling time,
- t_m: collection time.

The decay data for the half-life (decay constant) and γ-ray branching ratio were taken from Ref. 43). The neutron yield fluctuation monitored with the MCS was used for the calculation of correction factor for the decay during irradiation, S_a. One dimensional model was assumed in the estimation of γ-ray self absorption correction factor, μ.

Experimental Error and Results

Major sources of the error for the reaction rate were the γ-ray counting statistics (0.1 to several %) and the detector efficiency (2 to 3 %). The error for sum-peak correction was estimated less than 2 % depending on the decay mode and fraction of multiple γ-ray cascade. The error for the decay correction was reflected from the error of half-life of the activity. If the half-life was accurate, the error for the saturation factor should be less than 1 % even for the short half-life activities.

The other errors associated with foil weight, γ-ray self-absorption, irradiation time, cooling time and counting time were negligibly small. The error for neutron source yield was estimated to be 2 %. The overall error for the major part of reaction rate ranged from 3 to 6 %. Some data for high threshold reactions in the deep positions suffered from poor counting statistics due to low activation rate.

The measured activation reaction rates are shown in Figs. 3.2.1.1 and 3.2.1.2 for the

assembly #1 and #2, respectively. Tables 3.2.1.2 and 3.2.1.3 summarize the numerical data of the measured activation reaction rates. Because of poor counting statistics of gamma-rays, no activation reaction-rates except $^{197}Au(n,\gamma)^{198}Au$ could be obtained at 533 and/or 711 and 914 mm from the front surface of the test region, though large foils were used.

3.2.2 Fission Rate

Measurement

Fission rates of U-235 and U-238 were measured with two micro fission chambers. The chambers were 6.25 mm in outer diameter and 25.4 mm in active length. About 4 mg of uranium oxide was coated inside the chambers. The effective numbers of the atoms were experimentally determined with accuracy of 2.8 % as described in Ref. 44); 6.73×10^{18} and 7.32×10^{18} atoms/chamber for the U-235 and U-238 chambers, respectively.

The two chambers were tied with each other and located at the measurement position at the same time. Fission rates were measured in both experimental assemblies #1 and #2 at positions of -4, 102, 229, 356, 533, 711 and 914 mm from the front surface of the assemblies. Amplified signals were discriminated from gamma-ray and noise signals. Signals for fission events were counted by scalers.

Data Reduction

The measured fission counts were divided by the effective number of uranium atoms and the neutron yields to derive absolute fission rate per source neutron. Since thicknesses of the coated uranium oxide inside the chambers were not so thin, fission fragments lost their energies in the uranium oxide layer. Some portion of fragments did not have enough energy to produce signals, pulse heights of which were larger than those of noise signals. Proportions of the cut off signals were estimated by extrapolating the pulse height spectrum toward zero channel, and correction factors for the cut off were determined. The factors ranged between 1.11 and 1.13 for all the measurements. The absolute fission rates were corrected by the factors.

Uranium atoms in the U-235 chamber contained 7 % of U-238, and those in the U-238 chamber did 0.044 % of U-235. Corrections for these impurity uranium atoms were performed.

The obtained fission rates were presented in Table 3.2.2.1 and Figs. 3.2.2.1 - 3.2.2.2.

3.3 Gamma-Ray Spectrum

Gamma-Ray Spectrometer

An NE213 liquid organic scintillation counter [45] was used to measure gamma-ray spectra in the experimental assembly #1. The NE213 scintillator (Nuclear Enterprises, Scotland) was enclosed in a boric-silicic glass (Pyrex glass) container. Since some problems were found with the scintillator as described in the later section, a new spectrometer [46], which consisted of a deuterated benzene base scintillator, BC537 (BICRON, USA), and a quartz glass container, was used for the measurement in the assembly #2. A sectional view of the NE213 counter is shown in Fig. 3.3.1. The BC537 counter had just the same dimensions as the NE213 counter. Outer dimensions of the counters were 48 mm in diameter and 262 mm in length. The scintillators were spheres of 40 mm in diameter. An optical fiber was equipped for gain stabilization. Reference light pulses from an external light source were introduced to the light guide through the optical fiber.

Electric Circuit

The electric circuit used in the measurement is shown in Fig. 3.3.2. Dynode signals from Photomultiplier Tube (PMT) were fed to a pre-amplifier, and the output signals were put into two Delay Line Amplifiers (DLA) at the same time. Gains of the two DLAs were different by about 10 times to obtain energy spectra of wide dynamic range. Uni-polar pulse signals from each DLA were fed to a Rise-Time-to-Pulse-Height-Convertor and discriminated into neutron and gamma-ray signals according to difference of the rise time of signals. Pulse height signals of gamma-rays from DLA were selected by using the gate signals at Linear Gates, and stored in a Multichannel Analyzer.

In general, the gain of a photomultiplier tube drifts with counting rate or temperature change. To suppress the gain drift, a gain stabilization system was equipped. Light pulses of constant intensity generated by a light emitting diode in a thermostat were injected into the PMT through the light guide of scintillator. Drift of the detector pulses to the light pulses was monitored and the high voltage applied to the PMT was fed back to keep the pulse height constant. The light pulse signals mixed in a pulse height spectrum from gamma-rays were rejected from the spectrum by anti-coincidence. The gain was kept in accuracy of 1 % by the gain stabilization system.

Rejection of Decay Gamma-Rays by Pulsed Neutron Method

In a measurement of prompt gamma-rays, it is important to clearly reject decay gamma-rays since they are regarded as the background. As shown in Fig. 3.3.3, intensity of the decay gamma-rays changes at every moment depending on a history of neutron irradiations

to the experimental assembly. If the decay gamma-rays are measured before or after the prompt gamma-ray measurement, it is very difficult to determine the total amount of decay gamma-rays during the prompt gamma-ray measurement. Thus the pulsed neutron method was applied to accurately determine the background.

A period, between the times when D-T neutrons are injected into the experimental assembly and when neutrons disappear from the assembly due to captures and leakages, is almost equal to several hundreds μs. The period corresponds to the slowing down time of D-T neutrons to thermal neutrons. Prompt gamma-rays following neutron reactions are emitted until several hundreds μs after injection of D-T neutrons.

By utilizing this fact, decay gamma-rays can be accurately subtracted. Pulsed neutrons of several hundreds μs in width are generated and the periods of measurement for foreground and background gamma-rays are determined as shown in Fig. 3.3.3. Intensity of decay gamma-rays emitted by activated nuclei whose half-lives are usually longer than one second can be regarded as constant during the measurement periods of foreground and background runs. Pulse height spectra (PHS) for the foreground and the background runs are measured at the same time with different time-gate. Pulse height spectrum without decay gamma-rays is accurately derived subtracting the background spectrum from the foreground one.

Measurement

Prompt gamma-ray spectra were measured for both assemblies #1 and #2. The gamma-ray spectrometers were inserted in the experimental holes of 50 mm in diameter at four positions; 102, 356, 711 and 914 mm from the front surface of the assemblies, without a detector adapter. The center of the scintillators was set on the central axis of the assembly. The accelerator was operated in the arc-pulse mode with pulse width of 1.4 ms and repetition rate of 3.9 ms. Deuteron beam current was adjusted to between 50 nA and 1 mA depending on the measurement positions to keep the counting rates constant. The maximum counting rate was limited about 1000 cps for sum of neutron and gamma-ray events of high-gain circuit. Energy scale of measured pulse height spectra was calibrated with the Compton edge of 1.275 MeV gamma-rays from Sodium-22. Signals from a high precision research pulser were fed into the pre-amplifier to determine zero pulse height position of the ADCs.

Data Processing

Measured PHSs for high and low gains were connected to one PHS for both foreground and background runs. The background PHSs were subtracted from the foreground PHSs. The obtained PHSs were unfolded using the FORIST code [33] to derive energy spectra higher than about 0.3 MeV. The response matrix used in the unfolding process was calculated with the MARTHA code [47]. The original MARTHA code was the gamma-ray response matrix

calculation code for NaI(Tl) Scintillator, but the cross section data in the code were replaced for NE213 or BC537 scintillators. The obtained gamma-ray spectra at four positions are shown in Figs. 3.3.4 - 3.3.5 and Tables 3.3.1 - 3.3.2. The errors in the figure and tables are statistical ones only. The FORIST code provides a window function W(E) with the spectrum. The window function corresponds to the energy resolution of the unfolded spectrum in full width at half maximum in percentage. If a true spectrum and an observed spectrum are expressed as Φtrue(E) and Φobs(E), respectively, they are related with the next equation.

$$\Phi_{obs}(E) = \int_0^{\infty} \frac{1}{\sqrt{2\pi}\sigma(E)} \cdot \exp\left\{-\frac{(E-E')^2}{2\sigma^2(E)}\right\} \cdot \Phi_{true}(E')dE', \qquad (3.4.1)$$

where,

$$\sigma(E) = \frac{W(E) \cdot E}{235.5} \quad .$$

Namely, the obtained spectra are broadened ones by the Gaussian distribution with the above standard deviation.

Error Estimation and Results

Error sources are estimated as follows.

1.	Neutron Source Yield	±2 - 3 %
2.	Response Functions	± 5 %
3.	Perturbation Effect by the Counters	± 5 %
4.	Statistics Error	±4 - 10 %

Errors for the neutron yield include calibration errors of the small NE213 counter used as a neutron yield monitor. Errors for response functions are estimated by measuring gamma-rays from calibrated standard sources up to energy of 2.754 MeV[44]. Perturbation effect caused by the insertion of the scintillation detectors is examined by Monte Carlo calculations with and without detector modeling. Statistics errors are given in Tables 3.3.1 - 3.3.2. Errors except statistical ones are not included in the Tables and Fig. 3.3.4 - 3.3.5. The overall errors are roughly about 10 %.

Uncorrected Factors in the Measured Spectra

There are three components of parasitic and contamination gamma-rays in the measured gamma-ray spectra.

(i) The NE213 liquid scintillator is contained in a boric-silicic glass (Pyrex glass). The

following reaction takes place with boron-10 in the glass mainly with low energy neutrons.

$$^{10}B(n,\alpha)^{7}Li^{*}, \qquad ^{7}Li^{*} \rightarrow {}^{7}Li + \gamma\,(0.478\ MeV)$$

The gamma-rays of 0.478 MeV are not produced by the experimental assembly but by the detector itself. Annihilation gamma-rays arising from electron pair creations are seen at energy of 0.511 MeV in an usual gamma-ray spectrum. Gamma-ray peaks observed around 0.5 MeV in the measured spectra are sums of the 0.487 MeV gamma-rays and the annihilation gamma-rays. As the depth of detection position increases, a fraction of low energy neutron increases and the $^{10}B(n,\alpha)^{7}Li^{*}$ reaction occurs more frequently. Then the contribution of 0.478 MeV gamma-rays becomes dominant around 0.5 MeV.

(ii) The organic scintillator NE213 consists of hydrogen and carbon. Hydrogen atoms emit gamma-rays following the neutron capture reaction.

$$^{1}H(n,\gamma)^{2}H^{*}, \qquad ^{2}H^{*} \rightarrow {}^{2}H + \gamma\,(2.225\ MeV)$$

These gamma-rays of 2.225 MeV also disturb the measured gamma-ray spectra. According to another experiment, a ratio of observed gamma-rays from the $^{10}B(n,\alpha)^{7}Li^{*}$ reaction to those from $^{1}H(n,\gamma)^{2}H^{*}$ reaction for the NE213 counter has been found to be about 20. Hence small bumps at 2.2 MeV observed in the measured spectra at 102, 356 and 711 mm can be identified as the gamma-rays associated with the $^{1}H(n,\gamma)^{2}H^{*}$ reaction.

(iii) Target gamma-rays, i. e., gamma-rays generated by neutron interactions with the structural materials of the target, are emitted along with neutrons. The target gamma-rays are also included in the measured spectra. The target gamma-rays contribute most to the spectra at 102 mm since the position is closest to the target. According to an estimation by a transport calculation, a fraction of a gamma-ray heating rate by the target gamma-rays to that by gamma-rays produced by neutron reactions in the assembly is at most 5 % for both assemblies. Contribution of the target gamma-rays is not so large even at the closest position to the target. At the measurement positions deeper than 356 mm, contribution of the target gamma-rays can be negligibly small (less than 1 %).

Components (i), (ii) and (iii) are included in the spectra measured with the NE213 counter for the assembly #1, while only component (iii) is in the spectra measured with the BC537 counter for the assembly #2.

3.4 Gamma-Ray Heating Rate

Principle of Measurement

Gamma-ray heating rate is defined as absorbed dose of gamma-rays in a medium. To measure the gamma-ray heating rate, a method which utilizes different kinds of thermoluminescence dosimeters (TLD) was proposed [48] by Tanaka, et al. The principle is described in the Ref. 48), and examples of the application of the method in D-T neutron fields are seen in Refs. 49) and 50). Here, brief explanations are given. Absorbed doses of gamma-rays in a medium measured by different kinds of TLDs monotonously increase as a function of effective atomic numbers of the TLDs. Hence the absorbed dose of the medium can be derived by interpolating absorbed doses measured by different kinds of TLDs.

Irradiation

Since the atomic number of SS316 was 26.4, two kinds of TLDs whose effective atomic numbers (Zeff) were around 26.4 were selected; MSO (Mg_2SiO_4, Zeff=11.1) and SSO (Sr_2SiO_4, Zeff=32.5). These TLDs were powder form and sealed in glass capsules of 2 mm in diameter and 12 mm in length. All TLDs were calibrated by a cobalt-60 standard gamma-ray field. After washed with ethyl alcohol, TLDs were annealed for 30 minutes at 500 °C. Four samples of each TLD were packed in a thin aluminum foil. These procedures were adopted for both experiment of assemblies #1 and #2.

As for the irradiation for the assembly #1, one TLD package was put on the front surface of the test region and six packages were set in the center of the hole of 100 mm x 10 mm filled with SS316 spacers in the detector adapters for TLD, which were inserted to the experimental holes. Positions of TLD packages were -1, 102, 229, 356, 533, 711 and 914 mm from the front surface of the test region. One package was kept without irradiation for the background estimation. The irradiation was carried out for about 3 hours with d^+ beam current of 1.5 mA, and the total neutron yield was 2.26×10^{15}. About 15 minutes after the irradiation, TLD packages were taken out from the experimental hole and kept in a dark place. One week later from the irradiation, thermoluminescence (TL) was read out by a TLD reader (KYOKKO 2500).

In order to give the optimum amount of doses for TLDs, two irradiations, light and heavy irradiations, were carried out for the assembly #2. Positions of TLD packages were -1, 102, 229, 356, 533 and 711 mm for the light irradiation and 356, 533, 711 and 914 mm for the heavy irradiation. Durations and neutron yields of the irradiations were 12 minutes and 9.92×10^{13} for the light irradiation, and 6 hours and 2.05×10^{15} for the heavy irradiation. The rest of the experimental procedure was just the same as that for the assembly #1.

Data Processing and Results

Average values and standard deviations of measured TL were calculated for each group of four TLDs. Averaged TL of unirradiated TLDs, as the background, was subtracted from that of irradiated TLDs. The obtained TL was converted to the unit of exposure dose of ^{60}Co equivalence. In the experiment for the assembly #2, measurements at 336, 533 and 711 mm were duplicated by the heavy and light irradiations. The exposure doses per source neutron for both irradiation agreed within their error ranges. The exposure doses by the light irradiation were chosen for -1, 102, 229 and 345 mm positions, and those by the heavy irradiation were for the rest of the positions.

Since TLDs were sensitive to not only gamma-rays but also neutrons, neutron contribution on the TLDs had to be subtracted from the total TL response. The subtraction was done as follows. The neutron contribution can be calculated by energy-integration of the products of neutron response function and neutron flux. The used response function of each kind of TLD as a function of energy were calculated with a code developed by Hashikura, et al [51]. However, in comparison with experimental values of the response functions, significant discrepancies between the experiment and the calculation were observed for MSO in a high energy region. Hence the calculated response function of MSO in an energy range higher than 4 MeV was normalized by the experimental values. The neutron response functions used are shown in Fig. 3.4.1. The neutron energy spectra at the measurement points were calculated by the Monte Carlo transport code MCNP. The products of the neutron response function and the spectrum were integrated to yield neutron contribution of the TLDs in a unit of equivalent exposure dose of ^{60}Co. The obtained neutron contributions were subtracted from the total responses to derive pure gamma-ray responses. Proportions of the neutron response to the total response are presented in Table 3.4.1.

Both kinds of TLDs had been calibrated in a ^{60}Co standard field. Obtained gamma-ray responses on the TLDs were converted to absorbed doses. Since the atomic number of SS316 was 26.4, absorbed dose of SS316, i.e., gamma-ray heating rate, was derived by interpolation of absorbed dose for MSO and SSO as shown in Figs. 3.4.2 and 3.4.3. As shown in the figures, absorbed doses measured by MSO and SSO at each position are not different so much. Thus errors associated with the interpolation process are considered to be small.

The gamma-rays were produced by interaction of source neutron and structural materials of the target. In order to obtain gamma-ray heating rates only by gamma-rays produced in the assembly, contribution of target gamma-rays to the measured gamma-ray heating rates was estimated by an MCNP calculation. In the calculation, experimental assemblies made of SS316 were modeled and calculated source spectrum of the target gamma-rays was used. Gamma-ray spectrum at each measurement position was calculated and gamma-ray heating

rate by the target gamma-rays was derived by integration of the product of the gamma-ray spectrum and kerma factor of SS316. The obtained gamma-ray heating rate due to target gamma-ray was subtracted from the total gamma-ray heating rate. Proportions of the target gamma-ray were 33 and 5.3 % at -1 and 102 mm in the assembly #1, respectively, and 14 % at -1 mm in the assembly #2. At the rest of measurement positions, contributions of target gamma-rays were less than 3 %.

The measured gamma-ray heating rates of SS316 are presented in Table 3.4.2 and Fig. 3.4.4.

Error Estimation

In the subtraction of neutron response and the target gamma-ray contribution, the following errors were taken into account and added to the measured data according to the law of error propagation.

Neutron response function	30 %
Neutron Flux	10 %
Contribution of target gamma-ray	20 %

Error sources in the measured gamma-ray heating rates were as follows.

Deviation of four TLDs	(for assembly #1)	4 - 22 %
	(for assembly #2)	3 - 12 %
Neutron Source yield		2 %
Calibration of the TLD reader	(for assembly #1)	5 %
	(for assembly #2)	10 %
Interpolation of atomic number		5 %

The error for deviation of four TLDs is considered as a random error, and the other errors are systematic ones. The overall errors range between 14 and 22 % for assembly #1 and between 13 - 18 % for the assembly #2 depending on measurement points.

4. Discussions

4.1 Comparison among the Measured Data

Various experimental data (neutron spectrum, neutron activation reaction rate, fission rate, gamma-ray spectrum and gamma-ray heating) were obtained in the present experiments. The ratios of typical experimental data to neutron flux above 10 MeV which was obtained from the measured neutron spectrum were derived in order to examine the consistency among the measured data. As the typical experimental data, (1) neutron flux from 10 keV to 1000 keV which was reduced from the neutron spectrum, (2) reaction rates of ^{58}Ni(n,p)^{58}Co [threshold energy (Eth) is 2 MeV], ^{93}Nb(n,2n)^{92m}Nb [Eth is 9 MeV], ^{115}In(n,n')^{115m}In [Eth is 0.34 MeV] and ^{197}Au(n,γ)^{198}Au [non threshold reaction], (3) fission rate of ^{235}U [non threshold reaction] and (4) gamma-ray heating rate were selected since they have quite different neutron responses each other. Figures 4.1.1 and 4.1.2 show the ratios for the assemblies #1 and #2, respectively, where all the ratios are normalized to be unity at the front surface of the test region to clarify the difference of the profiles. The reaction rate of ^{93}Nb(n,2n)^{92m}Nb has the same tendency as the neutron flux above 10 MeV. The ratios of the other reaction rates and the fission rate increase more rapidly with decrease in the threshold energy. The profile of the neutron flux from 10 keV to 1000 keV is similar to that of the fission rate of ^{235}U. The gamma-ray heating rate exhibits a different profile from other data. The trend of the gamma-ray heating rate changes at the depth of about 300 mm; it is close to that of ^{115}In(n,n')^{115m}In in the front region and it approach to those of ^{197}Au(n,γ)^{198}Au and ^{235}U(n,fission) in the rear region. As the reason for such a trend, it is considered that the gamma-rays by threshold reactions such as (n,2n) and (n,n') are dominant in the front region, while the gamma-ray heating is dominated by those produced by (n,γ) reaction in the rear region. Figures 4.1.1 and 4.1.2 demonstrate the consistency of the measured data, since the measured data with sensitivity for the similar neutron energy show the similar tendency.

4.2 Comparison of Measured Data between the Assemblies #1 and #2

Two experimental assemblies with and without the source reflector were used in these experiments. The effects of the source reflector were examined experimentally. The neutron spectra at the front surface of the test region in the assemblies #1 and #2 were shown in Fig. 4.2.1. Neutrons lower than 1 MeV increase eminently due to the source reflector. Figure 4.2.2 shows the ratios of the integrated neutron fluxes above 10 MeV and from 10 keV to 1000 keV, reaction rates of ^{115}In(n,n')^{115m}In and ^{197}Au(n,γ)^{198}Au, fission rate of ^{235}U and gamma-ray heating rate in the assembly #2 to those in the assembly #1 along the center line

of the test region. The source reflector dose not affect the neutron flux above 10 MeV at all. The reaction-rate of $^{115}In(n,n')^{115m}In$, the threshold energy of which is 335 keV, increases by 30 % at the front surface of the test region, but the effect disappears inside the assembly. As for the neutron flux from 10 keV to 1000 keV, $^{197}Au(n,\gamma)^{198}Au$ and fission-rate of ^{235}U, the ratios at the front surface of the test region are more than three and the effect remains at the deeper positions. The ratio of the gamma-ray heating rate shows a complicated variation with the depth. It is 1.8 at the surface but it decreases just inside the test region and increases again. The tendency at the region deeper than 300 mm is very similar to those of reaction-rate of $^{197}Au(n,\gamma)^{198}Au$ and fission-rate of ^{235}U. This phenomenon is considered as followed : The increase at the surface is due to not lower energy neutrons reflected in the source reflector but gamma-rays from the source reflector. Since the direct gamma-ray from the source reflector is shielded by the assembly itself inside the test region and the gamma-ray heating is caused mainly by gamma-rays produced via threshold reactions such as (n,2n) and (n,n') at the front region around 100 mm depth, the ratio of the gamma-ray heating dose not increase so much. In the deeper positions gamma-rays produced by (n,γ) reaction are the main source of the gamma-ray heating. As the result, the tendency of the ratio of gamma-ray heating rate is similar to those of reaction-rate of $^{197}Au(n,\gamma)^{198}Au$ and fission-rate of ^{235}U in the deeper positions.

5. Concluding Remarks

Bulk shielding experiments on SS316 were performed by using the large SS316 assembly of 1200 mm in diameter and 1118 mm in thickness as one of the fusion shielding experiments. The various experimental data for neutron and gamma-ray were obtained at the positions of 0 to 914 mm in depth.

In-situ neutron spectra were measured not only in MeV region but also in keV and eV regions, which were rarely measured in the previous experiments. They are the most basic data for validation of the neutron transport calculation. Neutron activation reaction rates for thirteen reactions with various neutron responses and fission-rates of ^{235}U and ^{238}U were also measured. These reaction rates and fission rates are expected to serve as the neutron spectrum index, which are complementary data to the neutron spectra. The measurement of gamma-ray spectra and gamma-ray heating rates was performed in the present experiments. The experimental data for gamma-ray have various informations for not only neutron transport but also gamma-ray production, gamma-ray transport and so on. Particularly gamma-ray heating rates will be directly related with the nuclear heating in the troidal field coils.

These experimental data are provided as benchmark data for validation of the nuclear data and calculation codes used in nuclear design of fusion devices. The analysis by JAERI is described in detail in the Volume II[28]. The analysis using FENDL will be carried out by the U. S. and other parties in the frame of ITER/EDA.

Acknowledgment

The authors gratefully acknowledge Drs. S. Matsuda and H. Takatsu, Department of ITER Project in JAERI/Naka, for their supports to this work. They also thank Messrs. C. Kutsukake, S. Tanaka, Y. Abe, M. Seki and J. kusano for their good operation of FNS accelerator.

5. Concluding Remarks

Bulk shielding experiments on SS316 were performed by using the large SS316 assembly of 1200 mm in diameter and 1118 mm in thickness as one of the fusion shielding experiments. The various experimental data for neutron and gamma-ray were obtained at the positions of 0 to 914 mm in depth.

In-situ neutron spectra were measured not only in MeV region but also in keV and eV regions, which were rarely measured in the previous experiments. They are the most basic data for validation of the neutron transport calculation. Neutron activation reaction rates for thirteen reactions with various neutron responses and fission-rates of ^{235}U and ^{238}U were also measured. These reaction rates and fission rates are expected to serve as the neutron spectrum index, which are complementary data to the neutron spectra. The measurement of gamma-ray spectra and gamma-ray heating rates was performed in the present experiments. The experimental data for gamma-ray have various informations for not only neutron transport but also gamma-ray production, gamma-ray transport and so on. Particularly gamma-ray heating rates will be directly related with the nuclear heating in the troidal field coils.

These experimental data are provided as benchmark data for validation of the nuclear data and calculation codes used in nuclear design of fusion devices. The analysis by JAERI is described in detail in the Volume II[28]. The analysis using FENDL will be carried out by the U. S. and other parties in the frame of ITER/EDA.

Acknowledgment

The authors gratefully acknowledge Drs. S. Matsuda and H. Takatsu, Department of ITER Project in JAERI/Naka, for their supports to this work. They also thank Messrs. C. Kutsukake, S. Tanaka, Y. Abe, M. Seki and J. kusano for their good operation of FNS accelerator.

References

1) ITER Conceptual Design Report, ITER DS No. 18 (1991).
2) ITER Blanket, Shield and Material Data Base, ITER DS No. 29 (1991).
3) Dänner W., El-Guebaly L.A., Sawan M., Gohar Y.,. Maki K, Rado V. and Schchipakin O.: "Neutron Shielding and its Impact on the ITER Machine Design," Fusion Eng. Design, 18, pp. 183-193 (1991).
4) Maki K., Takatsu H., Kuroda T., Seki Y., Kajiura M. Tachikawa N., Saito R. and Kawasaki H.: "Shielding Design of Reactor Core Region in the Fusion Experimental Reactor," JAERI-M 91-017 (1991, in Japanese).
5) Maki K., Takatsu H., Kuroda T., Seki Y., Nakamura T., Mori S. and Kawasaki H.: "Japanese Contributions ITER Shielding Neutronics Design," JAERI-M 91-046 (1991).
6) Zimin A.S.: "Definition of All Relevant Local Nuclear Responses and the Total Heating in the Toroidal Field Coils During the Conceptual Design Phase of ITER," Fusion Technol., 20, pp. 144-163 (1991).
7) El-Guebaly L.A.: "Magnet Shielding Effectiveness of the Proposed Blankets for ITER," Proc. 14th IEEE/NPSS Symp. on Fusion Engineering at San Diego, California, 2, pp. 1127-1130 (1992).
8) Brésard I., Diop C.M., Giancarli L. and Gervaise F.: "A Three Dimensional Calculation of Neutron Streaming through ITER Tokamak Pumping Ducts with the Monte Carlo Code TRIPOLI-2," Fusion Eng. Des., 18, pp. 377-385 (1991).
9) Sato S, Maki K., Seki Y., Takatsu H., Mori S., Kuroda T. and Zimin S.,: "Streaming through the Gaps around Divertor Pipings in ITER," JAERI-M 93-093 (1993).
10) Zimin S., Takatsu H., Mori S., Maki K., Seki Y., Sato S, Tada E.: "Two-dimensional Over-all Neutronics Analysis of the ITER device," JAERI-M 93-141 (1993).
11) Santro R.T., Gohar Y., Parker R.R., Shatarov G., Sawan M.E. and Kharter H.Y: "ITER Shielding Analysis," Proc. Third Int. Symp. on Fusion Nuclear Technology, California (1994), to be published.
12) Sawan M.E. and El-Guebaly L.A.: "Neutronics and Shielding Results of the U.S. ITER Blanket Trade-Off Study," Proc. Third Int. Symp. on Fusion Nuclear Technology, California (1994), to be published.
13) Sawan M.E., Gohar Y. and Santro R.T.: "Shielding Analysis for the ITER Divertor and Vacuum Pumping Ducts," Proc. Third Int. Symp. on Fusion Nuclear Technology, California (1994), to be published.
14) Detail of the ITER Outline Design Report, ITER TAC-4 (1994).
15) Johnson R.H., Dorning J.J. and Wehring B.W.: "Integral Tests of Neutron Cross Sections for Iron Above 1.0 MeV," Trans. Am. Nucl. Sci., 22, 799 (1975).

16) Hansen L.F., Wong C., Komoto T. and Anderson J.D.: "Measurement of the Neutron Spectra from Materials Used in Fusion Reactors and Calculations Using the ENDF/B-III and -IV Neutron Libraries," Nucl. Sci. Eng., 60, 27 (1976).

17) Santro R.T., Alsmiller R.G., Barnes J.M. Jr. and Chapman G.T.: "Calculation of Neutron and Gamma-Ray Energy Spectra for Fusion Reactor Shield Design : Comparison with Experiment," Nucl. Sci. Eng., 78, pp. 259-272 (1982).

18) Santro R.T., Alsmiller R.G., Barnes J.M. Jr., Chapman G.T. and Tang J.S.: "Calculated Neutron and Gamma-Ray Energy Spectra from 14-MeV Neutrons Streaming Through an Iron Duct : Comparison with Experiment," Nucl. Sci. Eng., 80, pp. 586-602 (1982).

19) Hertel N.E., Johnson R.H., Wehring B.W. and Dorning J.J.: "Transmission of Fast Neutrons through an Iron Sphere," Fusion Technology, 9, 345 (1986).

20) Nakashima H., Tanaka S. and Maekawa H.: "Experiments and Calculations of 14 MeV Neutron Streaming through Multi-Layered Slit Assembly," J. Nucl. Sci. and Technol., 24, pp. 601-609 (1987).

21) Oishi K., Ikeda Y., Konno C. and Nakamura T.: "Measurement and Analysis of Neutron Spectra in a Large Cylindrical Iron Assembly Irradiated by 14 MeV Neutrons," Proc. 7th International Conference on Radiation Shielding, Bournemouth, pp. 331-340 (1988).

22) Nakashima H., Tanaka S., Oyama Y., Sasamoto N. and Suzuki T.: "Experiment and analysis of 14 MeV neutron deep penetration in a type 316L stainless steel assembly," Fusion Eng. Des., 10, pp. 121-125 (1989).

23) Oka. Y, Shin K., Ida T., Ohno S., Yokozawa M., Yamamoto J., Takahashi A., Sekimoto H. and Sakamoto S.: "Fusion Neutron Streaming Benchmark Experiments and the Analysis by the Tree-Dimensional Transport Calculation Code, TRISTAN," Fusion Eng. Des., 10, pp. 127-132 (1989).

24) Borisov A.A., Zagryadskij V.A., Chuvilin D.Yu., Kralik M., Pulpan Ya. and Tikhy M.: "The Neutron Leakage Spectrum for an Iron Sphere with a Central 14 MeV Neutron Source," INDC(CCP)-314 (1990).

25) Nakamura T., Maekawa H., Ikeda Y. and Oyama Y.: "A DT Neutron Source for Fusion Neutronics Experiments at the JAERI," Proc. Int. Ion Eng. Congress - ISIAT '83 & IAPT '83, Kyoto, Japan, Vol. 1, pp. 567-570 (1983).

26) Konno C., Maekawa F., Ikeda Y., Oyama Y., Kosako K. and Maekawa H.: "Bulk Shielding Experiments on Large SS316 Assemblies," Fusion Technol., 21, pp. 2169-2173 (1992).

27) Konno C., Maekawa F., Iwai A., Kosako K., Ikeda Y., Oyama Y. and Maekawa H.: "Pre-analyses of SS316 and SS316/Water Bulk Shielding Experiments," JAERI-Tech 94-019 (1994).

28) Maekawa F., Konno C., Kosako K., Ikeda Y., Oyama Y. and Maekawa H.: "Bulk

Shielding Experiments on Large SS316 Assemblies Bombarded by D-T Neutrons, Volume II : Analysis," JAERI-Research 94-044 (1994).

29) Maekawa H., Ikeda Y., Oyama Y., Yamaguchi S. and Nakamura T.: "Neutron Yield Monitors for the Fusion Neutronics Source (FNS) -- for 80° Beam Line --," JAERI-M 83-219 (1983).

30) Mori T., Nakagawa M. and Sasaki M.: "One-, Two- and Three-Dimensional Transport Code Using Multi-Group Double Differential Form Cross Section," JAERI 1314 (1988).

31) Oyama Y., Tanaka S., Tsuda K., Ikeda Y. and Maekawa H.: "A small spherical NE213 scintillation detector for use in in-assembly fast neutron spectrum measurements", Nucl. Instr. and Meth., A256, pp. 333- (1987).

32) Kimbara S. and Kumahara T.: ibid., 70, pp. 173 (1969).

33) FORIST Spectrum Unfolding code: Radiation Shielding Information Center, Oak Ridge National Laboratory, PSR-92 (1975).

34) Nakashima H.: "Study on Shielding Design Methods for Fusion Reactors Using Benchmark Experiments," pp. 20-45, JAERI-M 92-025 (1992, in Japanese).

35) Oyama Y., et al.: " Phase IIA and IIB Experiments of JAERI/USDOE Collaborative Program on Fusion Blanket Neutronics," JAERI-M 89-215 (1989).

36) Oyama Y., et al.: " Phase IIC Experiments of JAERI/USDOE Collaborative Program on Fusion Blanket Neutronics," JAERI-M 92-182 (1992).

37) Oyama Y., et al.: " Phase III Experiments of JAERI/USDOE Collaborative Program on Fusion Blanket Neutronics - Line Source and Annular Blanket Experiments -," JAERI-M 94-015 (1994).

38) Bennett E.F.: " A Continuous Mode Data Acquisition Technique for Proton Recoil Proportional Counter Neutron Spectrometers," ANL/FPP/TM-239 (1989).

39) Bennett E.F.: " Induction Filtering for Proportional Counter Amplifiers," ANL/FPP/TM-234 (1989).

40) Bergman A. A., et al.: Proc. 1st Int. Conf. on Peaceful Uses Atomic Energy, United Nations, 4, 135 (1955).

41) Maekawa F. and Oyama Y.: "Development of Measurement Technique for Neutron Spectrum in Energy Region of eV in Large Assemblies," JAERI-M 93-181, pp. 96 - 98, (1993).

42) Briesmeister J.F. (Ed.): "MCNP - A General Monte Carlo Code for Neutron and Photon Transport, Version 4," RSIC/CCC-200 (1991).

43) Lederer C. M. and Shireley V.S.: Table of Isotopes, 7th edition (1978).

44) Maekawa H., Ikeda Y., Oyama Y., Yamaguchi S., Tsuda K., Fukumoto T., Kosako K., Yoshizawa M. and Nakamura T.: "Benchmark Experiments on a 60 cm-thick Graphite Cylindrical Assembly," JAERI-M 88-034 (1988).

45) Maekawa F. and Oyama Y.: "Characteristics of a 40 mm Diameter NE213 Scintillation Counter for In-System Gamma-Ray Spectrum Measurement." JAERI-M 91-138, pp. 97 - 99 (1991).

46) Maekawa F. and Oyama Y.: "Techniques of Integral Experiment and Method for Validation of Evaluated Nuclear Data Libraries for Secondary Gamma-Ray Data under D-T Neutron Field," JAERI-M 94-19, pp. 369 - 379 (1994).

47) Saito K. and Moriuchi S.: Nucl. Instrum. Meth. 185, pp. 299 (1981).

48) Tanaka S. and Sasamoto N: "Gamma-Ray Absorbed Dose Measurements in Media with Plural Thermoluminescent Dosimeters Having Different Atomic Numbers," J. Nucl. Sci. Technol., 22, pp. 109-119 (1985).

49) Yamaguchi S., Maekawa H., Kosako K., Nakamura T. and Porges K.G.: "Measurements of Gamma-Ray Heating in Lithium-Oxide, Graphite and Iron Slab Assemblies Bombarded by D-T Neutrons," Fusion Eng. Des., 10, pp. 163-167 (1989).

50) Maekawa F., Oyama Y., C. Konno, Ikeda Y., Kosako K. and Maekawa H.: "Benchmark Experiment on a Copper Slab Assembly Bombarded by D-T Neutrons," JAERI-M 94-38 (1994).

51) Hashikura H., Haikawa K., Tanaka S. and Kondo S.: "Calculation of Neutron Response of Thermoluminescent Dosimeters," J. Faculty of Eng., Univ. of Tokyo, 39, pp. 7 (1987).

Table 1.1 Shielding performance design limits in ITER/CDA.

Responses	Design Limit
Total nuclear heating in troidal field coils [kW]	55
Peak nuclear heating in winding pack [mW/cm^3]	5
Peak dose to electrical insulator [rads]	$5X10^9$
Peak fast (E>0.1MeV) neutron fluence to superconductor [n/cm^2]	10^{19}
Peak displacement in copper stabilizer [dpa]	$6X10^{-3}$
Biological dose outside cryostat one day after shutdown [mrem/h]	0.5

Table 1.2 Recommended correction and safety factors in ITER/CDA.

Responses	1D Analysis		3D Analysis	
	Local	Integral	Local	Integral
Correction factors for :				
Assembly gaps	1.7	1.2	—— *	—— *
Modeling	1.3	1.3	1.1	1.1
Uncertainties in cross section data	1.4	1.3	1.4	1.3
Safety factors for inboard and divertor regions	3	2	1.5	1.4
Safety factors for outboard regions	>3#	>2#		
Safety factors for biological shield	10	10		

* Gaps included in 3-D models

Outboard blanket/shield design dependent

Table 2.1 Atomic number densities of SS316 in the test region and source reflector.

Material	Test Region	Source Reflector
C	7.1697×10^{-5} *	1.9879×10^{-4}
Si	9.8440×10^{-4}	8.1608×10^{-4}
P	4.3162×10^{-5}	4.8895×10^{-5}
S	1.8780×10^{-6}	4.4677×10^{-6}
Cr	1.5476×10^{-2}	1.5025×10^{-2}
Mn	9.7963×10^{-4}	1.3561×10^{-3}
Fe	5.7589×10^{-2}	5.8332×10^{-2}
Ni	9.7128×10^{-3}	9.1456×10^{-3}
Mo	1.0503×10^{-3}	1.0254×10^{-3}

* Unit is in [$\times 10^{24}$ atoms/cm^3]

Table 3.1.1.1 Systematic errors in various energy ranges. Errors expected in the ranges below 10 MeV are originating from the response error of 14.8 MeV neutrons.

No.	Energy range (MeV)	Efficiency	Energy Calibration	Neutron Source	Response Shape [fraction*1]	Total
0	>10	±2%	±3%	±2%	1	±4%
1	8.3 - 10.1	2	2	2	~ - 0.02	-20%*2
2	5.8 - 8.3	2	2	2	~ - 0.01	-11%*2
3	4.1 - 5.8	2	2	2	~ - 0.001	-3.4%*2
4	2.0 - 4.1	2	2	2	~ + 0.01	+3.5%*2
5	1.1 - 2.0	2	2	2	~ + 0.01	+3.5%*2

*1 Fraction is ratio of the error due to the response to the peak flux around 14 MeV.
*2 Example in the case of $\Phi_{peak}/\Phi(E_n) \sim 10$.

Table 3.1.1.2 Neutron spectra at -10, 102, 228, 356, 553, 711 and 914 mm from the front surface of the test region in the assembly #1 measured by the NE213 spectrometer.

	-10 mm			102 mm			228 mm			356 mm		
Neutron Energy [eV]	Flux [n/leth/ source]	Absolute Error	Window [%]	Flux [n/leth/ source]	Absolute Error	Window [%]	Flux [n/leth/ source]	Absolute Error	Wimdow [%]	Flux [n/leth/ source]	Absolute Error	Window [%]
1.99E+6	1.99E-5	1.11E-5	36.0	1.65E-5	5.76E-6	36.0	4.08E-6	1.13E-6	36.0	7.47E-7	1.79E-7	35.3
2.10E+6	1.98E-5	3.86E-6	35.1	1.76E-5	1.97E-6	35.1	4.03E-6	3.88E-7	34.3	7.18E-7	6.14E-8	33.2
2.20E+6	1.96E-5	1.52E-6	34.3	1.75E-5	7.10E-7	34.2	3.85E-6	1.41E-7	32.8	6.70E-7	2.26E-8	31.5
2.32E+6	1.99E-5	1.20E-6	33.5	1.69E-5	5.04E-7	33.4	3.64E-6	9.80E-8	31.3	6.15E-7	1.57E-8	29.9
2.44E+6	2.07E-5	1.17E-6	32.8	1.62E-5	4.78E-7	32.6	3.40E-6	8.95E-8	30.2	5.55E-7	1.38E-8	28.9
2.56E+6	2.13E-5	1.15E-6	32.0	1.53E-5	4.58E-7	31.9	3.12E-6	8.60E-8	29.5	4.90E-7	1.32E-8	28.9
2.69E+6	2.11E-5	1.10E-6	31.2	1.42E-5	4.40E-7	31.1	2.79E-6	8.20E-8	29.5	4.23E-7	1.23E-8	29.3
2.83E+6	2.03E-5	1.12E-6	30.5	1.30E-5	4.29E-7	30.4	2.45E-6	7.73E-8	29.5	3.61E-7	1.13E-8	29.5
2.98E+6	1.91E-5	1.32E-6	29.7	1.19E-5	4.30E-7	29.7	2.15E-6	7.55E-8	29.4	3.14E-7	1.08E-8	29.5
3.13E+6	1.81E-5	1.55E-6	29.0	1.10E-5	4.45E-7	29.0	1.93E-6	7.33E-8	29.0	2.84E-7	1.04E-8	29.0
3.29E+6	1.73E-5	1.63E-6	28.3	1.03E-5	4.52E-7	28.3	1.78E-6	7.07E-8	28.3	2.67E-7	9.81E-9	28.3
3.46E+6	1.64E-5	1.49E-6	27.6	9.74E-6	4.27E-7	27.6	1.68E-6	6.62E-8	27.6	2.59E-7	9.14E-9	27.6
3.63E+6	1.49E-5	1.27E-6	26.8	9.22E-6	3.93E-7	26.8	1.62E-6	6.15E-8	26.8	2.51E-7	8.47E-9	26.8
3.82E+6	1.30E-5	1.14E-6	26.1	8.68E-6	3.71E-7	26.1	1.56E-6	5.78E-8	26.1	2.38E-7	8.04E-9	26.1
4.02E+6	1.11E-5	1.18E-6	25.3	8.10E-6	3.70E-7	25.3	1.48E-6	5.69E-8	25.3	2.20E-7	7.84E-9	25.3
4.22E+6	9.58E-6	1.28E-6	24.5	7.45E-6	3.78E-7	24.5	1.39E-6	5.70E-8	24.5	1.98E-7	7.75E-9	24.5
4.44E+6	8.18E-6	1.36E-6	23.9	6.79E-6	3.83E-7	23.9	1.28E-6	5.67E-8	23.9	1.74E-7	7.68E-9	23.9
4.67E+6	6.55E-6	1.44E-6	23.3	6.18E-6	3.89E-7	23.3	1.14E-6	5.64E-8	23.3	1.51E-7	7.62E-9	23.3
4.91E+6	4.70E-6	1.53E-6	22.7	5.57E-6	4.01E-7	22.7	9.91E-7	5.69E-8	22.7	1.29E-7	7.69E-9	22.7
5.16E+6	3.18E-6	1.60E-6	22.2	4.85E-6	4.10E-7	22.2	8.55E-7	5.73E-8	22.2	1.16E-7	7.68E-9	22.2
5.42E+6	2.48E-6	1.72E-6	21.7	4.05E-6	4.28E-7	21.7	7.39E-7	5.92E-8	21.7	1.13E-7	7.90E-9	21.7
5.70E+6	2.24E-6	1.87E-6	21.1	3.35E-6	4.51E-7	21.1	6.40E-7	6.17E-8	21.1	1.11E-7	8.34E-9	21.1
5.99E+6	1.65E-6	1.98E-6	20.6	2.95E-6	4.62E-7	20.6	5.74E-7	6.24E-8	20.6	1.00E-7	8.45E-9	20.6
6.30E+6	4.09E-7	2.28E-6	20.0	2.88E-6	5.08E-7	20.0	5.48E-7	6.68E-8	20.0	8.50E-8	8.93E-9	20.0
6.62E+6	-1.32E-6	2.61E-6	19.5	2.85E-6	5.68E-7	19.5	5.26E-7	7.39E-8	19.5	7.41E-8	9.71E-9	19.5
6.96E+6	-3.07E-6	2.69E-6	19.0	2.69E-6	5.82E-7	19.0	4.87E-7	7.57E-8	19.0	7.20E-8	9.78E-9	19.0
7.32E+6	-3.63E-6	3.16E-6	18.5	2.64E-6	6.61E-7	18.5	4.72E-7	8.45E-8	18.5	7.28E-8	1.11E-8	18.5
7.69E+6	-2.27E-6	3.80E-6	18.0	2.76E-6	7.71E-7	18.0	4.73E-7	9.82E-8	18.0	6.88E-8	1.28E-8	18.0
8.09E+6	-1.19E-6	4.16E-6	17.6	2.53E-6	8.28E-7	17.6	4.08E-7	1.06E-7	17.6	6.39E-8	1.35E-8	17.6
8.50E+6	-2.83E-6	4.86E-6	17.2	1.58E-6	9.52E-7	17.2	3.39E-7	1.19E-7	17.2	6.26E-8	1.52E-8	17.2
8.94E+6	-5.17E-6	6.25E-6	16.8	5.51E-7	1.21E-6	16.8	4.29E-7	1.47E-7	16.8	5.53E-8	1.90E-8	16.8
9.40E+6	-4.88E-6	6.99E-6	16.4	8.22E-7	1.33E-6	16.4	5.65E-7	1.62E-7	16.4	4.14E-8	2.10E-8	16.4
9.88E+6	-3.62E-6	7.28E-6	15.9	2.36E-6	1.38E-6	15.9	4.79E-7	1.69E-7	15.9	4.61E-8	2.14E-8	15.9
1.04E+7	-2.43E-6	8.34E-6	15.5	3.05E-6	1.58E-6	15.5	2.93E-7	1.88E-7	15.5	7.52E-8	2.43E-8	15.5
1.09E+7	1.67E-6	8.44E-6	15.1	2.18E-6	1.57E-6	15.1	3.14E-7	1.86E-7	15.1	1.03E-7	2.38E-8	15.1
1.15E+7	9.37E-6	8.67E-6	14.8	2.38E-6	1.58E-6	14.8	5.34E-7	1.89E-7	14.8	1.26E-7	2.37E-8	14.8
1.21E+7	3.44E-5	1.04E-5	14.5	7.56E-6	1.91E-6	14.5	9.11E-7	2.27E-7	14.5	1.76E-7	2.82E-8	14.5
1.27E+7	1.18E-4	1.09E-5	14.4	2.21E-5	2.06E-6	14.4	1.73E-6	2.64E-7	14.4	3.47E-7	3.37E-8	14.4
1.33E+7	3.07E-4	1.35E-5	14.4	5.41E-5	2.49E-6	14.4	4.52E-6	3.13E-7	14.4	7.71E-7	3.88E-8	14.4
1.40E+7	5.01E-4	1.69E-5	14.4	9.20E-5	3.18E-6	14.4	1.02E-5	4.07E-7	14.4	1.33E-6	5.39E-8	14.4
1.47E+7	4.65E-4	1.94E-5	14.4	9.12E-5	4.21E-6	14.4	1.29E-5	6.70E-7	14.4	1.38E-6	9.32E-8	14.4
1.55E+7	2.44E-4	8.30E-6	14.4	4.80E-5	1.73E-6	14.4	7.58E-6	2.68E-7	14.4	7.01E-7	3.54E-8	14.4
1.63E+7	1.07E-4	9.84E-6	13.3	1.58E-5	2.03E-6	14.4	2.03E-6	3.24E-7	14.4	1.53E-7	4.66E-8	14.4
1.71E+7	8.66E-5	6.90E-6	12.1	9.59E-6	1.54E-6	14.4	1.09E-6	2.45E-7	14.4	7.87E-8	3.51E-8	14.4
1.80E+7	5.36E-5	1.56E-6	11.0	7.47E-6	4.11E-7	14.4	1.04E-6	6.70E-8	14.4	8.96E-8	1.01E-8	14.4

Table 3.1.1.2 (Continued)

	553mm			711 mm			914 mm		
Neutron Energy [eV]	Flux [n/leth/ source]	Absolute Error	Window [%]	Flux [n/leth/ source]	Absolute Error	Window [%]	Flux [n/leth/ source]	Absolute Error	Wimdow [%]
1.99E+6	5.59E-08	1.41E-08	34.5	4.99E-09	2.07E-09	33.5	2.14E-09	1.07E-09	33.0
2.10E+6	5.90E-08	4.84E-09	32.0	8.47E-09	6.98E-10	30.2	4.52E-09	3.60E-10	29.1
2.20E+6	5.61E-08	1.83E-09	29.8	8.97E-09	2.65E-10	27.1	5.09E-09	1.40E-10	25.3
2.32E+6	5.12E-08	1.26E-09	27.8	8.17E-09	1.83E-10	24.5	4.79E-09	9.44E-11	21.9
2.44E+6	4.57E-08	1.08E-09	26.5	6.83E-09	1.38E-10	23.3	4.01E-09	6.86E-11	19.3
2.56E+6	3.95E-08	1.02E-09	27.2	5.23E-09	1.27E-10	25.0	2.89E-09	6.99E-11	20.4
2.69E+6	3.26E-08	9.55E-10	28.0	3.67E-09	1.14E-10	26.6	1.75E-09	5.04E-11	22.5
2.83E+6	2.63E-08	8.13E-10	28.7	2.49E-09	8.16E-11	28.2	9.46E-10	3.07E-11	24.3
2.98E+6	2.16E-08	7.60E-10	29.2	1.85E-09	7.59E-11	29.2	6.13E-10	3.11E-11	26.0
3.13E+6	1.89E-08	7.16E-10	29.0	1.60E-09	7.08E-11	29.0	5.46E-10	2.06E-11	26.7
3.29E+6	1.76E-08	6.48E-10	28.3	1.53E-09	6.13E-11	28.3	5.23E-10	1.64E-11	27.0
3.46E+6	1.66E-08	5.96E-10	27.6	1.47E-09	5.69E-11	27.6	4.77E-10	1.38E-11	26.3
3.63E+6	1.56E-08	5.33E-10	26.8	1.39E-09	5.25E-11	26.8	4.25E-10	1.17E-11	26.1
3.82E+6	1.44E-08	4.96E-10	26.1	1.28E-09	5.10E-11	26.1	3.82E-10	1.08E-11	25.6
4.02E+6	1.31E-08	4.85E-10	25.3	1.13E-09	5.20E-11	25.3	3.39E-10	1.03E-11	25.2
4.22E+6	1.18E-08	4.89E-10	24.5	9.75E-10	5.43E-11	24.5	2.86E-10	1.02E-11	24.5
4.44E+6	1.08E-08	4.88E-10	23.9	8.48E-10	5.64E-11	23.9	2.32E-10	1.01E-11	23.9
4.67E+6	1.00E-08	4.90E-10	23.3	7.79E-10	5.81E-11	23.3	1.92E-10	1.00E-11	23.3
4.91E+6	9.19E-09	4.99E-10	22.7	7.46E-10	6.13E-11	22.7	1.74E-10	1.02E-11	22.7
5.16E+6	8.17E-09	5.07E-10	22.2	7.11E-10	6.41E-11	22.2	1.67E-10	1.05E-11	22.2
5.42E+6	7.25E-09	5.30E-10	21.7	6.82E-10	6.65E-11	21.7	1.60E-10	1.06E-11	21.7
5.70E+6	6.73E-09	5.59E-10	21.1	6.92E-10	6.93E-11	21.1	1.52E-10	1.07E-11	21.1
5.99E+6	6.55E-09	5.76E-10	20.6	6.98E-10	7.15E-11	20.6	1.37E-10	1.08E-11	20.6
6.30E+6	6.08E-09	6.31E-10	20.0	6.15E-10	7.74E-11	20.0	1.14E-10	1.10E-11	20.0
6.62E+6	4.91E-09	6.97E-10	19.5	4.72E-10	8.33E-11	19.5	9.40E-11	1.12E-11	19.5
6.96E+6	4.00E-09	7.16E-10	19.0	3.79E-10	8.46E-11	19.0	9.03E-11	1.10E-11	19.0
7.32E+6	4.63E-09	8.05E-10	18.5	3.52E-10	9.57E-11	18.5	8.79E-11	1.22E-11	18.5
7.69E+6	5.96E-09	9.43E-10	18.0	3.50E-10	1.09E-10	18.0	7.24E-11	1.34E-11	18.0
8.09E+6	5.48E-09	1.02E-09	17.6	3.48E-10	1.17E-10	17.6	5.88E-11	1.33E-11	17.6
8.50E+6	3.61E-09	1.07E-09	17.2	2.98E-10	1.22E-10	17.2	5.36E-11	1.37E-11	17.2
8.94E+6	3.35E-09	1.29E-09	16.8	2.64E-10	1.41E-10	16.8	4.57E-11	1.60E-11	16.8
9.40E+6	5.22E-09	1.45E-09	16.4	3.98E-10	1.61E-10	16.4	5.02E-11	1.69E-11	16.4
9.88E+6	7.08E-09	1.47E-09	15.9	5.34E-10	1.62E-10	15.9	6.97E-11	1.68E-11	15.9
1.04E+7	7.11E-09	1.61E-09	15.5	4.35E-10	1.76E-10	15.5	6.31E-11	1.81E-11	15.5
1.09E+7	6.47E-09	1.70E-09	15.1	3.53E-10	1.89E-10	15.1	3.89E-11	1.87E-11	15.1
1.15E+7	6.69E-09	1.85E-09	14.8	4.24E-10	2.05E-10	14.8	4.06E-11	1.93E-11	14.8
1.21E+7	1.23E-08	2.22E-09	14.5	6.32E-10	2.45E-10	14.5	4.82E-11	2.40E-11	14.5
1.27E+7	3.43E-08	2.52E-09	14.4	1.77E-09	2.58E-10	14.4	4.45E-11	2.54E-11	14.4
1.33E+7	6.43E-08	2.97E-09	14.4	3.95E-09	3.21E-10	14.4	9.32E-11	3.36E-11	14.4
1.40E+7	7.03E-08	3.99E-09	14.4	4.48E-09	3.85E-10	14.4	2.17E-10	3.67E-11	14.4
1.47E+7	4.43E-08	6.21E-09	14.4	2.70E-09	4.91E-10	14.4	2.42E-10	4.72E-11	14.4
1.55E+7	1.98E-08	2.46E-09	14.4	1.10E-09	2.23E-10	14.4	8.94E-11	2.36E-11	14.4
1.63E+7	1.18E-08	3.03E-09	14.4	3.82E-10	2.42E-10	14.4	-2.52E-11	2.00E-11	14.4
1.71E+7	7.03E-09	2.30E-09	14.4	1.06E-10	1.68E-10	14.4	-2.38E-11	1.48E-11	14.4
1.80E+7	2.46E-09	6.63E-10	14.4	1.77E-11	3.62E-11	14.4	-5.01E-12	3.35E-12	14.4

Table 3.1.1.3 Neutron spectra at -10, 102, 228, 356, 553, 711 and 914 mm from the front surface of the test region in the assembly #2 measured by the NE213 spectrometer.

	-10 mm			102 mm			228 mm			356 mm		
Neutron Energy [eV]	Flux [n/leth/ source]	Absolute Error	Window [%]	Flux [n/leth/ source]	Absolute Error	Window [%]	Flux [n/leth/ source]	Absolute Error	Wimdow [%]	Flux [n/leth/ source]	Absolute Error	Window [%]
1.99E+6	4.03E-5	1.19E-5	36.0	2.36E-5	5.51E-6	36.0	5.07E-6	1.07E-6	36.0	8.71E-7	1.60E-7	35.9
2.10E+6	3.01E-5	4.14E-6	35.1	1.87E-5	1.90E-6	35.1	4.13E-6	3.73E-7	34.5	6.85E-7	5.58E-8	34.0
2.20E+6	2.61E-5	1.60E-6	34.3	1.66E-5	6.94E-7	34.3	3.66E-6	1.36E-7	33.1	5.91E-7	2.07E-8	32.3
2.32E+6	2.50E-5	1.25E-6	33.5	1.56E-5	4.95E-7	33.5	3.42E-6	9.49E-8	31.7	5.40E-7	1.41E-8	30.7
2.44E+6	2.49E-5	1.22E-6	32.8	1.50E-5	4.68E-7	32.8	3.22E-6	8.76E-8	30.6	5.02E-7	1.30E-8	29.4
2.56E+6	2.51E-5	1.20E-6	32.0	1.43E-5	4.50E-7	32.0	3.00E-6	8.45E-8	29.9	4.64E-7	1.26E-8	28.6
2.69E+6	2.48E-5	1.16E-6	31.2	1.35E-5	4.35E-7	31.2	2.74E-6	8.15E-8	29.7	4.20E-7	1.20E-8	28.8
2.83E+6	2.41E-5	1.17E-6	30.5	1.25E-5	4.29E-7	30.5	2.46E-6	7.73E-8	29.5	3.73E-7	1.13E-8	29.0
2.98E+6	2.33E-5	1.33E-6	29.7	1.16E-5	4.32E-7	29.7	2.19E-6	7.58E-8	29.4	3.28E-7	1.09E-8	29.0
3.13E+6	2.28E-5	1.53E-6	29.0	1.09E-5	4.51E-7	29.0	1.98E-6	7.40E-8	29.0	2.92E-7	1.02E-8	28.9
3.29E+6	2.23E-5	1.60E-6	28.3	1.04E-5	4.55E-7	28.3	1.83E-6	7.18E-8	28.3	2.67E-7	9.51E-9	28.3
3.46E+6	2.11E-5	1.48E-6	27.6	9.94E-6	4.36E-7	27.6	1.73E-6	6.76E-8	27.6	2.52E-7	8.88E-9	27.6
3.63E+6	1.91E-5	1.28E-6	26.8	9.46E-6	3.99E-7	26.8	1.65E-6	6.24E-8	26.8	2.42E-7	8.26E-9	26.8
3.82E+6	1.64E-5	1.19E-6	26.1	8.94E-6	3.73E-7	26.1	1.58E-6	5.83E-8	26.1	2.32E-7	7.88E-9	26.1
4.02E+6	1.38E-5	1.21E-6	25.3	8.40E-6	3.69E-7	25.3	1.49E-6	5.74E-8	25.3	2.17E-7	7.70E-9	25.3
4.22E+6	1.19E-5	1.29E-6	24.5	7.85E-6	3.79E-7	24.5	1.39E-6	5.79E-8	24.5	1.98E-7	7.59E-9	24.5
4.44E+6	1.09E-5	1.37E-6	23.9	7.22E-6	3.83E-7	23.9	1.28E-6	5.73E-8	23.9	1.79E-7	7.46E-9	23.9
4.67E+6	1.03E-5	1.44E-6	23.3	6.48E-6	3.83E-7	23.3	1.16E-6	5.61E-8	23.3	1.62E-7	7.36E-9	23.3
4.91E+6	9.40E-6	1.53E-6	22.7	5.70E-6	3.90E-7	22.7	1.03E-6	5.66E-8	22.7	1.46E-7	7.45E-9	22.7
5.16E+6	7.87E-6	1.59E-6	22.2	4.95E-6	3.97E-7	22.2	8.97E-7	5.73E-8	22.2	1.28E-7	7.47E-9	22.2
5.42E+6	5.97E-6	1.70E-6	21.7	4.30E-6	4.12E-7	21.7	7.58E-7	5.86E-8	21.7	1.09E-7	7.64E-9	21.7
5.70E+6	4.23E-6	1.84E-6	21.1	3.74E-6	4.32E-7	21.1	6.53E-7	6.06E-8	21.1	9.12E-8	7.90E-9	21.1
5.99E+6	2.83E-6	1.94E-6	20.6	3.19E-6	4.42E-7	20.6	6.16E-7	6.08E-8	20.6	7.96E-8	8.02E-9	20.6
6.30E+6	1.54E-6	2.22E-6	20.0	2.68E-6	4.85E-7	20.0	6.24E-7	6.46E-8	20.0	7.61E-8	8.50E-9	20.0
6.62E+6	2.52E-7	2.53E-6	19.5	2.37E-6	5.38E-7	19.5	6.03E-7	7.08E-8	19.5	7.78E-8	9.30E-9	19.5
6.96E+6	-9.23E-7	2.63E-6	19.0	2.37E-6	5.50E-7	19.0	5.18E-7	7.33E-8	19.0	7.89E-8	9.56E-9	19.0
7.32E+6	-1.04E-6	3.07E-6	18.5	2.51E-6	6.30E-7	18.5	4.42E-7	8.11E-8	18.5	7.68E-8	1.06E-8	18.5
7.69E+6	1.27E-6	3.65E-6	18.0	2.47E-6	7.36E-7	18.0	4.54E-7	9.31E-8	18.0	7.34E-8	1.21E-8	18.0
8.09E+6	3.46E-6	3.99E-6	17.6	2.19E-6	7.90E-7	17.6	4.70E-7	1.01E-7	17.6	6.76E-8	1.29E-8	17.6
8.50E+6	8.34E-7	4.65E-6	17.2	1.76E-6	9.03E-7	17.2	4.03E-7	1.14E-7	17.2	6.17E-8	1.45E-8	17.2
8.94E+6	-4.54E-6	5.99E-6	16.8	1.39E-6	1.14E-6	16.8	3.61E-7	1.43E-7	16.8	6.44E-8	1.79E-8	16.8
9.40E+6	-5.95E-6	6.67E-6	16.4	1.42E-6	1.26E-6	16.4	4.50E-7	1.55E-7	16.4	6.69E-8	1.96E-8	16.4
9.88E+6	-2.28E-6	6.96E-6	15.9	1.82E-6	1.29E-6	15.9	5.49E-7	1.60E-7	15.9	5.27E-8	2.04E-8	15.9
1.04E+7	2.65E-6	7.99E-6	15.5	1.94E-6	1.48E-6	15.5	4.84E-7	1.80E-7	15.5	4.50E-8	2.28E-8	15.5
1.09E+7	6.66E-6	8.07E-6	15.1	1.65E-6	1.48E-6	15.1	2.97E-7	1.78E-7	15.1	6.97E-8	2.24E-8	15.1
1.15E+7	1.19E-5	8.26E-6	14.8	2.32E-6	1.50E-6	14.8	2.22E-7	1.80E-7	14.8	1.19E-7	2.23E-8	14.8
1.21E+7	3.98E-5	9.85E-6	14.5	4.71E-6	1.84E-6	14.5	4.64E-7	2.21E-7	14.5	2.16E-7	2.64E-8	14.5
1.27E+7	1.36E-4	1.01E-5	14.4	1.19E-5	2.08E-6	14.4	1.03E-6	2.70E-7	14.4	4.33E-7	3.01E-8	14.4
1.33E+7	3.28E-4	1.24E-5	14.4	3.63E-5	2.52E-6	14.4	3.15E-6	3.20E-7	14.4	8.55E-7	3.42E-8	14.4
1.40E+7	4.80E-4	1.55E-5	14.4	7.97E-5	3.26E-6	14.4	8.80E-6	4.24E-7	14.4	1.27E-6	4.72E-8	14.4
1.47E+7	3.91E-4	1.57E-5	14.4	9.79E-5	4.84E-6	14.4	1.29E-5	7.38E-7	14.4	1.15E-6	7.61E-8	14.4
1.55E+7	2.02E-4	7.03E-6	14.4	6.14E-5	2.03E-6	14.4	8.58E-6	2.96E-7	14.4	5.42E-7	2.86E-8	14.4
1.63E+7	1.05E-4	7.72E-6	14.1	2.23E-5	2.37E-6	14.2	2.77E-6	3.61E-7	14.4	1.33E-7	3.86E-8	14.4
1.71E+7	6.65E-5	5.70E-6	13.9	1.39E-5	1.76E-6	14.0	1.64E-6	2.72E-7	14.4	7.35E-8	2.82E-8	14.4
1.80E+7	3.56E-5	1.43E-6	13.6	1.12E-5	4.56E-7	13.8	1.49E-6	7.41E-8	14.4	6.49E-8	7.68E-9	14.4

Table 3.1.1.3 (Continued)

	553mm			711 mm			914 mm		
Neutron Energy [eV]	Flux [n/leth/ source]	Absolute Error	Window [%]	Flux [n/leth/ source]	Absolute Error	Window [%]	Flux [n/leth/ source]	Absolute Error	Wimdow [%]
1.99E+6	8.53E-08	1.31E-08	35.3	1.46E-08	1.83E-09	35.6	4.94E-09	3.95E-10	34.4
2.10E+6	6.23E-08	4.56E-09	33.4	9.40E-09	6.41E-10	34.1	2.72E-09	1.39E-10	32.1
2.20E+6	5.05E-08	1.68E-09	31.9	6.96E-09	2.33E-10	33.0	1.75E-09	5.26E-11	30.2
2.32E+6	4.40E-08	1.14E-09	30.5	5.82E-09	1.53E-10	32.0	1.35E-09	3.32E-11	28.3
2.44E+6	3.95E-08	1.01E-09	29.4	5.20E-09	1.38E-10	31.0	1.16E-09	2.91E-11	26.3
2.56E+6	3.57E-08	9.60E-10	29.3	4.79E-09	1.31E-10	30.5	1.04E-09	2.87E-11	25.8
2.69E+6	3.20E-08	9.19E-10	29.6	4.48E-09	1.28E-10	30.4	9.61E-10	2.75E-11	25.0
2.83E+6	2.86E-08	8.53E-10	29.5	4.21E-09	1.25E-10	29.9	9.06E-10	2.59E-11	23.8
2.98E+6	2.58E-08	8.26E-10	29.3	3.99E-09	1.23E-10	29.3	8.65E-10	2.45E-11	23.1
3.13E+6	2.39E-08	8.04E-10	29.0	3.83E-09	1.23E-10	28.6	8.06E-10	2.31E-11	22.9
3.29E+6	2.26E-08	7.66E-10	28.3	3.76E-09	1.20E-10	27.4	7.10E-10	2.08E-11	23.1
3.46E+6	2.17E-08	7.10E-10	27.6	3.78E-09	1.15E-10	26.0	5.98E-10	1.86E-11	23.8
3.63E+6	2.08E-08	6.42E-10	26.8	3.82E-09	1.09E-10	24.6	5.02E-10	1.60E-11	24.5
3.82E+6	1.98E-08	5.97E-10	26.1	3.77E-09	1.03E-10	23.6	4.30E-10	1.48E-11	24.9
4.02E+6	1.85E-08	5.79E-10	25.3	3.56E-09	1.01E-10	23.1	3.75E-10	1.36E-11	24.9
4.22E+6	1.70E-08	5.73E-10	24.5	3.22E-09	9.79E-11	23.0	3.31E-10	1.24E-11	24.5
4.44E+6	1.53E-08	5.65E-10	23.9	2.85E-09	9.49E-11	23.1	2.97E-10	1.20E-11	23.9
4.67E+6	1.37E-08	5.44E-10	23.3	2.52E-09	8.77E-11	23.0	2.62E-10	1.16E-11	23.3
4.91E+6	1.20E-08	5.56E-10	22.7	2.22E-09	8.61E-11	22.7	2.21E-10	1.15E-11	22.7
5.16E+6	1.04E-08	5.64E-10	22.2	1.93E-09	8.47E-11	22.2	1.79E-10	1.14E-11	22.2
5.42E+6	9.10E-09	5.85E-10	21.7	1.64E-09	8.48E-11	21.7	1.47E-10	1.11E-11	21.7
5.70E+6	7.87E-09	6.22E-10	21.1	1.32E-09	8.62E-11	21.1	1.32E-10	1.13E-11	21.1
5.99E+6	6.33E-09	6.41E-10	20.6	1.04E-09	8.40E-11	20.6	1.22E-10	1.15E-11	20.6
6.30E+6	4.85E-09	6.90E-10	20.0	8.65E-10	8.65E-11	20.0	1.08E-10	1.16E-11	20.0
6.62E+6	4.34E-09	7.63E-10	19.5	7.33E-10	9.50E-11	19.5	9.48E-11	1.18E-11	19.5
6.96E+6	5.08E-09	7.85E-10	19.0	5.77E-10	9.59E-11	19.0	8.59E-11	1.20E-11	19.0
7.32E+6	6.31E-09	8.86E-10	18.5	5.03E-10	1.06E-10	18.5	7.59E-11	1.31E-11	18.5
7.69E+6	6.95E-09	1.03E-09	18.0	5.48E-10	1.23E-10	18.0	7.33E-11	1.36E-11	18.0
8.09E+6	6.65E-09	1.09E-09	17.6	5.84E-10	1.30E-10	17.6	8.46E-11	1.41E-11	17.6
8.50E+6	5.97E-09	1.14E-09	17.2	6.09E-10	1.34E-10	17.2	9.17E-11	1.42E-11	17.2
8.94E+6	5.61E-09	1.35E-09	16.8	6.73E-10	1.60E-10	16.8	7.75E-11	1.60E-11	16.8
9.40E+6	5.87E-09	1.54E-09	16.4	6.48E-10	1.80E-10	16.4	4.97E-11	1.71E-11	16.4
9.88E+6	4.88E-09	1.54E-09	15.9	4.75E-10	1.76E-10	15.9	2.44E-11	1.67E-11	15.9
1.04E+7	1.39E-09	1.67E-09	15.5	3.29E-10	1.88E-10	15.5	1.28E-11	1.76E-11	15.5
1.09E+7	-4.33E-10	1.85E-09	15.1	3.10E-10	2.05E-10	15.1	9.02E-12	1.98E-11	15.1
1.15E+7	3.22E-09	2.01E-09	14.8	4.13E-10	2.23E-10	14.8	7.69E-12	2.11E-11	14.8
1.21E+7	1.13E-08	2.50E-09	14.5	7.50E-10	2.81E-10	14.5	3.25E-11	2.67E-11	14.5
1.27E+7	2.80E-08	2.88E-09	14.4	9.57E-10	3.74E-10	14.4	8.58E-11	3.19E-11	14.4
1.33E+7	5.56E-08	3.41E-09	14.4	1.12E-09	4.36E-10	14.4	1.42E-10	3.72E-11	14.4
1.40E+7	7.51E-08	4.56E-09	14.4	2.73E-09	6.26E-10	14.4	1.31E-10	5.25E-11	14.4
1.47E+7	6.27E-08	7.33E-09	14.4	3.93E-09	1.18E-09	14.4	4.77E-11	8.83E-11	14.4
1.55E+7	2.83E-08	2.93E-09	14.4	2.77E-09	4.34E-10	14.4	3.65E-11	3.34E-11	14.4
1.63E+7	7.31E-09	3.52E-09	14.4	1.45E-09	6.11E-10	14.4	7.96E-11	4.40E-11	14.4
1.71E+7	3.34E-09	2.69E-09	14.4	9.03E-10	4.45E-10	14.4	6.87E-11	3.42E-11	14.4
1.80E+7	1.71E-09	7.75E-10	14.4	5.80E-10	1.28E-10	14.4	2.83E-11	1.11E-11	14.4

Table 3.1.2.1 Neutron spectra at -10, 102, 228, 356, 553, 711 and 914 mm from the front surface of the test region in the assembly #1 measured by the proton-recoil gas proportional counters.

-10 mm			102 mm			228 mm			356 mm		
Neutron Energy [eV]	Flux [n/leth/ source]	Absolute Error	Neutron Energy [eV]	Flux [n/leth/ source]	Absolute Error	Neutron Energy [eV]	Flux [n/leth/ source]	Absolute Error	Neutron Energy [eV]	Flux [n/leth/ source]	Absolute Error
3.10E+3	1.89E-6	1.05E-6	3.06E+3	2.75E-6	2.22E-6	3.02E+3	1.40E-6	1.62E-6	2.98E+3	1.09E-6	9.39E-7
3.24E+3	2.11E-6	1.01E-6	3.19E+3	2.04E-6	2.16E-6	3.15E+3	3.88E-6	1.55E-6	3.10E+3	2.34E-6	8.98E-7
3.38E+3	5.11E-7	9.53E-7	3.33E+3	6.05E-6	2.03E-6	3.28E+3	4.09E-6	1.49E-6	3.24E+3	3.25E-6	8.57E-7
3.53E+3	2.19E-6	9.15E-7	3.48E+3	6.34E-6	2.01E-6	3.43E+3	3.90E-6	1.44E-6	3.38E+3	1.84E-6	8.32E-7
3.68E+3	1.53E-6	8.88E-7	3.63E+3	2.14E-6	1.87E-6	3.58E+3	3.01E-6	1.39E-6	3.53E+3	1.78E-6	7.97E-7
3.84E+3	1.71E-7	8.56E-7	3.79E+3	2.39E-6	1.88E-6	3.74E+3	3.19E-6	1.35E-6	3.68E+3	3.46E-6	7.79E-7
4.01E+3	6.54E-8	8.38E-7	3.96E+3	3.02E-7	1.82E-6	3.90E+3	2.34E-6	1.33E-6	3.84E+3	2.22E-6	7.49E-7
4.19E+3	1.50E-6	8.19E-7	4.13E+3	4.95E-6	1.79E-6	4.07E+3	3.79E-6	1.29E-6	4.01E+3	2.30E-6	7.36E-7
4.38E+3	8.19E-7	8.08E-7	4.32E+3	6.39E-6	1.75E-6	4.25E+3	4.33E-6	1.25E-6	4.19E+3	2.38E-6	7.17E-7
4.58E+3	2.73E-7	7.98E-7	4.51E+3	2.05E-6	1.72E-6	4.44E+3	1.62E-6	1.23E-6	4.38E+3	2.74E-6	7.01E-7
4.78E+3	8.28E-7	7.87E-7	4.71E+3	3.99E-6	1.67E-6	4.64E+3	3.57E-6	1.21E-6	4.58E+3	2.03E-6	6.84E-7
5.00E+3	1.43E-6	7.76E-7	4.92E+3	4.32E-6	1.65E-6	4.85E+3	3.38E-6	1.20E-6	4.78E+3	2.00E-6	6.73E-7
5.22E+3	-2.00E-6	7.88E-7	5.14E+3	4.36E-6	1.63E-6	5.07E+3	2.54E-6	1.18E-6	5.00E+3	2.82E-6	6.63E-7
5.46E+3	-1.61E-6	7.87E-7	5.38E+3	4.68E-6	1.62E-6	5.30E+3	4.20E-6	1.17E-6	5.22E+3	2.15E-6	6.55E-7
5.70E+3	-6.38E-8	8.13E-7	5.62E+3	1.42E-6	1.58E-6	5.54E+3	3.42E-6	1.15E-6	5.46E+3	9.19E-7	6.48E-7
5.96E+3	7.52E-7	8.02E-7	5.87E+3	4.38E-6	1.58E-6	5.79E+3	3.25E-6	1.14E-6	5.70E+3	2.78E-6	6.43E-7
6.24E+3	1.83E-6	7.98E-7	6.14E+3	2.00E-6	1.57E-6	6.05E+3	2.25E-6	1.13E-6	5.96E+3	2.79E-6	6.38E-7
6.52E+3	1.76E-6	7.87E-7	6.42E+3	4.19E-6	1.55E-6	6.33E+3	5.18E-6	1.12E-6	6.24E+3	2.10E-6	6.30E-7
6.82E+3	3.93E-7	7.73E-7	6.72E+3	3.98E-6	1.54E-6	6.62E+3	3.40E-6	1.11E-6	6.52E+3	2.40E-6	6.26E-7
7.13E+3	5.34E-7	7.78E-7	7.03E+3	2.42E-6	1.54E-6	6.92E+3	3.21E-6	1.10E-6	6.82E+3	3.45E-6	6.20E-7
7.46E+3	1.90E-6	7.70E-7	7.35E+3	4.48E-6	1.53E-6	7.24E+3	3.64E-6	1.10E-6	7.13E+3	1.66E-6	6.15E-7
7.80E+3	1.52E-6	7.61E-7	7.69E+3	3.77E-6	1.53E-6	7.57E+3	2.29E-6	1.09E-6	7.46E+3	2.08E-6	6.14E-7
8.16E+3	2.66E-6	7.63E-7	8.04E+3	1.39E-6	1.52E-6	7.92E+3	1.83E-6	1.10E-6	7.80E+3	2.75E-6	6.10E-7
8.54E+3	6.34E-7	7.63E-7	8.41E+3	3.80E-6	1.53E-6	8.29E+3	4.48E-6	1.10E-6	8.16E+3	2.88E-6	6.10E-7
8.93E+3	3.94E-7	7.73E-7	8.80E+3	7.85E-6	1.54E-6	8.67E+3	3.50E-6	1.11E-6	8.54E+3	2.66E-6	6.15E-7
9.35E+3	2.64E-6	7.84E-7	9.21E+3	6.20E-6	1.57E-6	9.07E+3	3.88E-6	1.13E-6	8.93E+3	2.72E-6	6.21E-7
9.78E+3	1.28E-6	7.98E-7	9.64E+3	3.55E-6	1.58E-6	9.49E+3	7.18E-6	1.13E-6	9.35E+3	4.35E-6	6.26E-7
1.02E+4	2.54E-6	7.93E-7	1.01E+4	5.06E-6	1.59E-6	9.93E+3	7.77E-6	1.15E-6	9.78E+3	4.66E-6	6.30E-7
1.07E+4	2.52E-6	8.05E-7	1.06E+4	9.38E-6	1.60E-6	1.04E+4	7.31E-6	1.15E-6	1.02E+4	4.94E-6	6.33E-7
1.12E+4	6.13E-7	8.07E-7	1.10E+4	9.29E-6	1.62E-6	1.09E+4	7.98E-6	1.16E-6	1.07E+4	5.19E-6	6.35E-7
1.17E+4	1.83E-6	8.14E-7	1.16E+4	6.08E-6	1.62E-6	1.14E+4	8.39E-6	1.16E-6	1.12E+4	5.21E-6	6.39E-7
1.23E+4	2.61E-6	8.24E-7	1.21E+4	7.68E-6	1.63E-6	1.19E+4	7.99E-6	1.16E-6	1.17E+4	5.26E-6	6.43E-7
1.29E+4	2.89E-6	8.28E-7	1.27E+4	7.67E-6	1.65E-6	1.25E+4	7.08E-6	1.17E-6	1.23E+4	5.82E-6	6.45E-7
1.35E+4	9.04E-7	8.37E-7	1.33E+4	6.82E-6	1.65E-6	1.31E+4	6.75E-6	1.18E-6	1.29E+4	4.46E-6	6.48E-7
1.41E+4	1.65E-6	8.47E-7	1.39E+4	9.18E-6	1.67E-6	1.37E+4	7.86E-6	1.18E-6	1.35E+4	3.84E-6	6.53E-7
1.48E+4	2.04E-6	8.62E-7	1.45E+4	7.36E-6	1.69E-6	1.43E+4	6.25E-6	1.20E-6	1.41E+4	3.83E-6	6.59E-7
1.55E+4	2.39E-6	8.70E-7	1.52E+4	2.59E-6	1.69E-6	1.50E+4	6.31E-6	1.21E-6	1.48E+4	3.94E-6	6.68E-7
1.62E+4	2.46E-6	8.80E-7	1.59E+4	4.75E-6	1.74E-6	1.57E+4	4.40E-6	1.23E-6	1.55E+4	4.12E-6	6.74E-7
1.69E+4	-2.23E-7	8.94E-7	1.67E+4	6.03E-6	1.75E-6	1.64E+4	5.80E-6	1.24E-6	1.62E+4	4.65E-6	6.79E-7
1.77E+4	2.28E-6	9.08E-7	1.75E+4	8.37E-6	1.78E-6	1.72E+4	6.72E-6	1.26E-6	1.69E+4	5.09E-6	6.87E-7
1.86E+4	1.50E-6	9.24E-7	1.83E+4	8.83E-6	1.79E-6	1.80E+4	5.96E-6	1.28E-6	1.77E+4	4.33E-6	6.93E-7
1.95E+4	2.43E-6	9.32E-7	1.92E+4	7.91E-6	1.82E-6	1.89E+4	9.24E-6	1.29E-6	1.86E+4	4.55E-6	7.03E-7
2.04E+4	2.85E-6	9.47E-7	2.01E+4	9.09E-6	1.84E-6	1.98E+4	1.06E-5	1.29E-6	1.95E+4	6.91E-6	7.08E-7
2.13E+4	4.32E-6	9.48E-7	2.10E+4	1.18E-5	1.86E-6	2.07E+4	1.33E-5	1.30E-6	2.04E+4	7.65E-6	7.12E-7
2.24E+4	3.41E-6	9.57E-7	2.20E+4	1.27E-5	1.87E-6	2.17E+4	1.36E-5	1.30E-6	2.13E+4	9.32E-6	7.10E-7
2.34E+4	4.22E-6	9.56E-7	2.31E+4	1.64E-5	1.87E-6	2.27E+4	1.50E-5	1.30E-6	2.24E+4	9.56E-6	7.12E-7
2.45E+4	3.70E-6	9.71E-7	2.41E+4	1.93E-5	1.86E-6	2.38E+4	1.67E-5	1.29E-6	2.34E+4	1.10E-5	7.06E-7
2.57E+4	3.54E-6	9.70E-7	2.53E+4	1.84E-5	1.86E-6	2.49E+4	1.77E-5	1.29E-6	2.45E+4	1.30E-5	6.97E-7
2.69E+4	3.45E-6	9.86E-7	2.65E+4	1.46E-5	1.86E-6	2.61E+4	1.64E-5	1.28E-6	2.57E+4	1.22E-5	6.87E-7
2.82E+4	1.30E-6	9.95E-7	2.77E+4	1.10E-5	1.87E-6	2.73E+4	1.22E-5	1.28E-6	2.69E+4	7.63E-6	6.82E-7
2.95E+4	2.27E-6	1.02E-6	2.91E+4	5.38E-6	1.89E-6	2.86E+4	6.17E-6	1.29E-6	2.82E+4	5.78E-6	6.86E-7
3.09E+4	3.02E-6	1.03E-6	3.04E+4	-1.19E-6	1.94E-6	3.00E+4	2.55E-6	1.31E-6	2.95E+4	3.21E-6	6.96E-7
3.24E+4	-3.66E-8	1.06E-6	3.19E+4	5.82E-6	1.99E-6	3.14E+4	4.41E-6	1.34E-6	3.09E+4	2.22E-6	7.07E-7
3.39E+4	-3.38E-8	1.08E-6	3.34E+4	7.55E-6	2.03E-6	3.29E+4	8.23E-6	1.36E-6	3.24E+4	2.25E-6	7.23E-7
3.55E+4	2.92E-6	1.11E-6	3.50E+4	8.87E-6	2.06E-6	3.45E+4	7.72E-6	1.39E-6	3.39E+4	4.40E-6	7.39E-7
3.72E+4	3.89E-6	1.13E-6	3.67E+4	1.12E-5	2.10E-6	3.61E+4	6.12E-6	1.41E-6	3.55E+4	5.13E-6	7.47E-7
3.90E+4	2.62E-6	1.15E-6	3.84E+4	1.08E-5	2.12E-6	3.78E+4	7.49E-6	1.44E-6	3.72E+4	5.49E-6	7.60E-7
4.09E+4	2.24E-6	1.18E-6	4.02E+4	1.07E-5	2.16E-6	3.96E+4	1.15E-5	1.45E-6	3.90E+4	7.17E-6	7.66E-7
4.28E+4	4.07E-6	1.20E-6	4.21E+4	1.51E-5	2.20E-6	4.15E+4	1.20E-5	1.48E-6	4.09E+4	8.10E-6	7.75E-7
4.48E+4	4.32E-6	1.22E-6	4.42E+4	1.89E-5	2.20E-6	4.35E+4	1.35E-5	1.49E-6	4.28E+4	8.87E-6	7.81E-7
4.70E+4	5.00E-6	1.23E-6	4.63E+4	1.53E-5	2.23E-6	4.55E+4	1.44E-5	1.50E-6	4.48E+4	8.58E-6	7.85E-7
4.92E+4	3.53E-6	1.26E-6	4.85E+4	1.10E-5	2.27E-6	4.77E+4	1.40E-5	1.52E-6	4.70E+4	9.30E-6	7.90E-7
5.16E+4	2.33E-6	1.28E-6	5.08E+4	1.05E-5	2.30E-6	5.00E+4	1.46E-5	1.53E-6	4.92E+4	8.42E-6	7.97E-7
5.40E+4	4.57E-6	1.31E-6	5.32E+4	1.53E-5	2.35E-6	5.24E+4	1.18E-5	1.55E-6	5.16E+4	8.57E-6	8.03E-7
5.66E+4	5.54E-6	1.34E-6	5.57E+4	2.06E-5	2.39E-6	5.49E+4	1.22E-5	1.58E-6	5.40E+4	7.99E-6	8.13E-7
5.93E+4	5.51E-6	1.36E-6	5.84E+4	1.98E-5	2.40E-6	5.75E+4	1.48E-5	1.59E-6	5.66E+4	8.13E-6	8.19E-7

Table 3.1.2.1 (Continued-1)

-10 mm			102 mm			228 mm			356 mm		
Neutron Energy [eV]	Flux [n/leth/ source]	Absolute Error	Neutron Energy [eV]	Flux [n/leth/ source]	Absolute Error	Neutron Energy [eV]	Flux [n/leth/ source]	Absolute Error	Neutron Energy [eV]	Flux [n/leth/ source]	Absolute Error
6.21E+4	4.86E-6	1.39E-6	6.12E+4	1.95E-5	2.44E-6	6.02E+4	1.80E-5	1.60E-6	5.93E+4	9.89E-6	8.31E-7
6.51E+4	7.88E-6	1.40E-6	6.41E+4	1.64E-5	2.47E-6	6.31E+4	1.97E-5	1.62E-6	6.21E+4	1.22E-5	8.32E-7
6.82E+4	5.95E-6	1.43E-6	6.72E+4	2.05E-5	2.50E-6	6.61E+4	1.76E-5	1.63E-6	6.51E+4	1.06E-5	8.37E-7
7.15E+4	6.27E-6	1.44E-6	7.04E+4	2.07E-5	2.54E-6	6.93E+4	1.99E-5	1.64E-6	6.82E+4	1.02E-5	8.45E-7
7.49E+4	7.77E-6	1.48E-6	7.37E+4	2.16E-5	2.56E-6	7.26E+4	1.73E-5	1.65E-6	7.15E+4	1.16E-5	8.48E-7
7.85E+4	7.92E-6	1.49E-6	7.73E+4	2.30E-5	2.61E-6	7.61E+4	1.73E-5	1.67E-6	7.49E+4	1.22E-5	8.52E-7
8.22E+4	1.07E-5	1.52E-6	8.10E+4	2.49E-5	2.63E-6	7.97E+4	2.16E-5	1.69E-6	7.85E+4	1.40E-5	8.53E-7
8.62E+4	6.37E-6	1.54E-6	8.48E+4	2.47E-5	2.68E-6	8.35E+4	2.20E-5	1.69E-6	8.22E+4	1.42E-5	8.52E-7
9.03E+4	4.26E-6	1.57E-6	8.89E+4	2.61E-5	2.69E-6	8.75E+4	1.97E-5	1.72E-6	8.62E+4	1.13E-5	8.57E-7
9.46E+4	5.86E-6	1.62E-6	9.31E+4	2.22E-5	2.74E-6	9.17E+4	1.68E-5	1.73E-6	9.03E+4	1.05E-5	8.62E-7
9.91E+4	6.78E-6	1.65E-6	9.76E+4	1.76E-5	2.78E-6	9.61E+4	1.62E-5	1.75E-6	9.46E+4	9.56E-6	8.72E-7
1.04E+5	6.13E-6	1.69E-6	1.02E+5	1.85E-5	2.84E-6	1.01E+5	1.88E-5	1.78E-6	9.91E+4	8.09E-6	8.86E-7
1.09E+5	7.36E-6	1.73E-6	1.07E+5	2.54E-5	2.88E-6	1.06E+5	1.80E-5	1.81E-6	1.04E+5	1.03E-5	8.94E-7
1.14E+5	1.06E-5	1.77E-6	1.12E+5	2.82E-5	2.94E-6	1.11E+5	2.40E-5	1.82E-6	1.09E+5	1.33E-5	9.06E-7
1.20E+5	1.39E-5	1.79E-6	1.18E+5	3.20E-5	2.98E-6	1.16E+5	2.82E-5	1.83E-6	1.14E+5	1.39E-5	9.06E-7
1.25E+5	1.42E-5	1.86E-6	1.23E+5	3.98E-5	3.02E-6	1.21E+5	2.91E-5	1.86E-6	1.20E+5	1.71E-5	9.13E-7
1.31E+5	1.66E-5	1.89E-6	1.29E+5	4.75E-5	3.09E-6	1.27E+5	3.78E-5	1.87E-6	1.25E+5	2.19E-5	9.10E-7
1.38E+5	1.55E-5	1.96E-6	1.35E+5	4.74E-5	3.14E-6	1.33E+5	3.69E-5	1.88E-6	1.31E+5	2.14E-5	9.18E-7
1.44E+5	1.30E-5	2.01E-6	1.42E+5	3.54E-5	3.23E-6	1.40E+5	2.68E-5	1.93E-6	1.38E+5	1.75E-5	9.17E-7
1.51E+5	1.08E-5	2.08E-6	1.49E+5	3.26E-5	3.32E-6	1.46E+5	2.07E-5	1.97E-6	1.44E+5	1.37E-5	9.34E-7
1.58E+5	1.73E-5	2.47E-6	1.53E+5	3.29E-5	3.30E-6	1.51E+5	2.41E-5	1.57E-6	1.51E+5	9.76E-6	9.59E-7
1.65E+5	1.62E-5	2.45E-6	1.60E+5	2.95E-5	3.26E-6	1.58E+5	2.94E-5	1.52E-6	1.58E+5	1.34E-5	7.45E-7
1.73E+5	2.20E-5	2.41E-6	1.68E+5	3.54E-5	3.22E-6	1.65E+5	2.85E-5	1.48E-6	1.65E+5	1.44E-5	7.23E-7
1.81E+5	1.85E-5	2.41E-6	1.76E+5	4.58E-5	3.17E-6	1.73E+5	2.78E-5	1.45E-6	1.73E+5	1.57E-5	7.04E-7
1.90E+5	1.77E-5	2.39E-6	1.84E+5	4.90E-5	3.11E-6	1.81E+5	3.15E-5	1.41E-6	1.81E+5	1.57E-5	6.86E-7
1.99E+5	1.89E-5	2.37E-6	1.93E+5	3.88E-5	3.06E-6	1.90E+5	2.93E-5	1.39E-6	1.90E+5	1.40E-5	6.68E-7
2.09E+5	1.82E-5	2.37E-6	2.02E+5	4.03E-5	3.02E-6	1.99E+5	2.43E-5	1.36E-6	1.99E+5	1.23E-5	6.54E-7
2.19E+5	2.25E-5	2.36E-6	2.12E+5	4.02E-5	2.99E-6	2.09E+5	2.55E-5	1.34E-6	2.09E+5	1.31E-5	6.43E-7
2.29E+5	2.20E-5	2.35E-6	2.22E+5	4.49E-5	2.98E-6	2.19E+5	2.77E-5	1.33E-6	2.19E+5	1.40E-5	6.34E-7
2.40E+5	2.56E-5	2.35E-6	2.33E+5	4.22E-5	2.95E-6	2.29E+5	2.66E-5	1.31E-6	2.29E+5	1.43E-5	6.22E-7
2.52E+5	2.31E-5	2.35E-6	2.44E+5	3.95E-5	2.94E-6	2.40E+5	3.09E-5	1.30E-6	2.40E+5	1.57E-5	6.11E-7
2.64E+5	2.74E-5	2.35E-6	2.56E+5	5.07E-5	2.92E-6	2.52E+5	3.54E-5	1.29E-6	2.52E+5	1.68E-5	5.98E-7
2.77E+5	3.29E-5	2.34E-6	2.68E+5	5.82E-5	2.89E-6	2.64E+5	3.94E-5	1.25E-6	2.64E+5	1.92E-5	5.82E-7
2.90E+5	3.35E-5	2.32E-6	2.81E+5	6.20E-5	2.85E-6	2.77E+5	3.97E-5	1.23E-6	2.77E+5	1.95E-5	5.63E-7
3.04E+5	3.60E-5	2.31E-6	2.94E+5	6.34E-5	2.80E-6	2.90E+5	3.84E-5	1.20E-6	2.90E+5	1.95E-5	5.44E-7
3.18E+5	3.33E-5	2.31E-6	3.09E+5	7.09E-5	2.76E-6	3.04E+5	4.35E-5	1.17E-6	3.04E+5	2.13E-5	5.21E-7
3.34E+5	3.08E-5	2.30E-6	3.23E+5	6.38E-5	2.73E-6	3.18E+5	4.18E-5	1.13E-6	3.18E+5	1.84E-5	5.02E-7
3.50E+5	3.96E-5	2.32E-6	3.39E+5	5.92E-5	2.69E-6	3.34E+5	3.69E-5	1.11E-6	3.34E+5	1.55E-5	4.85E-7
3.66E+5	3.56E-5	2.34E-6	3.55E+5	6.47E-5	2.68E-6	3.50E+5	3.74E-5	1.09E-6	3.50E+5	1.70E-5	4.71E-7
3.84E+5	3.24E-5	2.36E-6	3.72E+5	6.73E-5	2.68E-6	3.66E+5	3.76E-5	1.07E-6	3.66E+5	1.58E-5	4.60E-7
4.02E+5	2.94E-5	2.40E-6	3.90E+5	5.40E-5	2.68E-6	3.84E+5	3.35E-5	1.06E-6	3.84E+5	1.33E-5	4.49E-7
4.22E+5	2.95E-5	2.42E-6	4.09E+5	4.85E-5	2.68E-6	4.02E+5	2.76E-5	1.05E-6	4.02E+5	1.14E-5	4.41E-7
4.42E+5	3.06E-5	2.47E-6	4.28E+5	5.25E-5	2.69E-6	4.22E+5	2.65E-5	1.04E-6	4.22E+5	1.01E-5	4.36E-7
4.63E+5	3.04E-5	2.51E-6	4.49E+5	5.51E-5	2.70E-6	4.42E+5	2.83E-5	1.04E-6	4.42E+5	1.08E-5	4.31E-7
4.85E+5	4.46E-5	2.54E-6	4.70E+5	5.36E-5	2.70E-6	4.63E+5	2.73E-5	1.03E-6	4.63E+5	1.07E-5	4.25E-7
5.08E+5	4.72E-5	2.61E-6	4.93E+5	5.92E-5	2.73E-6	4.85E+5	3.13E-5	1.02E-6	4.85E+5	1.17E-5	4.18E-7
5.33E+5	4.78E-5	2.66E-6	5.16E+5	6.68E-5	2.75E-6	5.08E+5	3.35E-5	1.02E-6	5.08E+5	1.25E-5	4.14E-7
5.58E+5	5.10E-5	2.73E-6	5.41E+5	6.97E-5	2.80E-6	5.33E+5	3.28E-5	1.02E-6	5.33E+5	1.21E-5	4.09E-7
5.85E+5	5.60E-5	2.76E-6	5.67E+5	7.00E-5	2.80E-6	5.58E+5	3.56E-5	1.01E-6	5.58E+5	1.28E-5	4.00E-7
6.13E+5	6.05E-5	2.84E-6	5.94E+5	7.38E-5	2.83E-6	5.85E+5	3.49E-5	9.97E-7	5.85E+5	1.30E-5	3.90E-7
6.43E+5	5.85E-5	2.87E-6	6.23E+5	7.88E-5	2.83E-6	6.13E+5	3.58E-5	9.80E-7	6.13E+5	1.27E-5	3.75E-7
6.73E+5	5.74E-5	2.92E-6	6.53E+5	7.11E-5	2.83E-6	6.43E+5	3.34E-5	9.59E-7	6.43E+5	1.11E-5	3.60E-7
7.06E+5	5.19E-5	2.98E-6	6.84E+5	6.30E-5	2.83E-6	6.73E+5	2.86E-5	9.42E-7	6.73E+5	9.01E-6	3.45E-7
7.40E+5	4.38E-5	3.06E-6	7.17E+5	5.85E-5	2.85E-6	7.06E+5	2.42E-5	9.22E-7	7.06E+5	7.48E-6	3.33E-7
7.75E+5	4.12E-5	3.14E-6	7.51E+5	5.05E-5	2.89E-6	7.40E+5	2.07E-5	9.18E-7	7.40E+5	5.96E-6	3.26E-7
8.12E+5	4.16E-5	3.27E-6	7.87E+5	5.24E-5	2.92E-6	7.75E+5	1.75E-5	9.15E-7	7.75E+5	5.02E-6	3.22E-7
8.51E+5	4.58E-5	3.37E-6	8.25E+5	5.07E-5	2.97E-6	8.12E+5	1.79E-5	9.13E-7	8.12E+5	4.84E-6	3.17E-7
8.92E+5	5.11E-5	3.47E-6	8.65E+5	4.81E-5	3.02E-6	8.51E+5	1.69E-5	9.19E-7	8.51E+5	4.86E-6	3.14E-7
9.35E+5	5.10E-5	3.57E-6	9.06E+5	5.36E-5	3.04E-6	8.92E+5	1.70E-5	9.09E-7	8.92E+5	4.30E-6	3.07E-7
9.80E+5	5.63E-5	3.66E-6	9.50E+5	5.45E-5	3.07E-6	9.35E+5	1.67E-5	9.17E-7	9.35E+5	4.29E-6	3.03E-7
1.03E+6	6.59E-5	3.76E-6	9.95E+5	5.15E-5	3.08E-6	9.80E+5	1.65E-5	8.90E-7	9.80E+5	4.04E-6	2.94E-7
			1.04E+6	4.81E-5	3.09E-6	1.03E+6	1.59E-5	8.91E-7	1.03E+6	3.58E-6	2.84E-7

Table 3.1.2.1 (Continued-2)

553mm			711 mm			914 mm		
Neutron Energy [eV]	Flux [n/leth/ source]	Absolute Error	Neutron Energy [eV]	Flux [n/leth/ source]	Absolute Error	Neutron Energy [eV]	Flux [n/leth/ source]	Absolute Error
2.98E+3	9.84E-7	3.65E-7	3.02E+3	3.50E-7	1.38E-7	3.02E+3	1.03E-7	3.62E-8
3.10E+3	1.24E-6	3.52E-7	3.15E+3	2.31E-7	1.31E-7	3.15E+3	1.44E-7	3.41E-8
3.24E+3	6.80E-7	3.37E-7	3.28E+3	4.07E-7	1.26E-7	3.28E+3	1.41E-7	3.26E-8
3.38E+3	9.28E-7	3.24E-7	3.43E+3	4.71E-7	1.22E-7	3.43E+3	9.13E-8	3.13E-8
3.53E+3	1.97E-6	3.12E-7	3.58E+3	4.42E-7	1.17E-7	3.58E+3	9.47E-8	3.03E-8
3.68E+3	9.34E-7	3.02E-7	3.74E+3	4.48E-7	1.13E-7	3.74E+3	1.00E-7	2.97E-8
3.84E+3	8.54E-7	2.93E-7	3.90E+3	4.35E-7	1.10E-7	3.90E+3	9.69E-8	2.89E-8
4.01E+3	1.21E-6	2.85E-7	4.07E+3	2.25E-7	1.08E-7	4.07E+3	1.06E-7	2.80E-8
4.19E+3	9.35E-7	2.79E-7	4.25E+3	3.64E-7	1.05E-7	4.25E+3	1.29E-7	2.73E-8
4.38E+3	7.45E-7	2.73E-7	4.44E+3	6.18E-7	1.03E-7	4.44E+3	8.08E-8	2.66E-8
4.58E+3	9.86E-7	2.69E-7	4.64E+3	3.81E-7	1.01E-7	4.64E+3	7.74E-8	2.64E-8
4.78E+3	8.22E-7	2.65E-7	4.85E+3	1.56E-7	9.97E-8	4.85E+3	1.16E-7	2.59E-8
5.00E+3	1.48E-6	2.59E-7	5.07E+3	4.10E-7	9.86E-8	5.07E+3	1.18E-7	2.55E-8
5.22E+3	1.04E-6	2.55E-7	5.30E+3	4.33E-7	9.67E-8	5.30E+3	1.43E-7	2.47E-8
5.46E+3	3.82E-7	2.51E-7	5.54E+3	4.81E-7	9.53E-8	5.54E+3	1.08E-7	2.45E-8
5.70E+3	1.27E-6	2.51E-7	5.79E+3	3.58E-7	9.43E-8	5.79E+3	4.87E-8	2.41E-8
5.96E+3	1.22E-6	2.47E-7	6.05E+3	4.19E-7	9.33E-8	6.05E+3	1.09E-7	2.40E-8
6.24E+3	1.03E-6	2.45E-7	6.33E+3	5.66E-7	9.20E-8	6.33E+3	1.25E-7	2.39E-8
6.52E+3	7.42E-7	2.44E-7	6.62E+3	3.63E-7	9.09E-8	6.62E+3	1.21E-7	2.35E-8
6.82E+3	1.03E-6	2.44E-7	6.92E+3	3.74E-7	9.03E-8	6.92E+3	1.15E-7	2.34E-8
7.13E+3	1.34E-6	2.41E-7	7.24E+3	3.83E-7	8.94E-8	7.24E+3	6.92E-8	2.32E-8
7.46E+3	1.24E-6	2.39E-7	7.57E+3	4.62E-7	8.90E-8	7.57E+3	8.54E-8	2.32E-8
7.80E+3	9.97E-7	2.37E-7	7.92E+3	2.38E-7	8.88E-8	7.92E+3	1.26E-7	2.31E-8
8.16E+3	7.83E-7	2.37E-7	8.29E+3	4.36E-7	8.88E-8	8.29E+3	1.31E-7	2.30E-8
8.54E+3	1.05E-6	2.39E-7	8.67E+3	6.34E-7	8.98E-8	8.67E+3	1.01E-7	2.32E-8
8.93E+3	1.61E-6	2.42E-7	9.07E+3	4.52E-7	9.01E-8	9.07E+3	1.60E-7	2.32E-8
9.35E+3	1.42E-6	2.44E-7	9.49E+3	6.19E-7	9.09E-8	9.49E+3	2.18E-7	2.35E-8
9.78E+3	2.06E-6	2.46E-7	9.93E+3	7.23E-7	9.13E-8	9.93E+3	1.93E-7	2.34E-8
1.02E+4	2.52E-6	2.47E-7	1.04E+4	8.63E-7	9.17E-8	1.04E+4	1.78E-7	2.36E-8
1.07E+4	2.48E-6	2.46E-7	1.09E+4	9.58E-7	9.19E-8	1.09E+4	2.29E-7	2.36E-8
1.12E+4	2.54E-6	2.47E-7	1.14E+4	8.65E-7	9.17E-8	1.14E+4	2.34E-7	2.37E-8
1.17E+4	1.95E-6	2.47E-7	1.19E+4	7.30E-7	9.23E-8	1.19E+4	2.34E-7	2.36E-8
1.23E+4	2.22E-6	2.49E-7	1.25E+4	7.85E-7	9.23E-8	1.25E+4	2.01E-7	2.37E-8
1.29E+4	1.87E-6	2.51E-7	1.31E+4	8.32E-7	9.33E-8	1.31E+4	2.08E-7	2.37E-8
1.35E+4	1.95E-6	2.53E-7	1.37E+4	6.29E-7	9.33E-8	1.37E+4	1.91E-7	2.39E-8
1.41E+4	2.28E-6	2.55E-7	1.43E+4	7.88E-7	9.38E-8	1.43E+4	1.57E-7	2.40E-8
1.48E+4	1.68E-6	2.56E-7	1.50E+4	7.25E-7	9.46E-8	1.50E+4	2.21E-7	2.41E-8
1.55E+4	2.11E-6	2.59E-7	1.57E+4	6.45E-7	9.52E-8	1.57E+4	1.80E-7	2.44E-8
1.62E+4	1.87E-6	2.61E-7	1.64E+4	6.86E-7	9.62E-8	1.64E+4	8.48E-8	2.46E-8
1.69E+4	1.30E-6	2.65E-7	1.72E+4	6.61E-7	9.71E-8	1.72E+4	1.92E-7	2.50E-8
1.77E+4	2.03E-6	2.68E-7	1.80E+4	8.20E-7	9.80E-8	1.80E+4	2.36E-7	2.50E-8
1.86E+4	2.73E-6	2.70E-7	1.89E+4	8.46E-7	9.87E-8	1.89E+4	3.19E-7	2.51E-8
1.95E+4	3.35E-6	2.70E-7	1.98E+4	1.17E-6	9.89E-8	1.98E+4	3.52E-7	2.49E-8
2.04E+4	3.70E-6	2.70E-7	2.07E+4	1.27E-6	9.90E-8	2.07E+4	3.19E-7	2.47E-8
2.13E+4	3.86E-6	2.69E-7	2.17E+4	1.45E-6	9.78E-8	2.17E+4	3.44E-7	2.46E-8
2.24E+4	4.42E-6	2.68E-7	2.27E+4	1.85E-6	9.71E-8	2.27E+4	4.24E-7	2.44E-8
2.34E+4	5.01E-6	2.65E-7	2.38E+4	1.94E-6	9.52E-8	2.38E+4	5.04E-7	2.39E-8
2.45E+4	5.34E-6	2.61E-7	2.49E+4	1.86E-6	9.29E-8	2.49E+4	4.84E-7	2.34E-8
2.57E+4	4.96E-6	2.56E-7	2.61E+4	1.65E-6	9.13E-8	2.61E+4	4.42E-7	2.27E-8
2.69E+4	4.02E-6	2.53E-7	2.73E+4	1.18E-6	9.05E-8	2.73E+4	2.77E-7	2.26E-8
2.82E+4	2.55E-6	2.54E-7	2.86E+4	6.07E-7	9.08E-8	2.86E+4	1.55E-7	2.26E-8
2.95E+4	8.04E-7	2.58E-7	3.00E+4	5.37E-7	9.13E-8	3.00E+4	1.21E-7	2.29E-8
3.09E+4	1.15E-6	2.60E-7	3.14E+4	4.08E-7	9.33E-8	3.14E+4	9.23E-8	2.32E-8
3.24E+4	1.68E-6	2.66E-7	3.29E+4	4.89E-7	9.44E-8	3.29E+4	1.16E-7	2.36E-8
3.39E+4	1.26E-6	2.70E-7	3.45E+4	6.21E-7	9.62E-8	3.45E+4	1.74E-7	2.40E-8
3.55E+4	2.14E-6	2.73E-7	3.61E+4	5.89E-7	9.75E-8	3.61E+4	1.56E-7	2.41E-8
3.72E+4	2.30E-6	2.78E-7	3.78E+4	7.41E-7	9.89E-8	3.78E+4	2.33E-7	2.44E-8
3.90E+4	2.53E-6	2.82E-7	3.96E+4	9.90E-7	9.99E-8	3.96E+4	2.42E-7	2.46E-8
4.09E+4	3.21E-6	2.83E-7	4.15E+4	1.23E-6	1.00E-7	4.15E+4	2.76E-7	2.46E-8
4.28E+4	3.77E-6	2.87E-7	4.35E+4	1.34E-6	9.99E-8	4.35E+4	2.88E-7	2.47E-8
4.48E+4	3.75E-6	2.85E-7	4.55E+4	1.36E-6	9.99E-8	4.55E+4	3.21E-7	2.47E-8
4.70E+4	3.96E-6	2.88E-7	4.77E+4	1.30E-6	9.99E-8	4.77E+4	3.69E-7	2.47E-8
4.92E+4	3.37E-6	2.88E-7	5.00E+4	1.06E-6	1.00E-7	5.00E+4	3.27E-7	2.45E-8
5.16E+4	3.35E-6	2.90E-7	5.24E+4	1.11E-6	1.01E-7	5.24E+4	2.79E-7	2.46E-8
5.40E+4	3.47E-6	2.92E-7	5.49E+4	1.07E-6	1.02E-7	5.49E+4	2.31E-7	2.46E-8
5.66E+4	3.63E-6	2.94E-7	5.75E+4	1.21E-6	1.02E-7	5.75E+4	3.10E-7	2.49E-8

Table 3.1.2.1 (Continued-3)

553mm			711 mm			914 mm		
Neutron Energy [eV]	Flux [n/leth/ source]	Absolute Error	Neutron Energy [eV]	Flux [n/leth/ source]	Absolute Error	Neutron Energy [eV]	Flux [n/leth/ source]	Absolute Error
5.93E+4	3.97E-6	2.95E-7	6.02E+4	1.50E-6	1.02E-7	6.02E+4	3.25E-7	2.47E-8
6.21E+4	4.35E-6	2.97E-7	6.31E+4	1.37E-6	1.02E-7	6.31E+4	3.37E-7	2.47E-8
6.51E+4	4.63E-6	2.98E-7	6.61E+4	1.37E-6	1.02E-7	6.61E+4	3.46E-7	2.47E-8
6.82E+4	4.25E-6	2.97E-7	6.93E+4	1.44E-6	1.02E-7	6.93E+4	3.52E-7	2.46E-8
7.15E+4	4.60E-6	2.97E-7	7.26E+4	1.69E-6	1.02E-7	7.26E+4	3.98E-7	2.45E-8
7.49E+4	4.85E-6	2.98E-7	7.61E+4	1.53E-6	1.01E-7	7.61E+4	3.72E-7	2.42E-8
7.85E+4	4.98E-6	2.98E-7	7.97E+4	1.74E-6	1.00E-7	7.97E+4	4.02E-7	2.40E-8
8.22E+4	5.39E-6	2.95E-7	8.35E+4	1.85E-6	9.92E-8	8.35E+4	4.11E-7	2.36E-8
8.62E+4	5.13E-6	2.94E-7	8.75E+4	1.31E-6	9.86E-8	8.75E+4	3.58E-7	2.35E-8
9.03E+4	3.89E-6	2.95E-7	9.17E+4	1.13E-6	9.90E-8	9.17E+4	2.81E-7	2.32E-8
9.46E+4	3.47E-6	2.97E-7	9.61E+4	1.03E-6	9.95E-8	9.61E+4	2.71E-7	2.34E-8
9.91E+4	3.30E-6	3.00E-7	1.01E+5	1.19E-6	1.00E-7	1.01E+5	2.54E-7	2.34E-8
1.04E+5	3.67E-6	3.04E-7	1.06E+5	1.27E-6	1.01E-7	1.06E+5	2.81E-7	2.35E-8
1.09E+5	4.44E-6	3.04E-7	1.11E+5	1.49E-6	1.00E-7	1.11E+5	3.44E-7	2.32E-8
1.14E+5	5.97E-6	3.04E-7	1.16E+5	1.78E-6	9.95E-8	1.16E+5	4.06E-7	2.31E-8
1.20E+5	6.43E-6	3.02E-7	1.21E+5	2.17E-6	9.80E-8	1.21E+5	4.64E-7	2.27E-8
1.25E+5	7.50E-6	3.02E-7	1.27E+5	2.28E-6	9.68E-8	1.27E+5	5.42E-7	2.22E-8
1.31E+5	7.81E-6	2.97E-7	1.33E+5	2.19E-6	9.49E-8	1.33E+5	5.03E-7	2.17E-8
1.38E+5	6.27E-6	2.97E-7	1.40E+5	1.75E-6	9.44E-8	1.40E+5	3.33E-7	2.13E-8
1.44E+5	4.47E-6	2.98E-7	1.46E+5	1.13E-6	9.44E-8	1.46E+5	2.52E-7	2.13E-8
1.51E+5	3.33E-6	3.06E-7	1.51E+5	1.29E-6	6.36E-8	1.53E+5	2.28E-7	2.15E-8
1.58E+5	3.99E-6	2.10E-7	1.58E+5	1.06E-6	6.14E-8	1.55E+5	2.65E-7	1.35E-8
1.65E+5	4.70E-6	2.02E-7	1.65E+5	1.22E-6	5.91E-8	1.63E+5	2.76E-7	1.30E-8
1.73E+5	5.15E-6	1.96E-7	1.73E+5	1.42E-6	5.71E-8	1.71E+5	2.72E-7	1.24E-8
1.81E+5	5.28E-6	1.88E-7	1.81E+5	1.42E-6	5.49E-8	1.79E+5	3.00E-7	1.19E-8
1.90E+5	4.00E-6	1.84E-7	1.90E+5	1.09E-6	5.28E-8	1.87E+5	2.48E-7	1.14E-8
1.99E+5	3.45E-6	1.79E-7	1.99E+5	9.67E-7	5.13E-8	1.96E+5	2.02E-7	1.10E-8
2.09E+5	4.47E-6	1.75E-7	2.09E+5	1.17E-6	5.01E-8	2.06E+5	2.08E-7	1.08E-8
2.19E+5	4.44E-6	1.72E-7	2.19E+5	1.26E-6	4.84E-8	2.15E+5	2.28E-7	1.04E-8
2.29E+5	4.56E-6	1.67E-7	2.29E+5	1.08E-6	4.68E-8	2.26E+5	2.45E-7	1.00E-8
2.40E+5	4.77E-6	1.63E-7	2.40E+5	1.21E-6	4.52E-8	2.37E+5	2.39E-7	9.63E-9
2.52E+5	5.25E-6	1.57E-7	2.52E+5	1.41E-6	4.33E-8	2.48E+5	2.51E-7	9.24E-9
2.64E+5	5.91E-6	1.51E-7	2.64E+5	1.49E-6	4.12E-8	2.60E+5	2.75E-7	8.77E-9
2.77E+5	5.56E-6	1.44E-7	2.77E+5	1.36E-6	3.90E-8	2.72E+5	2.88E-7	8.23E-9
2.90E+5	5.61E-6	1.38E-7	2.90E+5	1.27E-6	3.67E-8	2.85E+5	2.60E-7	7.70E-9
3.04E+5	5.82E-6	1.30E-7	3.04E+5	1.43E-6	3.45E-8	2.99E+5	2.51E-7	7.11E-9
3.18E+5	4.85E-6	1.24E-7	3.18E+5	1.14E-6	3.21E-8	3.13E+5	2.25E-7	6.63E-9
3.34E+5	4.02E-6	1.17E-7	3.34E+5	8.44E-7	3.02E-8	3.28E+5	1.64E-7	6.12E-9
3.50E+5	4.12E-6	1.13E-7	3.50E+5	8.81E-7	2.85E-8	3.44E+5	1.46E-7	5.76E-9
3.66E+5	3.69E-6	1.09E-7	3.66E+5	8.23E-7	2.73E-8	3.61E+5	1.44E-7	5.49E-9
3.84E+5	3.20E-6	1.05E-7	3.84E+5	6.15E-7	2.59E-8	3.78E+5	1.14E-7	5.20E-9
4.02E+5	2.47E-6	1.02E-7	4.02E+5	4.47E-7	2.52E-8	3.96E+5	8.62E-8	4.99E-9
4.22E+5	2.12E-6	1.00E-7	4.22E+5	3.85E-7	2.45E-8	4.15E+5	7.52E-8	4.82E-9
4.42E+5	2.46E-6	9.82E-8	4.42E+5	4.67E-7	2.40E-8	4.35E+5	7.05E-8	4.67E-9
4.63E+5	2.51E-6	9.62E-8	4.63E+5	4.95E-7	2.34E-8	4.56E+5	7.32E-8	4.52E-9
4.85E+5	2.50E-6	9.33E-8	4.85E+5	4.76E-7	2.23E-8	4.78E+5	7.41E-8	4.34E-9
5.08E+5	2.49E-6	9.13E-8	5.08E+5	4.64E-7	2.16E-8	5.01E+5	7.33E-8	4.23E-9
5.33E+5	2.56E-6	8.90E-8	5.33E+5	4.59E-7	2.08E-8	5.25E+5	7.36E-8	4.01E-9
5.58E+5	2.59E-6	8.57E-8	5.58E+5	4.27E-7	1.98E-8	5.50E+5	6.95E-8	3.84E-9
5.85E+5	2.57E-6	8.17E-8	5.85E+5	3.99E-7	1.89E-8	5.76E+5	5.53E-8	3.69E-9
6.13E+5	2.32E-6	7.69E-8	6.13E+5	4.16E-7	1.74E-8	6.04E+5	5.71E-8	3.38E-9
6.43E+5	1.99E-6	7.21E-8	6.43E+5	3.52E-7	1.62E-8	6.33E+5	7.17E-8	3.17E-9
6.73E+5	1.59E-6	6.72E-8	6.73E+5	2.48E-7	1.45E-8	6.63E+5	4.45E-8	2.78E-9
7.06E+5	1.20E-6	6.39E-8	7.06E+5	1.82E-7	1.35E-8	6.95E+5	2.73E-8	2.49E-9
7.40E+5	8.76E-7	6.10E-8	7.40E+5	1.24E-7	1.26E-8	7.28E+5	2.05E-8	2.34E-9
7.75E+5	7.98E-7	5.92E-8	7.75E+5	9.31E-8	1.21E-8	7.63E+5	1.45E-8	2.22E-9
8.12E+5	7.13E-7	5.82E-8	8.12E+5	9.71E-8	1.16E-8	8.00E+5	1.15E-8	2.11E-9
8.51E+5	5.47E-7	5.56E-8	8.51E+5	9.03E-8	1.10E-8	8.38E+5	1.38E-8	2.07E-9
8.92E+5	7.37E-7	5.44E-8	8.92E+5	8.45E-8	1.03E-8	8.78E+5	1.24E-8	1.93E-9
9.35E+5	6.75E-7	5.08E-8	9.35E+5	6.58E-8	9.81E-9	9.20E+5	1.08E-8	1.75E-9
9.80E+5	4.43E-7	4.78E-8	9.80E+5	5.67E-8	8.69E-9	9.65E+5	8.62E-9	1.64E-9
1.03E+6	3.90E-7	4.54E-8	1.03E+6	4.36E-8	8.71E-9	1.01E+6	4.44E-9	1.52E-9

Table 3.1.2.2 Neutron spectra at -10, 102, 228, 356, 553, 711 and 914 mm from the front surface of the test region in the assembly #2 measured by the proton-recoil gas proportional counters.

-10 mm			102 mm			228 mm			356 mm		
Neutron Energy [eV]	Flux [n/leth/ source]	Absolute Error	Neutron Energy [eV]	Flux [n/leth/ source]	Absolute Error	Neutron Energy [eV]	Flux [n/leth/ source]	Absolute Error	Neutron Energy [eV]	Flux [n/leth/ source]	Absolute Error
3.02E+3	1.20E-5	4.92E-6	3.02E+3	4.83E-6	3.74E-6	2.98E+3	4.66E-6	2.36E-6	3.02E+3	4.93E-6	1.28E-6
3.15E+3	1.06E-5	4.67E-6	3.15E+3	1.15E-5	3.57E-6	3.10E+3	8.53E-6	2.26E-6	3.15E+3	6.45E-6	1.22E-6
3.28E+3	9.12E-6	4.47E-6	3.28E+3	1.27E-5	3.42E-6	3.24E+3	7.28E-6	2.16E-6	3.28E+3	4.20E-6	1.16E-6
3.43E+3	8.59E-6	4.32E-6	3.43E+3	1.17E-5	3.30E-6	3.38E+3	6.22E-6	2.10E-6	3.43E+3	4.39E-6	1.12E-6
3.58E+3	1.53E-5	4.18E-6	3.58E+3	1.07E-5	3.17E-6	3.53E+3	8.09E-6	2.01E-6	3.58E+3	5.55E-6	1.08E-6
3.74E+3	9.79E-6	3.98E-6	3.74E+3	9.00E-6	3.07E-6	3.68E+3	8.69E-6	1.96E-6	3.74E+3	4.51E-6	1.05E-6
3.90E+3	-5.42E-6	3.95E-6	3.90E+3	5.18E-6	3.00E-6	3.84E+3	5.88E-6	1.89E-6	3.90E+3	4.81E-6	1.02E-6
4.07E+3	9.13E-6	3.86E-6	4.07E+3	1.17E-5	2.95E-6	4.01E+3	6.95E-6	1.86E-6	4.07E+3	4.13E-6	9.90E-7
4.25E+3	1.14E-5	3.80E-6	4.25E+3	1.09E-5	2.88E-6	4.19E+3	9.47E-6	1.79E-6	4.25E+3	3.67E-6	9.75E-7
4.44E+3	1.40E-5	3.69E-6	4.44E+3	6.26E-6	2.80E-6	4.38E+3	6.94E-6	1.75E-6	4.44E+3	4.61E-6	9.51E-7
4.64E+3	1.17E-5	3.60E-6	4.64E+3	1.03E-5	2.78E-6	4.58E+3	5.08E-6	1.73E-6	4.64E+3	4.10E-6	9.39E-7
4.85E+3	3.76E-6	3.56E-6	4.85E+3	1.20E-5	2.71E-6	4.78E+3	7.50E-6	1.70E-6	4.85E+3	4.52E-6	9.19E-7
5.07E+3	8.34E-6	3.46E-6	5.07E+3	9.45E-6	2.66E-6	5.00E+3	5.00E-6	1.69E-6	5.07E+3	4.87E-6	9.05E-7
5.30E+3	1.64E-5	3.43E-6	5.30E+3	7.13E-6	2.64E-6	5.22E+3	4.00E-6	1.65E-6	5.30E+3	4.84E-6	8.95E-7
5.54E+3	2.71E-6	3.38E-6	5.54E+3	8.90E-6	2.61E-6	5.46E+3	8.33E-6	1.64E-6	5.54E+3	3.77E-6	8.85E-7
5.79E+3	6.88E-6	3.35E-6	5.79E+3	9.40E-6	2.59E-6	5.70E+3	7.34E-6	1.63E-6	5.79E+3	3.26E-6	8.76E-7
6.05E+3	1.42E-5	3.33E-6	6.05E+3	6.87E-6	2.58E-6	5.96E+3	7.55E-6	1.60E-6	6.05E+3	4.01E-6	8.70E-7
6.33E+3	8.29E-6	3.27E-6	6.33E+3	1.15E-5	2.55E-6	6.24E+3	7.96E-6	1.59E-6	6.33E+3	6.21E-6	8.62E-7
6.62E+3	6.99E-6	3.28E-6	6.62E+3	8.59E-6	2.54E-6	6.52E+3	7.26E-6	1.58E-6	6.62E+3	4.50E-6	8.55E-7
6.92E+3	5.02E-6	3.24E-6	6.92E+3	8.18E-6	2.52E-6	6.82E+3	4.21E-6	1.58E-6	6.92E+3	4.69E-6	8.45E-7
7.24E+3	8.92E-6	3.23E-6	7.24E+3	1.62E-5	2.50E-6	7.13E+3	8.09E-6	1.57E-6	7.24E+3	5.05E-6	8.42E-7
7.57E+3	1.25E-5	3.22E-6	7.57E+3	6.76E-6	2.49E-6	7.46E+3	9.15E-6	1.55E-6	7.57E+3	4.15E-6	8.31E-7
7.92E+3	1.08E-5	3.19E-6	7.92E+3	6.44E-6	2.49E-6	7.80E+3	6.38E-6	1.55E-6	7.92E+3	2.93E-6	8.37E-7
8.29E+3	7.99E-6	3.21E-6	8.29E+3	9.88E-6	2.50E-6	8.16E+3	5.72E-6	1.55E-6	8.29E+3	3.78E-6	8.38E-7
8.67E+3	9.56E-6	3.21E-6	8.67E+3	1.24E-5	2.52E-6	8.54E+3	8.63E-6	1.57E-6	8.67E+3	6.95E-6	8.48E-7
9.07E+3	1.37E-5	3.26E-6	9.07E+3	1.53E-5	2.54E-6	8.93E+3	9.82E-6	1.58E-6	9.07E+3	6.80E-6	8.53E-7
9.49E+3	1.43E-5	3.28E-6	9.49E+3	1.74E-5	2.56E-6	9.35E+3	1.25E-5	1.60E-6	9.49E+3	8.05E-6	8.61E-7
9.93E+3	1.61E-5	3.31E-6	9.93E+3	2.06E-5	2.59E-6	9.78E+3	1.52E-5	1.60E-6	9.93E+3	9.89E-6	8.62E-7
1.04E+4	1.74E-5	3.33E-6	1.04E+4	2.13E-5	2.59E-6	1.02E+4	1.52E-5	1.62E-6	1.04E+4	1.13E-5	8.66E-7
1.09E+4	1.84E-5	3.35E-6	1.09E+4	2.23E-5	2.60E-6	1.07E+4	1.63E-5	1.62E-6	1.09E+4	9.16E-6	8.67E-7
1.14E+4	2.13E-5	3.35E-6	1.14E+4	2.17E-5	2.61E-6	1.12E+4	1.86E-5	1.63E-6	1.14E+4	8.85E-6	8.71E-7
1.19E+4	2.02E-5	3.36E-6	1.19E+4	2.11E-5	2.63E-6	1.17E+4	1.64E-5	1.63E-6	1.19E+4	9.20E-6	8.74E-7
1.25E+4	1.44E-5	3.37E-6	1.25E+4	1.56E-5	2.65E-6	1.23E+4	1.52E-5	1.63E-6	1.25E+4	8.12E-6	8.84E-7
1.31E+4	1.86E-5	3.41E-6	1.31E+4	1.89E-5	2.66E-6	1.29E+4	1.29E-5	1.64E-6	1.31E+4	8.51E-6	8.88E-7
1.37E+4	1.33E-5	3.43E-6	1.37E+4	2.09E-5	2.70E-6	1.35E+4	1.43E-5	1.67E-6	1.37E+4	9.82E-6	8.93E-7
1.43E+4	1.37E-5	3.46E-6	1.43E+4	1.73E-5	2.70E-6	1.41E+4	1.30E-5	1.68E-6	1.43E+4	1.02E-5	8.98E-7
1.50E+4	1.87E-5	3.50E-6	1.50E+4	1.39E-5	2.75E-6	1.48E+4	9.61E-6	1.69E-6	1.50E+4	5.75E-6	9.06E-7
1.57E+4	9.82E-6	3.53E-6	1.57E+4	1.77E-5	2.78E-6	1.55E+4	1.20E-5	1.72E-6	1.57E+4	5.77E-6	9.18E-7
1.64E+4	1.46E-5	3.57E-6	1.64E+4	1.81E-5	2.82E-6	1.62E+4	1.63E-5	1.73E-6	1.64E+4	9.16E-6	9.30E-7
1.72E+4	1.80E-5	3.62E-6	1.72E+4	1.81E-5	2.84E-6	1.69E+4	1.40E-5	1.75E-6	1.72E+4	1.03E-5	9.38E-7
1.80E+4	1.55E-5	3.66E-6	1.80E+4	2.32E-5	2.87E-6	1.77E+4	1.30E-5	1.77E-6	1.80E+4	1.06E-5	9.46E-7
1.89E+4	2.20E-5	3.69E-6	1.89E+4	2.59E-5	2.90E-6	1.86E+4	1.96E-5	1.79E-6	1.89E+4	1.12E-5	9.51E-7
1.98E+4	2.34E-5	3.74E-6	1.98E+4	2.86E-5	2.92E-6	1.95E+4	2.28E-5	1.81E-6	1.98E+4	1.44E-5	9.54E-7
2.07E+4	2.27E-5	3.75E-6	2.07E+4	2.87E-5	2.93E-6	2.04E+4	2.31E-5	1.79E-6	2.07E+4	1.55E-5	9.57E-7
2.17E+4	2.91E-5	3.76E-6	2.17E+4	3.35E-5	2.95E-6	2.13E+4	2.68E-5	1.81E-6	2.17E+4	1.73E-5	9.52E-7
2.27E+4	3.36E-5	3.76E-6	2.27E+4	4.67E-5	2.94E-6	2.24E+4	3.19E-5	1.79E-6	2.27E+4	2.09E-5	9.43E-7
2.38E+4	4.20E-5	3.75E-6	2.38E+4	4.87E-5	2.93E-6	2.34E+4	3.52E-5	1.78E-6	2.38E+4	2.25E-5	9.34E-7
2.49E+4	3.99E-5	3.72E-6	2.49E+4	4.90E-5	2.89E-6	2.45E+4	3.65E-5	1.75E-6	2.49E+4	2.25E-5	9.20E-7
2.61E+4	3.26E-5	3.70E-6	2.61E+4	4.34E-5	2.88E-6	2.57E+4	3.44E-5	1.75E-6	2.61E+4	1.92E-5	9.09E-7
2.73E+4	2.63E-5	3.72E-6	2.73E+4	2.56E-5	2.89E-6	2.69E+4	2.70E-5	1.74E-6	2.73E+4	1.19E-5	9.09E-7
2.86E+4	1.17E-5	3.75E-6	2.86E+4	1.79E-5	2.92E-6	2.82E+4	1.40E-5	1.75E-6	2.86E+4	7.42E-6	9.14E-7
3.00E+4	1.35E-5	3.83E-6	3.00E+4	1.02E-5	2.98E-6	2.95E+4	8.37E-6	1.77E-6	3.00E+4	5.30E-6	9.29E-7
3.14E+4	1.63E-5	3.89E-6	3.14E+4	1.16E-5	3.03E-6	3.09E+4	8.78E-6	1.81E-6	3.14E+4	5.34E-6	9.46E-7
3.29E+4	1.35E-5	3.95E-6	3.29E+4	1.83E-5	3.08E-6	3.24E+4	6.37E-6	1.84E-6	3.29E+4	6.85E-6	9.65E-7
3.45E+4	1.38E-5	4.03E-6	3.45E+4	1.94E-5	3.14E-6	3.39E+4	1.21E-5	1.88E-6	3.45E+4	8.00E-6	9.78E-7
3.61E+4	1.94E-5	4.12E-6	3.61E+4	2.72E-5	3.18E-6	3.55E+4	1.71E-5	1.92E-6	3.61E+4	9.50E-6	9.89E-7
3.78E+4	1.97E-5	4.17E-6	3.78E+4	2.59E-5	3.23E-6	3.72E+4	1.98E-5	1.93E-6	3.78E+4	1.09E-5	1.00E-6
3.96E+4	2.61E-5	4.22E-6	3.96E+4	2.79E-5	3.27E-6	3.90E+4	2.38E-5	1.96E-6	3.96E+4	1.26E-5	1.01E-6
4.15E+4	3.14E-5	4.27E-6	4.15E+4	3.13E-5	3.31E-6	4.09E+4	2.29E-5	1.98E-6	4.15E+4	1.44E-5	1.02E-6
4.35E+4	2.57E-5	4.32E-6	4.35E+4	4.02E-5	3.36E-6	4.28E+4	2.50E-5	1.99E-6	4.35E+4	1.76E-5	1.03E-6
4.55E+4	3.33E-5	4.36E-6	4.55E+4	4.09E-5	3.38E-6	4.48E+4	2.76E-5	2.01E-6	4.55E+4	1.75E-5	1.03E-6
4.77E+4	3.63E-5	4.42E-6	4.77E+4	3.90E-5	3.41E-6	4.70E+4	2.93E-5	2.03E-6	4.77E+4	1.63E-5	1.03E-6
5.00E+4	3.21E-5	4.43E-6	5.00E+4	3.79E-5	3.45E-6	4.92E+4	2.61E-5	2.03E-6	5.00E+4	1.40E-5	1.04E-6
5.24E+4	2.93E-5	4.49E-6	5.24E+4	3.87E-5	3.48E-6	5.16E+4	2.58E-5	2.06E-6	5.24E+4	1.45E-5	1.05E-6
5.49E+4	2.25E-5	4.56E-6	5.49E+4	3.72E-5	3.51E-6	5.40E+4	2.45E-5	2.08E-6	5.49E+4	1.54E-5	1.06E-6
5.75E+4	3.68E-5	4.65E-6	5.75E+4	4.21E-5	3.56E-6	5.66E+4	2.83E-5	2.10E-6	5.75E+4	1.71E-5	1.07E-6

Table 3.1.2.2 (Continued-1)

-10 mm			102 mm			228 mm			356 mm		
Neutron Energy [eV]	Flux [n/leth/ source]	Absolute Error	Neutron Energy [eV]	Flux [n/leth/ source]	Absolute Error	Neutron Energy [eV]	Flux [n/leth/ source]	Absolute Error	Neutron Energy [eV]	Flux [n/leth/ source]	Absolute Error
6.02E+4	4.03E-5	4.70E-6	6.02E+4	4.55E-5	3.60E-6	5.93E+4	3.34E-5	2.12E-6	6.02E+4	1.97E-5	1.07E-6
6.31E+4	4.22E-5	4.75E-6	6.31E+4	4.76E-5	3.62E-6	6.21E+4	3.16E-5	2.13E-6	6.31E+4	1.89E-5	1.08E-6
6.61E+4	4.19E-5	4.78E-6	6.61E+4	4.31E-5	3.67E-6	6.51E+4	3.05E-5	2.15E-6	6.61E+4	1.84E-5	1.08E-6
6.93E+4	4.08E-5	4.84E-6	6.93E+4	4.37E-5	3.71E-6	6.82E+4	3.25E-5	2.17E-6	6.93E+4	1.93E-5	1.09E-6
7.26E+4	3.83E-5	4.91E-6	7.26E+4	5.51E-5	3.75E-6	7.15E+4	3.61E-5	2.18E-6	7.26E+4	2.16E-5	1.09E-6
7.61E+4	4.67E-5	4.96E-6	7.61E+4	5.38E-5	3.79E-6	7.49E+4	4.17E-5	2.20E-6	7.61E+4	2.17E-5	1.09E-6
7.97E+4	5.81E-5	5.00E-6	7.97E+4	6.02E-5	3.80E-6	7.85E+4	4.39E-5	2.20E-6	7.97E+4	2.35E-5	1.09E-6
8.35E+4	5.11E-5	5.02E-6	8.35E+4	6.47E-5	3.84E-6	8.22E+4	4.30E-5	2.20E-6	8.35E+4	2.33E-5	1.09E-6
8.75E+4	5.04E-5	5.08E-6	8.75E+4	5.15E-5	3.86E-6	8.62E+4	3.51E-5	2.21E-6	8.75E+4	2.03E-5	1.09E-6
9.17E+4	4.25E-5	5.11E-6	9.17E+4	4.75E-5	3.91E-6	9.03E+4	3.28E-5	2.22E-6	9.17E+4	1.71E-5	1.09E-6
9.61E+4	2.68E-5	5.24E-6	9.61E+4	4.66E-5	3.96E-6	9.46E+4	3.04E-5	2.25E-6	9.61E+4	1.64E-5	1.11E-6
1.01E+5	3.33E-5	5.32E-6	1.01E+5	4.90E-5	4.01E-6	9.91E+4	2.53E-5	2.29E-6	1.01E+5	1.55E-5	1.12E-6
1.06E+5	5.06E-5	5.40E-6	1.06E+5	5.26E-5	4.08E-6	1.04E+5	3.30E-5	2.30E-6	1.06E+5	1.93E-5	1.13E-6
1.11E+5	5.30E-5	5.49E-6	1.11E+5	5.76E-5	4.13E-6	1.09E+5	4.21E-5	2.34E-6	1.11E+5	2.47E-5	1.13E-6
1.16E+5	6.14E-5	5.54E-6	1.16E+5	7.08E-5	4.18E-6	1.14E+5	4.82E-5	2.35E-6	1.16E+5	2.72E-5	1.13E-6
1.21E+5	8.23E-5	5.62E-6	1.21E+5	9.77E-5	4.19E-6	1.20E+5	5.56E-5	2.35E-6	1.21E+5	3.18E-5	1.12E-6
1.27E+5	8.81E-5	5.68E-6	1.27E+5	1.02E-4	4.24E-6	1.25E+5	6.80E-5	2.35E-6	1.27E+5	3.69E-5	1.12E-6
1.33E+5	8.41E-5	5.79E-6	1.33E+5	9.38E-5	4.29E-6	1.31E+5	6.48E-5	2.37E-6	1.33E+5	3.17E-5	1.12E-6
1.40E+5	6.91E-5	5.92E-6	1.40E+5	7.00E-5	4.37E-6	1.38E+5	5.13E-5	2.39E-6	1.40E+5	2.46E-5	1.13E-6
1.46E+5	5.92E-5	6.07E-6	1.46E+5	5.80E-5	4.51E-6	1.44E+5	3.91E-5	2.44E-6	1.46E+5	1.74E-5	1.15E-6
1.53E+5	5.24E-5	6.30E-6	1.53E+5	6.13E-5	4.65E-6	1.51E+5	3.74E-5	2.50E-6	1.53E+5	1.81E-5	1.18E-6
1.55E+5	7.07E-5	4.84E-6	1.61E+5	7.00E-5	4.78E-6	1.55E+5	3.68E-5	2.02E-6	1.55E+5	1.83E-5	9.14E-7
1.63E+5	6.66E-5	4.73E-6	1.63E+5	7.38E-5	3.94E-6	1.63E+5	4.11E-5	1.98E-6	1.63E+5	2.04E-5	8.89E-7
1.71E+5	6.90E-5	4.66E-6	1.71E+5	6.94E-5	3.86E-6	1.71E+5	4.62E-5	1.93E-6	1.71E+5	2.25E-5	8.66E-7
1.79E+5	7.49E-5	4.60E-6	1.79E+5	8.21E-5	3.79E-6	1.79E+5	5.25E-5	1.89E-6	1.79E+5	2.38E-5	8.42E-7
1.87E+5	7.36E-5	4.51E-6	1.87E+5	8.01E-5	3.74E-6	1.87E+5	4.97E-5	1.83E-6	1.87E+5	2.27E-5	8.21E-7
1.96E+5	6.53E-5	4.46E-6	1.96E+5	6.99E-5	3.65E-6	1.96E+5	3.80E-5	1.79E-6	1.96E+5	1.87E-5	7.99E-7
2.06E+5	6.51E-5	4.44E-6	2.06E+5	6.92E-5	3.61E-6	2.06E+5	3.63E-5	1.78E-6	2.06E+5	1.87E-5	7.88E-7
2.15E+5	8.07E-5	4.39E-6	2.15E+5	7.34E-5	3.59E-6	2.15E+5	4.33E-5	1.75E-6	2.15E+5	2.05E-5	7.73E-7
2.26E+5	8.34E-5	4.36E-6	2.26E+5	7.78E-5	3.53E-6	2.26E+5	4.87E-5	1.73E-6	2.26E+5	2.30E-5	7.59E-7
2.37E+5	6.89E-5	4.32E-6	2.37E+5	8.52E-5	3.51E-6	2.37E+5	4.63E-5	1.69E-6	2.37E+5	2.30E-5	7.41E-7
2.48E+5	7.59E-5	4.31E-6	2.48E+5	8.20E-5	3.46E-6	2.48E+5	4.86E-5	1.67E-6	2.48E+5	2.15E-5	7.23E-7
2.60E+5	1.01E-4	4.28E-6	2.60E+5	8.85E-5	3.41E-6	2.60E+5	5.53E-5	1.63E-6	2.60E+5	2.63E-5	7.04E-7
2.72E+5	1.13E-4	4.20E-6	2.72E+5	1.02E-4	3.37E-6	2.72E+5	6.23E-5	1.60E-6	2.72E+5	2.94E-5	6.84E-7
2.85E+5	1.05E-4	4.13E-6	2.85E+5	1.03E-4	3.31E-6	2.85E+5	6.15E-5	1.55E-6	2.85E+5	2.83E-5	6.59E-7
2.99E+5	1.09E-4	4.08E-6	2.99E+5	1.18E-4	3.24E-6	2.99E+5	6.55E-5	1.50E-6	2.99E+5	3.00E-5	6.29E-7
3.13E+5	1.15E-4	4.01E-6	3.13E+5	1.22E-4	3.17E-6	3.13E+5	6.41E-5	1.45E-6	3.13E+5	2.95E-5	6.01E-7
3.28E+5	1.04E-4	3.98E-6	3.28E+5	1.01E-4	3.09E-6	3.28E+5	5.61E-5	1.40E-6	3.28E+5	2.37E-5	5.77E-7
3.44E+5	1.12E-4	3.93E-6	3.44E+5	1.06E-4	3.04E-6	3.44E+5	5.45E-5	1.36E-6	3.44E+5	2.25E-5	5.55E-7
3.61E+5	1.19E-4	3.91E-6	3.61E+5	1.13E-4	3.02E-6	3.61E+5	5.62E-5	1.34E-6	3.61E+5	2.30E-5	5.39E-7
3.78E+5	1.09E-4	3.89E-6	3.78E+5	1.02E-4	2.98E-6	3.78E+5	5.25E-5	1.31E-6	3.78E+5	1.97E-5	5.24E-7
3.96E+5	9.71E-5	3.88E-6	3.96E+5	8.38E-5	2.95E-6	3.96E+5	4.12E-5	1.29E-6	3.96E+5	1.59E-5	5.13E-7
4.15E+5	8.39E-5	3.89E-6	4.15E+5	7.85E-5	2.95E-6	4.15E+5	3.42E-5	1.28E-6	4.15E+5	1.39E-5	5.02E-7
4.35E+5	8.84E-5	3.90E-6	4.35E+5	7.56E-5	2.95E-6	4.35E+5	3.66E-5	1.26E-6	4.35E+5	1.36E-5	4.99E-7
4.56E+5	8.65E-5	3.94E-6	4.56E+5	8.10E-5	2.94E-6	4.56E+5	3.77E-5	1.26E-6	4.56E+5	1.49E-5	4.89E-7
4.78E+5	9.81E-5	3.94E-6	4.78E+5	8.98E-5	2.94E-6	4.78E+5	3.92E-5	1.25E-6	4.78E+5	1.51E-5	4.80E-7
5.01E+5	1.09E-4	3.99E-6	5.01E+5	9.26E-5	2.95E-6	5.01E+5	4.22E-5	1.24E-6	5.01E+5	1.56E-5	4.73E-7
5.25E+5	1.06E-4	4.04E-6	5.25E+5	9.16E-5	2.97E-6	5.25E+5	4.32E-5	1.24E-6	5.25E+5	1.50E-5	4.68E-7
5.50E+5	1.14E-4	4.09E-6	5.50E+5	9.40E-5	2.99E-6	5.50E+5	4.46E-5	1.22E-6	5.50E+5	1.51E-5	4.61E-7
5.76E+5	1.23E-4	4.15E-6	5.76E+5	1.02E-4	2.99E-6	5.76E+5	4.58E-5	1.22E-6	5.76E+5	1.69E-5	4.48E-7
6.04E+5	1.28E-4	4.15E-6	6.04E+5	1.12E-4	2.99E-6	6.04E+5	4.64E-5	1.18E-6	6.04E+5	1.65E-5	4.34E-7
6.33E+5	1.27E-4	4.19E-6	6.33E+5	1.07E-4	2.95E-6	6.33E+5	4.66E-5	1.15E-6	6.33E+5	1.51E-5	4.12E-7
6.63E+5	1.21E-4	4.20E-6	6.63E+5	1.00E-4	2.93E-6	6.63E+5	3.80E-5	1.12E-6	6.63E+5	1.28E-5	3.94E-7
6.95E+5	1.06E-4	4.25E-6	6.95E+5	8.42E-5	2.92E-6	6.95E+5	3.34E-5	1.09E-6	6.95E+5	1.00E-5	3.76E-7
7.28E+5	9.05E-5	4.29E-6	7.28E+5	7.72E-5	2.92E-6	7.28E+5	2.79E-5	1.07E-6	7.28E+5	8.38E-6	3.65E-7
7.63E+5	8.92E-5	4.37E-6	7.63E+5	6.66E-5	2.92E-6	7.63E+5	2.10E-5	1.06E-6	7.63E+5	6.15E-6	3.56E-7
8.00E+5	8.06E-5	4.47E-6	8.00E+5	6.30E-5	2.94E-6	8.00E+5	2.23E-5	1.06E-6	8.00E+5	5.70E-6	3.50E-7
8.38E+5	8.30E-5	4.56E-6	8.38E+5	5.92E-5	2.98E-6	8.38E+5	2.06E-5	1.06E-6	8.38E+5	5.87E-6	3.47E-7
8.78E+5	8.74E-5	4.67E-6	8.78E+5	5.96E-5	2.99E-6	8.78E+5	1.98E-5	1.04E-6	8.78E+5	5.70E-6	3.37E-7
9.20E+5	8.92E-5	4.76E-6	9.20E+5	6.44E-5	3.03E-6	9.20E+5	1.99E-5	1.04E-6	9.20E+5	5.41E-6	3.28E-7
9.65E+5	8.98E-5	4.82E-6	9.65E+5	6.08E-5	3.04E-6	9.65E+5	1.90E-5	1.02E-6	9.65E+5	4.77E-6	3.18E-7
1.01E+6	9.84E-5	4.92E-6	1.01E+6	6.00E-5	3.06E-6	1.01E+6	1.68E-5	1.01E-6	1.01E+6	4.09E-6	3.09E-7

Table 3.1.2.2 (Continued-2)

553mm			711 mm			914 mm		
Neutron Energy [eV]	Flux [n/leth/ source]	Absolute Error	Neutron Energy [eV]	Flux [n/leth/ source]	Absolute Error	Neutron Energy [eV]	Flux [n/leth/ source]	Absolute Error
3.02E+3	2.46E-6	5.24E-7	3.02E+3	6.96E-7	1.72E-7	3.02E+3	1.32E-7	3.64E-8
3.15E+3	2.48E-6	4.91E-7	3.15E+3	6.64E-7	1.65E-7	3.15E+3	1.39E-7	3.47E-8
3.28E+3	2.38E-6	4.73E-7	3.28E+3	7.44E-7	1.55E-7	3.28E+3	2.11E-7	3.32E-8
3.43E+3	1.58E-6	4.53E-7	3.43E+3	9.48E-7	1.50E-7	3.43E+3	1.72E-7	3.21E-8
3.58E+3	2.38E-6	4.38E-7	3.58E+3	4.94E-7	1.44E-7	3.58E+3	1.67E-7	3.07E-8
3.74E+3	1.81E-6	4.25E-7	3.74E+3	6.32E-7	1.40E-7	3.74E+3	1.64E-7	2.98E-8
3.90E+3	1.62E-6	4.12E-7	3.90E+3	6.15E-7	1.36E-7	3.90E+3	2.06E-7	2.88E-8
4.07E+3	1.65E-6	4.04E-7	4.07E+3	7.44E-7	1.31E-7	4.07E+3	1.59E-7	2.79E-8
4.25E+3	1.70E-6	3.94E-7	4.25E+3	7.45E-7	1.30E-7	4.25E+3	9.18E-8	2.73E-8
4.44E+3	2.07E-6	3.85E-7	4.44E+3	5.11E-7	1.25E-7	4.44E+3	1.54E-7	2.69E-8
4.64E+3	1.46E-6	3.79E-7	4.64E+3	5.18E-7	1.24E-7	4.64E+3	1.56E-7	2.64E-8
4.85E+3	1.67E-6	3.72E-7	4.85E+3	5.33E-7	1.22E-7	4.85E+3	1.28E-7	2.59E-8
5.07E+3	1.82E-6	3.67E-7	5.07E+3	5.43E-7	1.21E-7	5.07E+3	1.51E-7	2.55E-8
5.30E+3	1.48E-6	3.61E-7	5.30E+3	5.94E-7	1.18E-7	5.30E+3	1.74E-7	2.50E-8
5.54E+3	1.82E-6	3.59E-7	5.54E+3	7.11E-7	1.17E-7	5.54E+3	1.59E-7	2.46E-8
5.79E+3	1.95E-6	3.55E-7	5.79E+3	7.14E-7	1.15E-7	5.79E+3	1.66E-7	2.44E-8
6.05E+3	2.20E-6	3.48E-7	6.05E+3	4.83E-7	1.14E-7	6.05E+3	1.65E-7	2.40E-8
6.33E+3	1.91E-6	3.46E-7	6.33E+3	7.93E-7	1.13E-7	6.33E+3	1.37E-7	2.37E-8
6.62E+3	2.31E-6	3.41E-7	6.62E+3	6.96E-7	1.12E-7	6.62E+3	1.40E-7	2.37E-8
6.92E+3	1.71E-6	3.38E-7	6.92E+3	4.89E-7	1.11E-7	6.92E+3	1.58E-7	2.35E-8
7.24E+3	1.49E-6	3.36E-7	7.24E+3	6.58E-7	1.10E-7	7.24E+3	1.84E-7	2.32E-8
7.57E+3	1.54E-6	3.35E-7	7.57E+3	6.16E-7	1.10E-7	7.57E+3	1.33E-7	2.31E-8
7.92E+3	1.13E-6	3.36E-7	7.92E+3	4.20E-7	1.09E-7	7.92E+3	1.11E-7	2.30E-8
8.29E+3	1.56E-6	3.38E-7	8.29E+3	5.99E-7	1.10E-7	8.29E+3	1.78E-7	2.31E-8
8.67E+3	2.98E-6	3.40E-7	8.67E+3	8.54E-7	1.11E-7	8.67E+3	2.03E-7	2.32E-8
9.07E+3	3.01E-6	3.42E-7	9.07E+3	1.01E-6	1.11E-7	9.07E+3	1.92E-7	2.34E-8
9.49E+3	3.00E-6	3.45E-7	9.49E+3	1.17E-6	1.11E-7	9.49E+3	2.61E-7	2.35E-8
9.93E+3	3.66E-6	3.46E-7	9.93E+3	1.09E-6	1.12E-7	9.93E+3	3.47E-7	2.36E-8
1.04E+4	3.46E-6	3.47E-7	1.04E+4	1.29E-6	1.13E-7	1.04E+4	3.59E-7	2.36E-8
1.09E+4	4.24E-6	3.47E-7	1.09E+4	1.44E-6	1.13E-7	1.09E+4	3.41E-7	2.35E-8
1.14E+4	4.06E-6	3.50E-7	1.14E+4	1.36E-6	1.13E-7	1.14E+4	2.77E-7	2.36E-8
1.19E+4	3.97E-6	3.50E-7	1.19E+4	1.43E-6	1.13E-7	1.19E+4	3.08E-7	2.35E-8
1.25E+4	3.52E-6	3.51E-7	1.25E+4	1.25E-6	1.13E-7	1.25E+4	2.92E-7	2.37E-8
1.31E+4	3.79E-6	3.51E-7	1.31E+4	1.02E-6	1.13E-7	1.31E+4	3.16E-7	2.36E-8
1.37E+4	3.61E-6	3.55E-7	1.37E+4	9.48E-7	1.14E-7	1.37E+4	2.80E-7	2.37E-8
1.43E+4	3.04E-6	3.56E-7	1.43E+4	1.20E-6	1.15E-7	1.43E+4	2.46E-7	2.39E-8
1.50E+4	3.37E-6	3.60E-7	1.50E+4	1.14E-6	1.16E-7	1.50E+4	2.79E-7	2.41E-8
1.57E+4	3.00E-6	3.62E-7	1.57E+4	1.01E-6	1.17E-7	1.57E+4	2.60E-7	2.42E-8
1.64E+4	3.04E-6	3.66E-7	1.64E+4	9.71E-7	1.18E-7	1.64E+4	2.59E-7	2.44E-8
1.72E+4	3.24E-6	3.69E-7	1.72E+4	1.13E-6	1.19E-7	1.72E+4	2.79E-7	2.46E-8
1.80E+4	4.37E-6	3.72E-7	1.80E+4	1.63E-6	1.19E-7	1.80E+4	3.42E-7	2.47E-8
1.89E+4	5.06E-6	3.74E-7	1.89E+4	1.65E-6	1.19E-7	1.89E+4	4.15E-7	2.47E-8
1.98E+4	5.15E-6	3.75E-7	1.98E+4	1.82E-6	1.19E-7	1.98E+4	4.49E-7	2.46E-8
2.07E+4	6.46E-6	3.74E-7	2.07E+4	1.95E-6	1.19E-7	2.07E+4	4.70E-7	2.45E-8
2.17E+4	7.17E-6	3.71E-7	2.17E+4	2.15E-6	1.18E-7	2.17E+4	5.39E-7	2.45E-8
2.27E+4	7.78E-6	3.66E-7	2.27E+4	2.46E-6	1.17E-7	2.27E+4	6.93E-7	2.40E-8
2.38E+4	8.62E-6	3.62E-7	2.38E+4	3.00E-6	1.15E-7	2.38E+4	7.14E-7	2.34E-8
2.49E+4	9.00E-6	3.56E-7	2.49E+4	2.88E-6	1.13E-7	2.49E+4	6.48E-7	2.27E-8
2.61E+4	7.71E-6	3.50E-7	2.61E+4	2.44E-6	1.10E-7	2.61E+4	5.52E-7	2.23E-8
2.73E+4	4.60E-6	3.48E-7	2.73E+4	1.66E-6	1.10E-7	2.73E+4	3.73E-7	2.21E-8
2.86E+4	3.22E-6	3.48E-7	2.86E+4	8.95E-7	1.10E-7	2.86E+4	1.95E-7	2.21E-8
3.00E+4	2.03E-6	3.54E-7	3.00E+4	6.17E-7	1.11E-7	3.00E+4	1.40E-7	2.25E-8
3.14E+4	1.71E-6	3.59E-7	3.14E+4	6.66E-7	1.13E-7	3.14E+4	1.55E-7	2.29E-8
3.29E+4	2.33E-6	3.67E-7	3.29E+4	1.01E-6	1.15E-7	3.29E+4	1.74E-7	2.32E-8
3.45E+4	3.21E-6	3.72E-7	3.45E+4	9.67E-7	1.16E-7	3.45E+4	2.54E-7	2.35E-8
3.61E+4	3.68E-6	3.79E-7	3.61E+4	1.07E-6	1.17E-7	3.61E+4	3.18E-7	2.36E-8
3.78E+4	3.47E-6	3.83E-7	3.78E+4	1.48E-6	1.19E-7	3.78E+4	2.99E-7	2.37E-8
3.96E+4	5.13E-6	3.85E-7	3.96E+4	1.51E-6	1.19E-7	3.96E+4	3.43E-7	2.40E-8
4.15E+4	5.97E-6	3.86E-7	4.15E+4	1.72E-6	1.20E-7	4.15E+4	4.27E-7	2.40E-8
4.35E+4	6.35E-6	3.86E-7	4.35E+4	1.80E-6	1.19E-7	4.35E+4	4.37E-7	2.40E-8
4.55E+4	6.36E-6	3.88E-7	4.55E+4	1.95E-6	1.20E-7	4.55E+4	4.64E-7	2.39E-8
4.77E+4	6.10E-6	3.88E-7	4.77E+4	2.05E-6	1.19E-7	4.77E+4	4.65E-7	2.37E-8
5.00E+4	5.41E-6	3.89E-7	5.00E+4	1.95E-6	1.20E-7	5.00E+4	4.27E-7	2.37E-8
5.24E+4	4.99E-6	3.93E-7	5.24E+4	1.54E-6	1.20E-7	5.24E+4	3.84E-7	2.36E-8
5.49E+4	5.69E-6	3.94E-7	5.49E+4	1.61E-6	1.20E-7	5.49E+4	3.52E-7	2.39E-8
5.75E+4	6.54E-6	3.96E-7	5.75E+4	2.05E-6	1.21E-7	5.75E+4	4.56E-7	2.39E-8

Table 3.1.2.2 (Continued-3)

553mm			711 mm			914 mm		
Neutron Energy [eV]	Flux [n/leth/ source]	Absolute Error	Neutron Energy [eV]	Flux [n/leth/ source]	Absolute Error	Neutron Energy [eV]	Flux [n/leth/ source]	Absolute Error
6.02E+4	6.50E-6	3.98E-7	6.02E+4	2.03E-6	1.21E-7	6.02E+4	4.83E-7	2.37E-8
6.31E+4	6.63E-6	3.98E-7	6.31E+4	2.18E-6	1.21E-7	6.31E+4	4.63E-7	2.36E-8
6.61E+4	7.44E-6	3.99E-7	6.61E+4	2.14E-6	1.20E-7	6.61E+4	4.84E-7	2.35E-8
6.93E+4	7.80E-6	3.96E-7	6.93E+4	2.26E-6	1.20E-7	6.93E+4	4.94E-7	2.34E-8
7.26E+4	7.12E-6	3.96E-7	7.26E+4	2.41E-6	1.19E-7	7.26E+4	4.97E-7	2.32E-8
7.61E+4	8.42E-6	3.95E-7	7.61E+4	2.48E-6	1.18E-7	7.61E+4	5.51E-7	2.30E-8
7.97E+4	8.86E-6	3.93E-7	7.97E+4	2.35E-6	1.17E-7	7.97E+4	5.96E-7	2.27E-8
8.35E+4	7.68E-6	3.88E-7	8.35E+4	2.38E-6	1.16E-7	8.35E+4	5.17E-7	2.22E-8
8.75E+4	6.20E-6	3.90E-7	8.75E+4	2.03E-6	1.15E-7	8.75E+4	4.13E-7	2.21E-8
9.17E+4	5.54E-6	3.91E-7	9.17E+4	1.65E-6	1.15E-7	9.17E+4	3.64E-7	2.21E-8
9.61E+4	5.52E-6	3.94E-7	9.61E+4	1.49E-6	1.16E-7	9.61E+4	3.54E-7	2.20E-8
1.01E+5	6.26E-6	3.96E-7	1.01E+5	1.78E-6	1.16E-7	1.01E+5	3.79E-7	2.20E-8
1.06E+5	6.34E-6	3.98E-7	1.06E+5	1.88E-6	1.17E-7	1.06E+5	3.95E-7	2.21E-8
1.11E+5	8.03E-6	3.98E-7	1.11E+5	2.26E-6	1.15E-7	1.11E+5	4.71E-7	2.18E-8
1.16E+5	9.30E-6	3.96E-7	1.16E+5	2.78E-6	1.14E-7	1.16E+5	5.78E-7	2.15E-8
1.21E+5	1.03E-5	3.90E-7	1.21E+5	3.13E-6	1.11E-7	1.21E+5	6.77E-7	2.08E-8
1.27E+5	1.23E-5	3.85E-7	1.27E+5	3.34E-6	1.10E-7	1.27E+5	7.02E-7	2.03E-8
1.33E+5	1.10E-5	3.81E-7	1.33E+5	2.84E-6	1.07E-7	1.33E+5	5.62E-7	1.97E-8
1.40E+5	7.45E-6	3.81E-7	1.40E+5	2.15E-6	1.07E-7	1.40E+5	4.08E-7	1.94E-8
1.46E+5	4.95E-6	3.84E-7	1.46E+5	1.49E-6	1.07E-7	1.46E+5	3.18E-7	1.94E-8
1.53E+5	6.26E-6	3.91E-7	1.53E+5	1.42E-6	1.09E-7	1.53E+5	2.83E-7	1.94E-8
1.55E+5	5.62E-6	2.64E-7	1.55E+5	1.54E-6	6.86E-8	1.58E+5	3.31E-7	1.28E-8
1.63E+5	6.46E-6	2.56E-7	1.63E+5	1.66E-6	6.59E-8	1.65E+5	3.36E-7	1.22E-8
1.71E+5	6.76E-6	2.47E-7	1.71E+5	1.79E-6	6.34E-8	1.73E+5	3.41E-7	1.17E-8
1.79E+5	6.93E-6	2.40E-7	1.79E+5	1.82E-6	6.09E-8	1.81E+5	3.58E-7	1.12E-8
1.87E+5	7.12E-6	2.32E-7	1.87E+5	1.75E-6	5.86E-8	1.90E+5	3.09E-7	1.07E-8
1.96E+5	6.07E-6	2.23E-7	1.96E+5	1.37E-6	5.68E-8	1.99E+5	2.68E-7	1.03E-8
2.06E+5	5.06E-6	2.20E-7	2.06E+5	1.25E-6	5.53E-8	2.09E+5	2.46E-7	9.99E-9
2.15E+5	5.70E-6	2.13E-7	2.15E+5	1.53E-6	5.35E-8	2.19E+5	2.83E-7	9.67E-9
2.26E+5	6.60E-6	2.10E-7	2.26E+5	1.65E-6	5.18E-8	2.29E+5	2.94E-7	9.30E-9
2.37E+5	6.35E-6	2.02E-7	2.37E+5	1.58E-6	4.97E-8	2.40E+5	2.94E-7	8.90E-9
2.48E+5	6.38E-6	1.97E-7	2.48E+5	1.54E-6	4.82E-8	2.52E+5	2.88E-7	8.51E-9
2.60E+5	7.44E-6	1.91E-7	2.60E+5	1.77E-6	4.61E-8	2.64E+5	3.34E-7	8.02E-9
2.72E+5	8.23E-6	1.83E-7	2.72E+5	1.93E-6	4.38E-8	2.77E+5	3.46E-7	7.56E-9
2.85E+5	7.82E-6	1.74E-7	2.85E+5	1.78E-6	4.13E-8	2.90E+5	2.86E-7	6.97E-9
2.99E+5	7.59E-6	1.64E-7	2.99E+5	1.70E-6	3.85E-8	3.04E+5	3.01E-7	6.46E-9
3.13E+5	7.68E-6	1.54E-7	3.13E+5	1.71E-6	3.59E-8	3.18E+5	2.65E-7	5.91E-9
3.28E+5	6.17E-6	1.46E-7	3.28E+5	1.29E-6	3.35E-8	3.34E+5	1.91E-7	5.48E-9
3.44E+5	5.44E-6	1.39E-7	3.44E+5	1.12E-6	3.16E-8	3.50E+5	1.61E-7	5.09E-9
3.61E+5	5.25E-6	1.34E-7	3.61E+5	1.11E-6	2.98E-8	3.66E+5	1.56E-7	4.84E-9
3.78E+5	4.53E-6	1.28E-7	3.78E+5	8.94E-7	2.84E-8	3.84E+5	1.26E-7	4.54E-9
3.96E+5	3.65E-6	1.24E-7	3.96E+5	7.21E-7	2.69E-8	4.02E+5	9.07E-8	4.33E-9
4.15E+5	3.19E-6	1.21E-7	4.15E+5	5.36E-7	2.61E-8	4.22E+5	7.51E-8	4.15E-9
4.35E+5	2.81E-6	1.18E-7	4.35E+5	5.09E-7	2.54E-8	4.42E+5	7.94E-8	4.03E-9
4.56E+5	2.98E-6	1.15E-7	4.56E+5	5.41E-7	2.47E-8	4.63E+5	7.70E-8	3.86E-9
4.78E+5	3.28E-6	1.12E-7	4.78E+5	5.66E-7	2.39E-8	4.85E+5	7.34E-8	3.71E-9
5.01E+5	3.09E-6	1.09E-7	5.01E+5	5.33E-7	2.31E-8	5.08E+5	7.89E-8	3.59E-9
5.25E+5	3.09E-6	1.07E-7	5.25E+5	5.59E-7	2.23E-8	5.33E+5	6.97E-8	3.40E-9
5.50E+5	3.14E-6	1.03E-7	5.50E+5	5.47E-7	2.16E-8	5.58E+5	7.08E-8	3.23E-9
5.76E+5	3.01E-6	9.91E-8	5.76E+5	4.65E-7	2.03E-8	5.85E+5	4.79E-8	3.12E-9
6.04E+5	3.07E-6	9.43E-8	6.04E+5	4.44E-7	1.93E-8	6.13E+5	4.91E-8	2.87E-9
6.33E+5	2.72E-6	8.79E-8	6.33E+5	4.90E-7	1.78E-8	6.43E+5	7.29E-8	2.69E-9
6.63E+5	2.35E-6	8.21E-8	6.63E+5	3.82E-7	1.63E-8	6.73E+5	4.79E-8	2.32E-9
6.95E+5	1.63E-6	7.68E-8	6.95E+5	2.84E-7	1.45E-8	7.06E+5	2.72E-8	2.02E-9
7.28E+5	1.28E-6	7.15E-8	7.28E+5	1.80E-7	1.34E-8	7.40E+5	1.94E-8	1.86E-9
7.63E+5	9.98E-7	6.96E-8	7.63E+5	1.20E-7	1.25E-8	7.75E+5	1.36E-8	1.70E-9
8.00E+5	8.13E-7	6.69E-8	8.00E+5	1.10E-7	1.20E-8	8.12E+5	1.04E-8	1.62E-9
8.38E+5	8.53E-7	6.45E-8	8.38E+5	1.00E-7	1.17E-8	8.51E+5	9.59E-9	1.50E-9
8.78E+5	7.69E-7	6.22E-8	8.78E+5	8.74E-8	1.08E-8	8.92E+5	1.05E-8	1.39E-9
9.20E+5	6.55E-7	5.87E-8	9.20E+5	9.80E-8	1.04E-8	9.35E+5	8.47E-9	1.28E-9
9.65E+5	6.10E-7	5.59E-8	9.65E+5	7.55E-8	9.48E-9	9.80E+5	5.24E-9	1.19E-9
1.01E+6	4.45E-7	5.30E-8	1.01E+6	5.80E-8	8.69E-9	1.03E+6	4.06E-9	1.03E-9

Table 3.1.3.1 Measurement conditions for two mode runs.

Mode #	Target Neutron Energy to be Measured	Time Range of Measurement	Neutron Pulse	
			Repitition Rate	Pulse Width
#1	$10^{-7} \sim 10^{-4}$ MeV	200 μs	200 μs	0.5 μs
#2	$10^{-4} \sim 10^{-2}$ MeV	50 μs	128 μs	0.005 μs

Table 3.1.3.2 Propaties of resonance filters used in the measurement.

Material	Resonance Energy	Thickness	Form
In	1.46 eV	0.5 mm	Foil
W	4.15 eV	0.2 mm	Foil
Au	4.906 eV	0.1 mm	Foil
Co	132. eV	0.2 mm	Foil
Mn	336. eV	1.8 mm x 60 % density	Powder

Table 3.1.3.3 Comparison of measured and calculated slowing down time.

Position [mm]	Mode #	Filter	Energy [eV]	Expt. [μs]	Calc. [μs]	C/E
355.6	#1	Au	4.906	24.1	23.9	0.990
		Co	132	5.16	5.10	0.990
	#2	Co	132	4.98	5.10	1.024
		Mn	336	3.60	3.50	0.972
533.4	#1	In	1.46	44.7	44.5	0.994
		W	4.15	24.5	25.9	1.059
		Au	4.906	23.0	23.9	1.038
		Co	132	5.03	5.07	1.008
	#2	Co	132	5.14	5.07	0.988
		Mn	336	3.55	3.46	0.973
711.2	#1	Au	4.906	23.0	23.8	1.037
		Co	132	5.14	5.09	1.037
	#2	Co	132	5.08	5.09	1.003
914.4	#1	Co	132	5.12	5.14	1.004

Table 3.1.3.4 Neutron spectra at 356, 553, 711 and 914 mm from the front surface of the teste region in the assembly #2 measured by the slowing down time method.

	356 mm			553 mm			711 mm			914 mm		
Neutron Energy [eV]	Flux [n/leth/ source]	Absolute Error	FWHM [%]	Flux [n/leth/ source]	Absolute Error	FWHM [%]	Flux [n/leth/ source]	Absolute Error	FWHM [%]	Flux [n/leth/ source]	Absolute Error	FWHM [%]
2.82E-1	2.47E-10	1.15E-10	95.7	7.07E-10	1.11E-10	86.8	5.54E-11	1.99E-11	85.1	6.45E-11	2.19E-11	78.4
3.55E-1	2.58E-10	1.25E-10	103.3	1.57E-08	1.10E-09	72.4	1.08E-10	2.98E-11	80.8	5.69E-11	2.17E-11	73.6
4.47E-1	4.28E-08	3.14E-09	122.1	1.74E-08	1.22E-09	65.1	5.90E-09	4.30E-10	71.5	1.84E-09	1.72E-10	62.7
5.62E-1	6.87E-08	4.82E-09	77.5	2.98E-08	2.01E-09	75.6	1.46E-08	9.82E-10	76.5	3.96E-09	3.17E-10	76.7
7.08E-1	1.07E-07	7.26E-09	69.9	5.80E-08	3.78E-09	66.2	2.72E-08	1.77E-09	69.9	5.52E-09	4.24E-10	77.9
8.91E-1	1.78E-07	1.18E-08	68.4	7.43E-08	4.81E-09	65.9	2.57E-08	1.69E-09	62.6	1.01E-08	7.19E-10	72.2
1.12E+0	2.00E-07	1.32E-08	69.5	1.04E-07	6.67E-09	61.9	4.32E-08	2.79E-09	64.6	1.15E-08	8.22E-10	58.8
1.41E+0	2.58E-07	1.69E-08	64.1	1.42E-07	9.07E-09	66.9	4.99E-08	3.22E-09	61.4	1.98E-08	1.35E-09	67.8
1.78E+0	3.82E-07	2.47E-08	60.5	1.84E-07	1.17E-08	59.9	7.67E-08	4.89E-09	61.2	1.68E-08	1.18E-09	61.7
2.24E+0	4.23E-07	2.74E-08	68.9	2.31E-07	1.46E-08	59.5	8.47E-08	5.40E-09	55.7	2.36E-08	1.62E-09	58.6
2.82E+0	5.69E-07	3.66E-08	73.9	2.60E-07	1.65E-08	59.1	1.05E-07	6.69E-09	59.9	2.93E-08	1.99E-09	54.8
3.55E+0	7.22E-07	4.62E-08	58.5	3.30E-07	2.08E-08	55.4	1.33E-07	8.44E-09	56.9	4.07E-08	2.72E-09	57.6
4.47E+0	7.95E-07	5.09E-08	58.5	3.59E-07	2.27E-08	56.1	1.45E-07	9.21E-09	56.1	3.80E-08	2.58E-09	56.8
5.62E+0	8.43E-07	5.42E-08	58.0	4.32E-07	2.73E-08	54.7	1.65E-07	1.05E-08	55.2	4.59E-08	3.09E-09	53.1
7.08E+0	1.01E-06	6.47E-08	62.6	4.62E-07	2.92E-08	53.2	1.90E-07	1.21E-08	55.7	5.04E-08	3.40E-09	56.0
8.91E+0	1.16E-06	7.42E-08	58.4	5.38E-07	3.40E-08	55.1	2.00E-07	1.27E-08	55.0	5.96E-08	4.01E-09	52.6
1.12E+1	1.23E-06	7.91E-08	63.5	5.79E-07	3.66E-08	53.9	2.21E-07	1.40E-08	54.8	6.05E-08	4.10E-09	53.9
1.41E+1	1.42E-06	9.11E-08	64.6	6.41E-07	4.06E-08	55.1	2.44E-07	1.55E-08	54.2	7.03E-08	4.75E-09	52.9
1.78E+1	1.48E-06	9.50E-08	67.8	7.12E-07	4.51E-08	54.3	2.73E-07	1.74E-08	53.8	6.90E-08	4.71E-09	55.0
2.24E+1	1.64E-06	1.05E-07	66.2	7.35E-07	4.66E-08	57.6	2.91E-07	1.85E-08	53.5	8.48E-08	5.74E-09	57.1
2.82E+1	1.69E-06	1.09E-07	61.8	7.65E-07	4.86E-08	59.6	3.02E-07	1.93E-08	55.8	8.68E-08	5.93E-09	56.4
3.55E+1	1.69E-06	1.09E-07	63.2	8.40E-07	5.34E-08	61.0	3.19E-07	2.04E-08	57.8	8.57E-08	5.92E-09	58.1
4.47E+1	2.11E-06	1.36E-07	63.9	9.74E-07	6.18E-08	57.7	3.80E-07	2.43E-08	56.3	1.01E-07	6.92E-09	56.6
5.62E+1	2.53E-06	1.63E-07	59.9	1.18E-06	7.49E-08	57.5	4.65E-07	2.96E-08	55.3	1.33E-07	9.04E-09	54.9
7.08E+1	2.96E-06	1.90E-07	63.0	1.37E-06	8.68E-08	57.9	5.37E-07	3.42E-08	56.4	1.37E-07	9.37E-09	56.0
8.91E+1	3.06E-06	1.97E-07	65.6	1.38E-06	8.73E-08	59.0	5.21E-07	3.33E-08	56.6	1.40E-07	9.68E-09	55.1
1.12E+2	3.66E-06	2.36E-07	73.2	1.58E-06	1.05E-07	59.8	6.08E-07	4.16E-08	59.5	1.51E-07	1.03E-08	57.0
1.41E+2	3.86E-06	2.49E-07	75.2	1.76E-06	1.17E-07	61.5	6.59E-07	4.53E-08	57.8	1.77E-07	1.20E-08	59.6
1.78E+2	4.56E-06	2.93E-07	87.6	1.75E-06	1.17E-07	65.9	6.80E-07	4.71E-08	60.5	1.74E-07	1.19E-08	58.4
2.24E+2	4.27E-06	2.77E-07	90.6	1.82E-06	1.23E-07	75.4	6.33E-07	4.47E-08	67.8	1.69E-07	1.17E-08	65.9
2.82E+2	4.00E-06	2.61E-07	97.5	1.75E-06	1.19E-07	82.6	6.25E-07	4.48E-08	74.5	1.71E-07	1.20E-08	74.8
3.55E+2	4.09E-06	2.69E-07	107.0	1.97E-06	1.34E-07	82.7	6.58E-07	4.76E-08	76.0	1.78E-07	1.26E-08	73.9
4.47E+2	4.94E-06	3.23E-07	151.9	2.30E-06	1.56E-07	82.7	7.98E-07	5.71E-08	71.6	2.03E-07	1.44E-08	68.7
5.62E+2	5.76E-06	3.76E-07	150.3	2.27E-06	1.56E-07	94.0	9.28E-07	6.62E-08	68.2	2.50E-07	1.75E-08	64.0
7.08E+2	6.26E-06	4.09E-07	204.5	2.96E-06	2.00E-07	135.6	1.01E-06	7.25E-08	70.4	2.56E-07	1.81E-08	64.7
8.91E+2	6.57E-06	4.31E-07	179.4	2.96E-06	2.02E-07	110.2	1.06E-06	7.67E-08	72.9	2.86E-07	2.02E-08	66.4
1.12E+3	6.07E-06	4.02E-07	210.0	3.15E-06	2.16E-07	138.8	1.06E-06	7.79E-08	86.6	2.95E-07	2.10E-08	66.8
1.41E+3	6.59E-06	4.38E-07	250.4	3.11E-06	2.16E-07	143.7	1.16E-06	8.56E-08	121.3	2.79E-07	2.04E-08	75.1
1.78E+3	7.32E-06	4.86E-07	254.7	2.79E-06	1.99E-07	179.5	1.02E-06	7.76E-08	152.1	2.37E-07	1.81E-08	99.9
2.24E+3	6.45E-06	4.35E-07	290.4	2.79E-06	2.01E-07	225.0	1.01E-06	7.86E-08	158.3	2.49E-07	1.91E-08	128.9
2.82E+3	6.55E-06	4.44E-07	291.7	2.68E-06	1.96E-07	254.2	8.10E-07	6.73E-08	175.9	2.14E-07	1.72E-08	145.8
3.55E+3	5.34E-06	3.72E-07	292.5	2.71E-06	2.01E-07	256.3	7.29E-07	6.35E-08	193.8	1.90E-07	1.61E-08	156.8
4.47E+3	5.93E-06	4.13E-07	302.9	2.65E-06	2.00E-07	246.1	8.16E-07	7.08E-08	206.0	1.95E-07	1.68E-08	159.8
5.62E+3	6.01E-06	4.22E-07	301.8	2.65E-06	2.04E-07	232.2	9.14E-07	7.90E-08	209.5	1.98E-07	1.75E-08	160.9
7.08E+3	7.97E-06	5.49E-07	286.8	2.97E-06	2.28E-07	224.0	9.70E-07	8.50E-08	186.9	1.99E-07	1.80E-08	162.6
8.91E+3	8.36E-06	5.80E-07	260.8	2.89E-06	2.28E-07	215.0	1.02E-06	9.09E-08	175.6	2.11E-07	1.93E-08	156.3

Table 3.2.1.1 Dosimetry Reactions

	Reactions	Half-Life	Abundance [%]	γ-ray Energy [keV]	γ-ray Branching [%]	Threshold Energy [MeV]
1.	$^{27}Al(n,\alpha)^{24}Na$	15.02 h	100.0	1368.6	100.0	5
2.	$Ti(n,x)^{46}Sc$	83.83 d	100.0	889.3	99.98	4
3.	$Ti(n,x)^{47}Sc$	3.341 d	100.0	159.4	68.0	1.5
4.	$Ti(n,x)^{48}Sc$	1.821 d	100.0	983.5	100.0	5
5.	$^{56}Fe(n,p)^{56}Mn$	2.579 h	91.72	846.8	98.9	5
6.	$^{59}Co(n,\alpha)^{56}Mn$	2.579 h	100.0	846.8	98.9	6
7.	$^{58}Ni(n,p)^{58}Co$	70.92 d	68.26	810.8	99.5	2
8.	$^{58}Ni(n,2n)^{57}Ni$	1.503 d	68.27	1377.6	77.9	12.5
9.	$^{64}Zn(n,p)^{64}Cu$	12.70 h	48.6	511.0	74.2	1.5
10.	$^{90}Zr(n,2n)^{89}Zr$	3.268 d	51.45	909.2	99.01	12
11.	$^{93}Nb(n,2n)^{92m}Nb$	10.15 d	100.0	934.5	99.0	9
12.	$^{115}In(n,n')^{115m}In$	4.486 h	95.7	336.3	45.8	0.34
13.	$^{197}Au(n,\gamma)^{198}Au$	2.694 d	100.0	411.8	95.5	--------

Table 3.2.1.2 Measured neutron activation reaction rates in the assembly #1.

Distance from the front surface of the test region [mm]	$^{27}Al(n,\alpha)^{24}Na$ Reaction Rate [1/source]	Absolute Error	$Ti(n,x)^{46}Sc$ Reaction Rate [1/source]	Absolute Error	$Ti(n,x)^{47}Sc$ Reaction Rate [1/source]	Absolute Error	$Ti(n,x)^{48}Sc$ Reaction Rate [1/source]	Absolute Error	$Fe(n,x)^{56}Mn$ Reaction Rate [1/source]	Absolute Error
-1	1.12E-29	3.63E-31	1.48E-29	5.64E-31	2.83E-30	1.02E-31	5.68E-30	1.90E-31	9.89E-30	3.05E-31
101	2.08E-30	6.79E-32	2.83E-30	1.11E-31	5.19E-31	2.07E-32	1.05E-30	3.77E-32	1.81E-30	5.55E-32
227	2.52E-31	8.86E-33	3.70E-31	2.30E-32	6.77E-32	3.31E-33	1.22E-31	4.96E-33	2.31E-31	7.35E-33
355	3.15E-32	1.23E-33	4.24E-32	8.09E-33	8.28E-33	1.22E-33	1.41E-32	1.07E-33	2.82E-32	9.58E-34

Distance from the front surface of the test region [mm]	$^{59}Co(n,\alpha)^{56}Mn$ Reaction Rate [1/source]	Absolute Error	$^{58}Ni(n,2n)^{57}Ni$ Reaction Rate [1/source]	Absolute Error	$^{58}Ni(n,p)^{58}Co$ Reaction Rate [1/source]	Absolute Error	$^{64}Zn(n,p)^{64}Cu$ Reaction Rate [1/source]	Absolute Error	$^{90}Zr(n,2n)^{89}Zr$ Reaction Rate [1/source]	Absolute Error
-1	2.98E-30	9.67E-32	4.16E-30	1.34E-31	3.30E-29	1.04E-30	1.60E-29	4.98E-31	8.18E-29	2.41E-30
101	5.36E-31	1.69E-32	6.83E-31	2.40E-32	9.35E-30	2.91E-31	4.06E-30	1.30E-31	1.42E-29	4.21E-31
227	6.62E-32	2.32E-33	7.86E-32	2.99E-33	1.37E-30	4.27E-32	5.87E-31	2.11E-32	1.63E-30	5.06E-32
355	8.04E-33	3.76E-34	9.68E-33	5.41E-34	1.86E-31	7.06E-33	8.15E-32	3.91E-33	2.02E-31	7.20E-33
533	———	———	———	———	1.19E-32	5.31E-34	5.67E-33	3.43E-34	1.13E-32	9.45E-34

Distance from the front surface of the test region [mm]	$^{93}Nb(n,2n)^{92m}Nb$ Reaction Rate [1/source]	Absolute Error	$^{115}In(n,n')^{115m}In$ Reaction Rate [1/source]	Absolute Error	$^{197}Au(n,\gamma)^{198}Au$ Reaction Rate [1/source]	Absolute Error
-1	4.53E-29	1.32E-30	1.77E-29	5.20E-31	9.20E-29	4.83E-30
101	8.11E-30	2.41E-31	1.09E-29	3.21E-31	7.32E-28	3.70E-29
227	9.67E-31	2.97E-32	2.45E-30	7.53E-33	1.03E-27	5.07E-29
355	1.20E-31	4.36E-33	4.67E-31	1.92E-32	7.47E-28	3.70E-29
533	6.48E-33	3.48E-34	4.63E-32	3.03E-33	3.96E-28	1.94E-29
711	———	———	———	———	1.61E-28	5.03E-30
914	———	———	———	———	4.75E-29	1.60E-30

Table 3.2.1.3 Measured neutron activation reactionrates in the assembly #2.

Distance from the front surface of the test region [mm]	$^{27}Al(n,\alpha)^{24}Na$ Reaction Rate [1/source]	Absolute Error	$Ti(n,x)^{46}Sc$ Reaction Rate [1/source]	Absolute Error	$Ti(n,x)^{47}Sc$ Reaction Rate [1/source]	Absolute Error	$Ti(n,x)^{48}Sc$ Reaction Rate [1/source]	Absolute Error	$Fe(n,x)^{56}Mn$ Reaction Rate [1/source]	Absolute Error
-1	1.07E-29	3.40E-31	1.43E-29	5.35E-31	2.73E-30	9.95E-32	5.40E-30	1.85E-31	9.41E-30	2.88E-31
102	2.01E-30	6.74E-32	2.77E-30	1.07E-31	5.32E-31	2.05E-32	9.86E-31	3.60E-32	1.82E-30	5.59E-32
229	2.50E-31	8.91E-33	3.19E-31	2.17E-32	6.90E-32	3.88E-33	1.18E-31	6.46E-33	2.23E-31	7.14E-33
356	3.09E-32	1.45E-33	5.33E-32	9.81E-33	9.06E-33	1.61E-33	1.44E-32	1.59E-33	2.86E-32	1.13E-33

Distance from the front surface of the test region [mm]	$^{59}Co(n,\alpha)^{56}Mn$ Reaction Rate [1/source]	Absolute Error	$^{58}Ni(n,2n)^{57}Ni$ Reaction Rate [1/source]	Absolute Error	$^{58}Ni(n,p)^{58}Co$ Reaction Rate [1/source]	Absolute Error	$^{64}Zn(n,p)^{64}Cu$ Reaction Rate [1/source]	Absolute Error	$^{90}Zr(n,2n)^{89}Zr$ Reaction Rate [1/source]	Absolute Error
-1	2.81E-30	8.79E-32	4.01E-30	1.32E-31	3.38E-29	1.04E-30	1.62E-29	5.00E-31	7.92E-29	2.34E-30
102	5.30E-31	1.69E-32	6.75E-31	2.39E-32	9.34E-30	2.90E-31	4.00E-30	1.30E-31	1.39E-29	4.14E-31
229	6.60E-32	2.38E-33	7.67E-32	3.10E-33	1.35E-30	4.25E-32	5.78E-31	2.02E-32	1.63E-30	5.19E-32
356	7.46E-33	3.61E-34	9.03E-33	5.05E-34	1.90E-31	6.98E-33	7.90E-32	3.38E-33	1.97E-31	7.36E-33
533	———	———	———	———	1.18E-32	5.45E-34	6.83E-33	4.13E-34	9.88E-33	8.43E-34

Distance from the front surface of the test region [mm]	$^{93}Nb(n,2n)^{92m}Nb$ Reaction Rate [1/source]	Absolute Error	$^{115}In(n,n')^{115m}In$ Reaction Rate [1/source]	Absolute Error	$^{197}Au(n,\gamma)^{198}Au$ Reaction Rate [1/source]	Absolute Error
-1	4.40E-29	1.29E-30	2.26E-29	6.57E-31	1.91E-27	9.49E-29
102	7.90E-30	2.36E-31	1.12E-29	3.43E-31	2.83E-27	1.40E-28
229	9.52E-31	3.21E-32	2.38E-30	1.03E-31	2.59E-27	1.27E-28
356	1.25E-31	4.81E-33	4.97E-31	3.39E-32	1.59E-27	7.88E-29
533	6.36E-33	6.62E-34	4.01E-32	5.10E-33	7.52E-28	3.73E-29
711	———	———	———	———	2.72E-28	8.68E-30
914	———	———	———	———	7.30E-29	2.52E-30

Table 3.2.2.1 Measured fission rates.

(a) Assembly #1

Distance from the front surface of the test region [mm]	^{235}U(n,fission) Fission Rate [1/source]	Absolute Error	^{238}U(n,fission) Fission Rate [1/source]	Absolute Error
-4	4.11E-28	1.45E-29	1.36E-28	5.98E-30
102	5.90E-28	2.02E-29	3.31E-29	1.18E-30
229	5.23E-28	1.78E-29	5.05E-30	1.92E-31
356	3.71E-28	1.26E-29	8.00E-31	3.93E-32
533	1.71E-28	5.81E-30	—	—
711	6.47E-29	2.22E-30	—	—
914	1.78E-29	6.15E-31	—	—

(b) Assembly #2

Distance from the front surface of the test region [mm]	^{235}U(n,fission) Fission Rate [1/source]	Absolute Error	^{238}U(n,fission) Fission Rate [1/source]	Absolute Error
-4	1.39E-27	4.78E-29	1.41E-28	4.87E-30
102	1.55E-27	5.28E-29	3.48E-29	1.25E-30
229	1.16E-27	3.96E-29	5.39E-30	2.16E-31
356	7.39E-28	2.51E-29	8.86E-31	5.53E-32
533	3.05E-28	1.04E-29	—	—
711	1.08E-28	3.67E-30	—	—
914	2.74E-29	9.45E-31	—	—

Table 3.3.1 Gamma-ray spectra at 102, 356, 711 and 914 mm from the front surface of the test region in the assembly #1 measured by the NE213 spectrometer.

	102 mm			356 mm			711 mm			914 mm		
Neutron Energy [MeV]	Flux [n/leth/ source]	Absolute Error	Window [%]	Flux [n/leth/ source]	Absolute Error	Window [%]	Flux [n/leth/ source]	Absolute Error	Wimdow [%]	Flux [n/leth/ source]	Absolute Error	Window [%]
3.02E-1	2.00E-05	1.05E-06	29.8	1.68E-06	1.10E-07	29.8	2.15E-07	1.49E-08	29.8	5.92E-08	4.07E-09	29.8
3.16E-1	1.98E-05	1.04E-06	29.5	1.66E-06	1.11E-07	29.5	2.15E-07	1.52E-08	29.5	5.91E-08	4.15E-09	29.5
3.31E-1	1.95E-05	1.05E-06	29.2	1.67E-06	1.14E-07	29.2	2.16E-07	1.57E-08	29.2	5.88E-08	4.28E-09	29.2
3.47E-1	1.93E-05	1.06E-06	28.9	1.68E-06	1.20E-07	28.9	2.15E-07	1.67E-08	28.9	5.81E-08	4.54E-09	28.9
3.63E-1	1.92E-05	1.05E-06	28.6	1.69E-06	1.28E-07	28.6	2.13E-07	1.80E-08	28.6	5.70E-08	4.89E-09	28.6
3.80E-1	1.92E-05	1.05E-06	28.3	1.72E-06	1.33E-07	28.3	2.15E-07	1.89E-08	28.3	5.71E-08	5.15E-09	28.3
3.98E-1	1.95E-05	1.07E-06	27.9	1.87E-06	1.47E-07	27.5	2.41E-07	2.13E-08	27.5	6.39E-08	5.80E-09	27.5
4.17E-1	2.04E-05	1.12E-06	27.3	2.40E-06	1.78E-07	25.9	3.30E-07	2.69E-08	25.7	8.84E-08	7.32E-09	25.7
4.37E-1	2.21E-05	1.15E-06	26.4	3.55E-06	1.91E-07	24.1	5.27E-07	2.90E-08	23.7	1.43E-07	7.89E-09	23.8
4.57E-1	2.50E-05	1.18E-06	25.5	5.22E-06	1.98E-07	22.2	8.20E-07	2.94E-08	21.7	2.23E-07	8.02E-09	21.7
4.79E-1	2.83E-05	1.27E-06	24.6	6.71E-06	2.65E-07	20.4	1.08E-06	4.11E-08	19.8	2.95E-07	1.12E-08	19.8
5.01E-1	3.02E-05	1.32E-06	24.2	7.04E-06	2.68E-07	20.1	1.13E-06	4.11E-08	19.4	3.08E-07	1.12E-08	19.4
5.25E-1	2.95E-05	1.31E-06	24.5	5.90E-06	2.08E-07	21.4	9.16E-07	3.01E-08	20.8	2.50E-07	8.24E-09	20.8
5.49E-1	2.60E-05	1.31E-06	25.0	4.03E-06	2.21E-07	22.9	5.90E-07	3.23E-08	22.5	1.62E-07	8.83E-09	22.5
5.75E-1	2.17E-05	1.19E-06	25.6	2.43E-06	1.67E-07	24.5	3.24E-07	2.35E-08	24.3	8.97E-08	6.42E-09	24.3
6.03E-1	1.86E-05	1.12E-06	26.2	1.51E-06	1.21E-07	26.0	1.79E-07	1.58E-08	25.9	5.08E-08	4.35E-09	25.9
6.31E-1	1.73E-05	1.09E-06	26.5	1.18E-06	1.13E-07	26.6	1.33E-07	1.46E-08	26.6	3.82E-08	4.01E-09	26.6
6.61E-1	1.75E-05	1.06E-06	26.2	1.21E-06	8.59E-08	26.0	1.41E-07	1.02E-08	26.0	3.97E-08	2.81E-09	26.0
6.92E-1	1.88E-05	1.08E-06	25.4	1.41E-06	8.22E-08	25.1	1.66E-07	9.11E-09	25.2	4.57E-08	2.49E-09	25.3
7.24E-1	2.14E-05	1.11E-06	24.2	1.68E-06	8.29E-08	23.8	1.90E-07	8.95E-09	24.4	5.16E-08	2.43E-09	24.4
7.59E-1	2.59E-05	1.25E-06	22.5	1.97E-06	8.68E-08	22.4	2.06E-07	8.91E-09	23.6	5.58E-08	2.42E-09	23.7
7.94E-1	3.19E-05	1.43E-06	20.9	2.22E-06	9.88E-08	21.1	2.12E-07	9.35E-09	23.0	5.74E-08	2.53E-09	23.1
8.32E-1	3.70E-05	1.41E-06	20.0	2.33E-06	9.80E-08	20.7	2.07E-07	9.46E-09	23.0	5.58E-08	2.57E-09	23.2
8.71E-1	3.77E-05	1.54E-06	19.8	2.20E-06	9.54E-08	21.0	1.91E-07	8.87E-09	23.5	5.14E-08	2.40E-09	23.8
9.12E-1	3.23E-05	1.46E-06	20.9	1.88E-06	9.36E-08	22.1	1.71E-07	8.59E-09	24.3	4.56E-08	2.32E-09	24.5
9.55E-1	2.37E-05	1.14E-06	22.4	1.51E-06	7.72E-08	23.4	1.51E-07	7.99E-09	24.9	4.00E-08	2.16E-09	25.1
1.00E+0	1.72E-05	1.12E-06	23.9	1.22E-06	7.24E-08	24.5	1.36E-07	7.49E-09	25.4	3.61E-08	2.01E-09	25.6
1.05E+0	1.47E-05	9.07E-07	24.5	1.09E-06	6.33E-08	25.3	1.27E-07	7.14E-09	25.7	3.43E-08	1.94E-09	25.8
1.10E+0	1.50E-05	8.60E-07	24.2	1.05E-06	5.83E-08	25.6	1.22E-07	6.89E-09	25.8	3.40E-08	1.90E-09	25.8
1.15E+0	1.68E-05	8.77E-07	22.8	1.07E-06	5.66E-08	25.2	1.21E-07	6.83E-09	25.7	3.43E-08	1.90E-09	25.7
1.20E+0	1.98E-05	9.01E-07	21.1	1.11E-06	5.57E-08	24.6	1.21E-07	6.82E-09	25.7	3.45E-08	1.89E-09	25.7
1.26E+0	2.29E-05	1.04E-06	19.3	1.17E-06	5.64E-08	24.0	1.23E-07	6.82E-09	25.7	3.47E-08	1.89E-09	25.7
1.32E+0	2.49E-05	1.04E-06	18.1	1.23E-06	5.71E-08	23.5	1.25E-07	6.80E-09	25.7	3.51E-08	1.88E-09	25.7
1.38E+0	2.48E-05	1.07E-06	17.6	1.25E-06	5.80E-08	23.4	1.27E-07	6.84E-09	25.7	3.57E-08	1.90E-09	25.7
1.45E+0	2.25E-05	1.05E-06	17.9	1.22E-06	5.82E-08	23.5	1.30E-07	6.95E-09	25.7	3.65E-08	1.92E-09	25.7
1.51E+0	1.87E-05	9.05E-07	18.6	1.16E-06	5.69E-08	24.0	1.33E-07	7.06E-09	25.7	3.73E-08	1.95E-09	25.7
1.59E+0	1.50E-05	8.33E-07	19.4	1.09E-06	5.55E-08	24.6	1.36E-07	7.15E-09	25.7	3.81E-08	1.97E-09	25.7
1.66E+0	1.28E-05	7.20E-07	20.1	1.05E-06	5.43E-08	25.1	1.38E-07	7.25E-09	25.7	3.89E-08	2.00E-09	25.7
1.74E+0	1.23E-05	6.74E-07	20.5	1.04E-06	5.39E-08	25.3	1.41E-07	7.35E-09	25.7	3.95E-08	2.03E-09	25.7
1.82E+0	1.25E-05	6.38E-07	20.6	1.07E-06	5.44E-08	25.0	1.44E-07	7.48E-09	25.6	4.01E-08	2.06E-09	25.6
1.91E+0	1.25E-05	6.21E-07	20.7	1.11E-06	5.54E-08	24.4	1.48E-07	7.62E-09	25.3	4.08E-08	2.10E-09	25.3
2.00E+0	1.19E-05	5.95E-07	20.7	1.15E-06	5.62E-08	23.6	1.54E-07	7.73E-09	24.9	4.21E-08	2.12E-09	24.9
2.09E+0	1.12E-05	5.72E-07	20.9	1.20E-06	5.77E-08	22.9	1.62E-07	7.93E-09	24.5	4.43E-08	2.18E-09	24.4
2.19E+0	1.08E-05	5.62E-07	21.0	1.25E-06	5.99E-08	22.4	1.69E-07	8.22E-09	24.1	4.66E-08	2.26E-09	24.0
2.29E+0	1.07E-05	5.52E-07	21.0	1.27E-06	6.10E-08	22.5	1.73E-07	8.41E-09	24.1	4.80E-08	2.32E-09	24.0
2.40E+0	1.07E-05	5.42E-07	21.0	1.24E-06	6.02E-08	23.1	1.70E-07	8.41E-09	24.4	4.76E-08	2.33E-09	24.2
2.51E+0	1.09E-05	5.46E-07	20.8	1.15E-06	5.88E-08	23.9	1.63E-07	8.35E-09	24.8	4.55E-08	2.31E-09	24.7
2.63E+0	1.09E-05	5.44E-07	20.8	1.05E-06	5.77E-08	24.7	1.55E-07	8.31E-09	25.2	4.29E-08	2.30E-09	25.1
2.75E+0	1.09E-05	5.35E-07	20.8	9.75E-07	5.65E-08	25.4	1.49E-07	8.34E-09	25.6	4.07E-08	2.31E-09	25.5
2.88E+0	1.08E-05	5.30E-07	21.1	9.35E-07	5.67E-08	25.7	1.48E-07	8.56E-09	25.7	3.96E-08	2.36E-09	25.7
3.02E+0	1.06E-05	5.24E-07	21.4	9.36E-07	5.79E-08	25.7	1.49E-07	8.84E-09	25.7	3.95E-08	2.43E-09	25.7
3.16E+0	1.04E-05	5.07E-07	22.2	9.71E-07	5.82E-08	25.7	1.50E-07	8.89E-09	25.7	4.01E-08	2.45E-09	25.7
3.31E+0	1.01E-05	4.83E-07	23.1	1.02E-06	5.94E-08	25.7	1.51E-07	9.09E-09	25.7	4.11E-08	2.50E-09	25.7

Table 3.3.1 (Continued)

	102 mm			356 mm			711 mm			914 mm		
Neutron Energy [eV]	Flux [n/leth/ source]	Absolute Error	Window [%]	Flux [n/leth/ source]	Absolute Error	Window [%]	Flux [n/leth/ source]	Absolute Error	Wimdow [%]	Flux [n/leth/ source]	Absolute Error	Window [%]
3.47E+0	9.65E-06	4.84E-07	24.0	1.06E-06	6.50E-08	25.7	1.50E-07	1.00E-08	25.7	4.20E-08	2.77E-09	25.7
3.63E+0	9.16E-06	4.96E-07	24.8	1.07E-06	7.10E-08	25.7	1.49E-07	1.10E-08	25.7	4.20E-08	3.05E-09	25.7
3.80E+0	8.89E-06	4.67E-07	25.4	1.04E-06	7.08E-08	25.7	1.48E-07	1.09E-08	25.7	4.08E-08	3.03E-09	25.7
3.98E+0	8.77E-06	4.45E-07	25.7	1.00E-06	7.24E-08	25.7	1.48E-07	1.12E-08	25.7	3.88E-08	3.12E-09	25.7
4.17E+0	8.52E-06	4.66E-07	25.7	9.74E-07	7.78E-08	25.7	1.49E-07	1.21E-08	25.7	3.71E-08	3.38E-09	25.7
4.36E+0	7.94E-06	4.44E-07	25.7	9.76E-07	7.65E-08	25.7	1.47E-07	1.19E-08	25.7	3.69E-08	3.32E-09	25.7
4.57E+0	7.26E-06	4.86E-07	25.7	9.87E-07	8.65E-08	25.7	1.41E-07	1.34E-08	25.7	3.85E-08	3.74E-09	25.7
4.79E+0	6.93E-06	5.59E-07	25.7	9.73E-07	9.81E-08	25.7	1.35E-07	1.52E-08	25.7	4.07E-08	4.25E-09	25.7
5.01E+0	7.19E-06	4.51E-07	25.7	9.36E-07	8.06E-08	25.7	1.36E-07	1.25E-08	25.7	4.18E-08	3.50E-09	25.7
5.25E+0	7.56E-06	4.89E-07	25.7	9.21E-07	9.08E-08	25.7	1.46E-07	1.46E-08	25.7	4.09E-08	4.03E-09	25.7
5.49E+0	7.35E-06	6.49E-07	25.7	9.67E-07	1.20E-07	25.7	1.54E-07	1.94E-08	25.7	3.90E-08	5.32E-09	25.7
5.75E+0	6.49E-06	5.54E-07	25.7	1.03E-06	1.08E-07	25.7	1.49E-07	1.71E-08	25.7	3.79E-08	4.73E-09	25.7
6.03E+0	5.84E-06	5.46E-07	25.7	1.03E-06	1.08E-07	25.7	1.30E-07	1.66E-08	25.7	3.79E-08	4.64E-09	25.7
6.31E+0	6.10E-06	5.76E-07	25.7	9.20E-07	1.12E-07	25.7	1.12E-07	1.76E-08	25.7	3.74E-08	4.92E-09	25.7
6.61E+0	6.87E-06	4.64E-07	25.7	8.08E-07	9.21E-08	25.7	1.08E-07	1.44E-08	25.7	3.63E-08	4.02E-09	25.7
6.92E+0	7.23E-06	4.56E-07	25.5	8.39E-07	8.78E-08	24.7	1.32E-07	1.24E-08	23.6	3.86E-08	3.47E-09	23.8
7.24E+0	7.02E-06	4.08E-07	24.9	1.10E-06	8.54E-08	22.5	1.98E-07	1.24E-08	20.6	5.08E-08	3.40E-09	20.8
7.59E+0	6.82E-06	3.40E-07	24.1	1.54E-06	7.75E-08	20.1	2.95E-07	1.21E-08	17.3	7.29E-08	3.24E-09	17.4
7.94E+0	6.91E-06	3.36E-07	23.2	1.95E-06	7.63E-08	18.0	3.61E-07	1.11E-08	14.1	9.30E-08	2.96E-09	14.0
8.32E+0	6.83E-06	3.16E-07	23.2	2.04E-06	7.86E-08	16.7	3.44E-07	1.12E-08	11.5	9.67E-08	2.90E-09	11.0
8.71E+0	6.08E-06	2.80E-07	23.5	1.70E-06	7.06E-08	17.7	2.69E-07	9.79E-09	11.9	8.12E-08	2.62E-09	10.8
9.12E+0	4.77E-06	2.55E-07	24.0	1.17E-06	5.74E-08	19.9	1.91E-07	8.03E-09	14.9	5.66E-08	2.18E-09	13.7
9.55E+0	3.35E-06	2.46E-07	24.9	7.24E-07	5.17E-08	22.3	1.28E-07	6.27E-09	18.2	3.41E-08	1.53E-09	17.1
1.00E+1	2.18E-06	2.42E-07	25.7	4.51E-07	5.22E-08	24.4	7.49E-08	4.71E-09	21.4	1.86E-08	1.12E-09	20.5
1.05E+1	1.37E-06	2.24E-07	25.7	2.78E-07	4.86E-08	25.7	3.67E-08	2.96E-09	24.0	9.49E-09	7.20E-10	23.5
1.10E+1	9.01E-07	1.75E-07	25.7	1.60E-07	3.60E-08	25.7	1.51E-08	1.80E-09	25.7	4.40E-09	4.67E-10	25.7
1.15E+1	6.85E-07	1.16E-07	25.7	9.21E-08	1.84E-08	25.7	5.77E-09	9.51E-10	25.7	1.94E-09	2.70E-10	25.7
1.20E+1	5.80E-07	9.29E-08	25.7	5.91E-08	1.46E-08	25.7	2.70E-09	6.81E-10	25.7	9.25E-10	1.70E-10	25.7
1.26E+1	4.64E-07	9.29E-08	25.7	4.07E-08	2.25E-08	25.7	1.75E-09	7.10E-10	25.7	5.30E-10	1.54E-10	25.7
1.32E+1	3.07E-07	7.56E-08	25.7	2.56E-08	2.12E-08	25.7	1.17E-09	5.81E-10	25.7	3.18E-10	1.26E-10	25.7
1.38E+1	1.56E-07	4.47E-08	25.7	1.29E-08	1.33E-08	25.7	6.29E-10	3.37E-10	25.7	1.63E-10	7.56E-11	25.7
1.44E+1	5.85E-08	1.87E-08	25.7	4.86E-09	5.72E-09	25.7	2.49E-10	1.37E-10	25.7	6.30E-11	3.21E-11	25.7
1.51E+1	1.55E-08	5.38E-09	25.7	1.30E-09	1.66E-09	25.7	6.89E-11	3.86E-11	25.7	1.73E-11	9.33E-12	25.7

Table 3.3.2 Gamma-ray spectra at 102, 356, 711 and 914 mm from the front surface of the test region in the assembly #2 measured by the BC537 spectrometer.

	102 mm			356 mm			711 mm			914 mm		
Neutron Energy [MeV]	Flux [n/leth/ source]	Absolute Error	Window [%]	Flux [n/leth/ source]	Absolute Error	Window [%]	Flux [n/leth/ source]	Absolute Error	Wimdow [%]	Flux [n/leth/ source]	Absolute Error	Window [%]
3.02E-1	3.38E-05	1.59E-06	29.3	3.44E-06	1.65E-07	29.4	4.06E-07	1.97E-08	29.6	1.05E-07	5.06E-09	29.5
3.16E-1	3.21E-05	1.70E-06	29.0	3.32E-06	1.77E-07	29.1	3.96E-07	2.13E-08	29.2	1.01E-07	5.48E-09	29.2
3.31E-1	3.03E-05	1.62E-06	29.0	3.23E-06	1.69E-07	29.0	3.86E-07	2.02E-08	29.1	9.87E-08	5.21E-09	29.0
3.47E-1	2.91E-05	1.53E-06	28.9	3.20E-06	1.61E-07	28.9	3.81E-07	1.93E-08	28.9	9.77E-08	4.95E-09	28.9
3.63E-1	2.89E-05	1.49E-06	28.5	3.19E-06	1.58E-07	28.6	3.80E-07	1.91E-08	28.6	9.77E-08	4.90E-09	28.6
3.80E-1	2.94E-05	1.52E-06	28.0	3.19E-06	1.64E-07	28.2	3.83E-07	1.99E-08	28.2	9.86E-08	5.10E-09	28.1
3.98E-1	3.02E-05	1.53E-06	27.4	3.24E-06	1.69E-07	27.5	3.94E-07	2.09E-08	27.4	1.02E-07	5.36E-09	27.4
4.17E-1	3.13E-05	1.53E-06	26.7	3.37E-06	1.71E-07	26.7	4.19E-07	2.17E-08	26.4	1.08E-07	5.57E-09	26.3
4.37E-1	3.30E-05	1.56E-06	26.0	3.66E-06	1.75E-07	25.5	4.68E-07	2.23E-08	25.2	1.21E-07	5.72E-09	25.1
4.57E-1	3.52E-05	1.63E-06	25.4	4.16E-06	1.98E-07	24.1	5.43E-07	2.50E-08	23.7	1.40E-07	6.41E-09	23.6
4.79E-1	3.68E-05	1.71E-06	25.0	4.80E-06	2.26E-07	22.9	6.30E-07	2.94E-08	22.4	1.62E-07	7.57E-09	22.3
5.01E-1	3.70E-05	1.72E-06	24.9	5.33E-06	2.19E-07	22.3	6.95E-07	2.85E-08	21.9	1.78E-07	7.31E-09	21.9
5.25E-1	3.57E-05	1.67E-06	25.1	5.40E-06	2.25E-07	22.3	6.94E-07	2.81E-08	22.1	1.76E-07	7.14E-09	22.1
5.49E-1	3.33E-05	1.70E-06	25.5	4.83E-06	2.42E-07	23.1	6.07E-07	3.03E-08	23.0	1.54E-07	7.78E-09	23.0
5.75E-1	3.05E-05	1.63E-06	26.0	3.82E-06	1.99E-07	24.3	4.66E-07	2.44E-08	24.2	1.20E-07	6.26E-09	24.2
6.03E-1	2.80E-05	1.55E-06	26.3	2.87E-06	1.82E-07	25.3	3.39E-07	2.19E-08	25.4	8.99E-08	5.56E-09	25.4
6.31E-1	2.67E-05	1.51E-06	26.4	2.39E-06	1.66E-07	25.9	2.76E-07	2.01E-08	25.8	7.35E-08	5.09E-09	25.9
6.61E-1	2.72E-05	1.46E-06	25.9	2.39E-06	1.37E-07	25.8	2.76E-07	1.61E-08	25.5	7.15E-08	4.06E-09	25.7
6.92E-1	2.94E-05	1.52E-06	25.1	2.66E-06	1.38E-07	24.8	3.11E-07	1.59E-08	24.4	7.82E-08	3.97E-09	24.7
7.24E-1	3.30E-05	1.63E-06	23.8	3.01E-06	1.41E-07	23.6	3.58E-07	1.67E-08	23.2	8.77E-08	4.07E-09	23.5
7.59E-1	3.81E-05	1.82E-06	22.1	3.36E-06	1.48E-07	22.2	3.97E-07	1.69E-08	22.1	9.56E-08	4.12E-09	22.5
7.94E-1	4.49E-05	2.03E-06	20.6	3.65E-06	1.64E-07	21.0	4.08E-07	1.78E-08	21.6	9.89E-08	4.35E-09	21.8
8.32E-1	5.20E-05	1.97E-06	19.7	3.78E-06	1.61E-07	20.6	3.86E-07	1.79E-08	22.0	9.59E-08	4.37E-09	22.0
8.71E-1	5.46E-05	2.27E-06	19.5	3.65E-06	1.65E-07	20.7	3.42E-07	1.60E-08	22.9	8.73E-08	4.09E-09	22.6
9.12E-1	4.81E-05	2.18E-06	20.6	3.22E-06	1.64E-07	21.7	2.93E-07	1.58E-08	24.0	7.63E-08	4.05E-09	23.6
9.55E-1	3.55E-05	1.60E-06	22.1	2.66E-06	1.31E-07	23.0	2.53E-07	1.37E-08	24.9	6.66E-08	3.49E-09	24.5
1.00E+0	2.48E-05	1.52E-06	23.6	2.19E-06	1.21E-07	24.1	2.28E-07	1.19E-08	25.6	6.05E-08	3.13E-09	25.2
1.05E+0	2.03E-05	1.22E-06	24.3	1.91E-06	1.05E-07	25.0	2.18E-07	1.14E-08	25.8	5.77E-08	2.99E-09	25.5
1.10E+0	2.02E-05	1.15E-06	24.2	1.79E-06	9.76E-08	25.5	2.16E-07	1.10E-08	25.8	5.67E-08	2.87E-09	25.7
1.15E+0	2.18E-05	1.15E-06	22.9	1.78E-06	9.16E-08	25.3	2.16E-07	1.09E-08	25.7	5.58E-08	2.80E-09	25.7
1.20E+0	2.45E-05	1.17E-06	21.3	1.82E-06	8.91E-08	25.0	2.13E-07	1.07E-08	25.7	5.46E-08	2.74E-09	25.7
1.26E+0	2.79E-05	1.33E-06	19.6	1.88E-06	9.00E-08	24.7	2.10E-07	1.06E-08	25.7	5.37E-08	2.73E-09	25.7
1.32E+0	3.09E-05	1.37E-06	18.5	1.93E-06	9.12E-08	24.3	2.10E-07	1.08E-08	25.7	5.36E-08	2.75E-09	25.6
1.38E+0	3.20E-05	1.45E-06	17.9	1.94E-06	9.25E-08	24.0	2.12E-07	1.09E-08	25.5	5.44E-08	2.77E-09	25.4
1.45E+0	3.04E-05	1.40E-06	17.8	1.92E-06	9.26E-08	23.7	2.18E-07	1.10E-08	25.1	5.58E-08	2.79E-09	25.1
1.51E+0	2.69E-05	1.29E-06	18.2	1.90E-06	9.18E-08	23.5	2.26E-07	1.12E-08	24.6	5.78E-08	2.81E-09	24.8
1.58E+0	2.31E-05	1.17E-06	18.9	1.90E-06	9.22E-08	23.2	2.37E-07	1.14E-08	24.1	5.97E-08	2.86E-09	24.5
1.66E+0	2.00E-05	1.05E-06	19.8	1.92E-06	9.36E-08	23.1	2.47E-07	1.18E-08	23.7	6.11E-08	2.92E-09	24.3
1.74E+0	1.76E-05	9.63E-07	20.6	1.94E-06	9.48E-08	23.2	2.53E-07	1.22E-08	23.6	6.16E-08	2.97E-09	24.4
1.82E+0	1.62E-05	8.81E-07	21.3	1.93E-06	9.52E-08	23.6	2.51E-07	1.23E-08	23.9	6.11E-08	3.01E-09	24.6
1.91E+0	1.54E-05	8.43E-07	21.7	1.87E-06	9.51E-08	24.1	2.42E-07	1.23E-08	24.4	5.99E-08	3.02E-09	24.8
2.00E+0	1.51E-05	8.12E-07	21.7	1.79E-06	9.30E-08	24.6	2.30E-07	1.21E-08	24.9	5.87E-08	2.99E-09	25.1
2.09E+0	1.51E-05	7.91E-07	21.4	1.72E-06	8.96E-08	25.0	2.21E-07	1.17E-08	25.4	5.82E-08	2.97E-09	25.2
2.19E+0	1.57E-05	8.03E-07	20.8	1.73E-06	8.97E-08	24.9	2.19E-07	1.17E-08	25.7	5.87E-08	3.00E-09	25.2
2.29E+0	1.67E-05	8.11E-07	20.3	1.80E-06	9.14E-08	24.6	2.23E-07	1.18E-08	25.6	6.00E-08	3.03E-09	25.1
2.40E+0	1.75E-05	8.13E-07	20.0	1.88E-06	9.28E-08	24.2	2.32E-07	1.18E-08	25.4	6.16E-08	3.04E-09	25.0
2.51E+0	1.76E-05	8.29E-07	19.9	1.94E-06	9.50E-08	23.9	2.43E-07	1.21E-08	25.2	6.32E-08	3.10E-09	24.8
2.63E+0	1.70E-05	8.32E-07	20.3	1.98E-06	9.74E-08	23.6	2.54E-07	1.24E-08	24.9	6.44E-08	3.17E-09	24.7
2.75E+0	1.58E-05	7.94E-07	20.9	1.99E-06	9.80E-08	23.6	2.61E-07	1.27E-08	24.6	6.51E-08	3.20E-09	24.8
2.88E+0	1.49E-05	7.39E-07	21.9	2.01E-06	9.77E-08	23.8	2.65E-07	1.28E-08	24.7	6.53E-08	3.20E-09	25.0
3.02E+0	1.47E-05	7.20E-07	23.0	2.04E-06	9.82E-08	24.2	2.66E-07	1.30E-08	24.9	6.51E-08	3.23E-09	25.2
3.16E+0	1.48E-05	7.72E-07	24.0	2.07E-06	1.02E-07	24.6	2.67E-07	1.35E-08	25.2	6.48E-08	3.38E-09	25.4
3.31E+0	1.45E-05	8.50E-07	24.8	2.07E-06	1.08E-07	25.1	2.69E-07	1.44E-08	25.4	6.43E-08	3.60E-09	25.6

Table 3.3.2 (Continued)

	102 mm			356 mm			711 mm			914 mm		
Neutron Energy [eV]	Flux [n/leth/ source]	Absolute Error	Window [%]	Flux [n/leth/ source]	Absolute Error	Window [%]	Flux [n/leth/ source]	Absolute Error	Wimdow [%]	Flux [n/leth/ source]	Absolute Error	Window [%]
3.47E+0	1.38E-05	8.73E-07	25.5	2.02E-06	1.10E-07	25.5	2.73E-07	1.47E-08	25.7	6.41E-08	3.70E-09	25.7
3.63E+0	1.33E-05	8.07E-07	25.7	1.96E-06	1.03E-07	25.7	2.76E-07	1.40E-08	25.7	6.49E-08	3.54E-09	25.7
3.80E+0	1.38E-05	8.50E-07	25.7	1.90E-06	1.04E-07	25.7	2.72E-07	1.44E-08	25.7	6.77E-08	3.60E-09	25.7
3.98E+0	1.49E-05	1.22E-06	25.7	1.89E-06	1.38E-07	25.7	2.66E-07	1.90E-08	25.7	7.25E-08	4.70E-09	25.7
4.17E+0	1.58E-05	1.53E-06	25.7	1.97E-06	1.72E-07	25.7	2.62E-07	2.39E-08	25.7	7.75E-08	5.83E-09	25.7
4.37E+0	1.56E-05	1.41E-06	25.7	2.08E-06	1.62E-07	25.7	2.70E-07	2.33E-08	25.7	7.91E-08	5.55E-09	25.7
4.57E+0	1.46E-05	1.13E-06	25.7	2.15E-06	1.30E-07	25.7	2.85E-07	1.88E-08	25.7	7.55E-08	4.45E-09	25.7
4.79E+0	1.35E-05	1.12E-06	25.7	2.09E-06	1.30E-07	25.7	2.96E-07	1.71E-08	25.7	6.93E-08	4.41E-09	25.7
5.01E+0	1.34E-05	1.21E-06	25.7	1.96E-06	1.38E-07	25.7	2.92E-07	1.67E-08	25.7	6.63E-08	4.74E-09	25.7
5.25E+0	1.39E-05	1.40E-06	25.7	1.91E-06	1.52E-07	25.7	2.79E-07	1.50E-08	25.7	7.00E-08	5.11E-09	25.7
5.50E+0	1.37E-05	1.45E-06	25.7	2.04E-06	1.63E-07	25.7	2.79E-07	1.27E-08	25.7	7.69E-08	5.54E-09	25.7
5.75E+0	1.23E-05	1.32E-06	25.7	2.24E-06	1.46E-07	25.7	3.00E-07	1.17E-08	25.1	7.97E-08	5.19E-09	25.7
6.03E+0	1.05E-05	1.41E-06	25.7	2.33E-06	1.30E-07	25.7	3.24E-07	1.57E-08	23.6	7.61E-08	4.71E-09	25.7
6.31E+0	9.80E-06	1.26E-06	25.7	2.26E-06	1.14E-07	25.1	3.31E-07	2.42E-08	21.7	7.10E-08	4.27E-09	25.4
6.61E+0	1.02E-05	1.15E-06	25.7	2.20E-06	9.82E-08	23.8	3.37E-07	2.82E-08	19.6	6.96E-08	3.77E-09	24.2
6.92E+0	1.05E-05	1.22E-06	25.7	2.30E-06	9.89E-08	22.1	3.68E-07	3.04E-08	17.7	7.35E-08	3.71E-09	22.2
7.24E+0	9.89E-06	1.01E-06	25.7	2.49E-06	1.12E-07	20.0	3.96E-07	3.28E-08	16.5	8.61E-08	4.19E-09	19.4
7.59E+0	9.01E-06	8.89E-07	25.7	2.66E-06	1.28E-07	18.0	3.78E-07	2.71E-08	16.6	1.07E-07	4.76E-09	16.5
7.94E+0	8.65E-06	8.59E-07	25.7	2.66E-06	1.24E-07	17.3	3.29E-07	2.37E-08	18.6	1.20E-07	4.24E-09	14.4
8.32E+0	8.61E-06	8.00E-07	25.7	2.38E-06	1.10E-07	18.2	2.80E-07	1.77E-08	20.6	1.04E-07	4.07E-09	13.9
8.71E+0	8.28E-06	7.66E-07	25.7	1.87E-06	1.01E-07	19.9	2.29E-07	1.68E-08	22.6	7.46E-08	3.37E-09	15.9
9.12E+0	7.42E-06	7.35E-07	25.7	1.37E-06	8.19E-08	22.0	1.79E-07	2.11E-08	24.4	5.15E-08	2.57E-09	18.7
9.55E+0	6.23E-06	7.17E-07	25.7	9.99E-07	6.65E-08	24.0	1.33E-07	2.78E-08	25.7	3.62E-08	2.29E-09	21.6
1.00E+1	4.97E-06	6.93E-07	25.7	7.41E-07	5.87E-08	25.4	9.38E-08	3.05E-08	25.7	2.40E-08	2.13E-09	24.1
1.05E+1	3.89E-06	6.39E-07	25.7	5.29E-07	4.96E-08	25.7	6.26E-08	2.39E-08	25.7	1.43E-08	1.76E-09	25.7
1.10E+1	3.10E-06	5.63E-07	25.7	3.43E-07	3.74E-08	25.7	4.34E-08	1.34E-08	25.7	7.59E-09	1.14E-09	25.7
1.15E+1	2.54E-06	5.01E-07	25.7	1.98E-07	2.60E-08	25.7	3.62E-08	2.02E-08	25.7	3.56E-09	5.57E-10	25.7
1.20E+1	2.05E-06	4.65E-07	25.7	1.05E-07	1.87E-08	25.7	3.43E-08	3.08E-08	25.7	1.59E-09	8.41E-10	25.7
1.26E+1	1.48E-06	4.15E-07	25.7	5.53E-08	1.57E-08	25.7	2.99E-08	3.06E-08	25.7	7.54E-10	9.22E-10	25.7
1.32E+1	8.85E-07	3.13E-07	25.7	2.85E-08	1.23E-08	25.7	2.09E-08	2.18E-08	25.7	3.75E-10	7.14E-10	25.7
1.38E+1	4.13E-07	1.80E-07	25.7	1.30E-08	7.37E-09	25.7	1.10E-08	1.13E-08	25.7	1.66E-10	3.95E-10	25.7
1.45E+1	1.44E-07	7.53E-08	25.7	4.73E-09	3.16E-09	25.7	4.18E-09	4.31E-09	25.7	5.62E-11	1.55E-10	25.7
1.51E+1	3.60E-08	2.18E-08	25.7	1.26E-09	9.26E-10	25.7	1.12E-09	1.16E-09	25.7	1.37E-11	4.19E-11	25.7

Table 3.4.1 Contribution of neutron response to total one for MSO and SSO.

Position	#1 MSO	#1 SSO	#2 MSO	#2 SSO
-1 mm	39.1 %	25.8 %	41.5 %	22.6 %
102	24.1	13.2	25.8	13.1
229	19.1	10.9	15.4	8.4
356	12.6	8.0	10.5	5.0
533	6.3	3.6	5.2	2.7
711	3.3	1.8	3.0	1.4
914	1.8	1.1	1.8	0.8

Table 3.4.2 Measured gamma-ray heating rates of SS316 by the TLD.

(a) Assembly #1

Distance from the front surface of the test region [mm]	Gamma-ray Heating Rate [Gy/Source Neutron]	Absolute Error
-1	5.22E-16	1.16E-16
102	3.44E-16	5.96E-17
229	8.33E-17	1.20E-17
356	3.06E-17	5.33E-18
533	1.28E-17	2.17E-18
711	5.13E-18	7.84E-19
914	1.40E-18	2.02E-19

(b) Assembly #2

Distance from the front surface of the test region [mm]	Gamma-ray Heating Rate [Gy/Source Neutron]	Absolute Error
-1	9.48E-16	1.72E-16
102	3.93E-16	5.35E-17
229	1.28E-16	1.85E-17
356	5.85E-17	7.40E-18
533	2.31E-17	3.11E-18
711	8.47E-18	1.10E-18
914	2.27E-18	2.93E-19

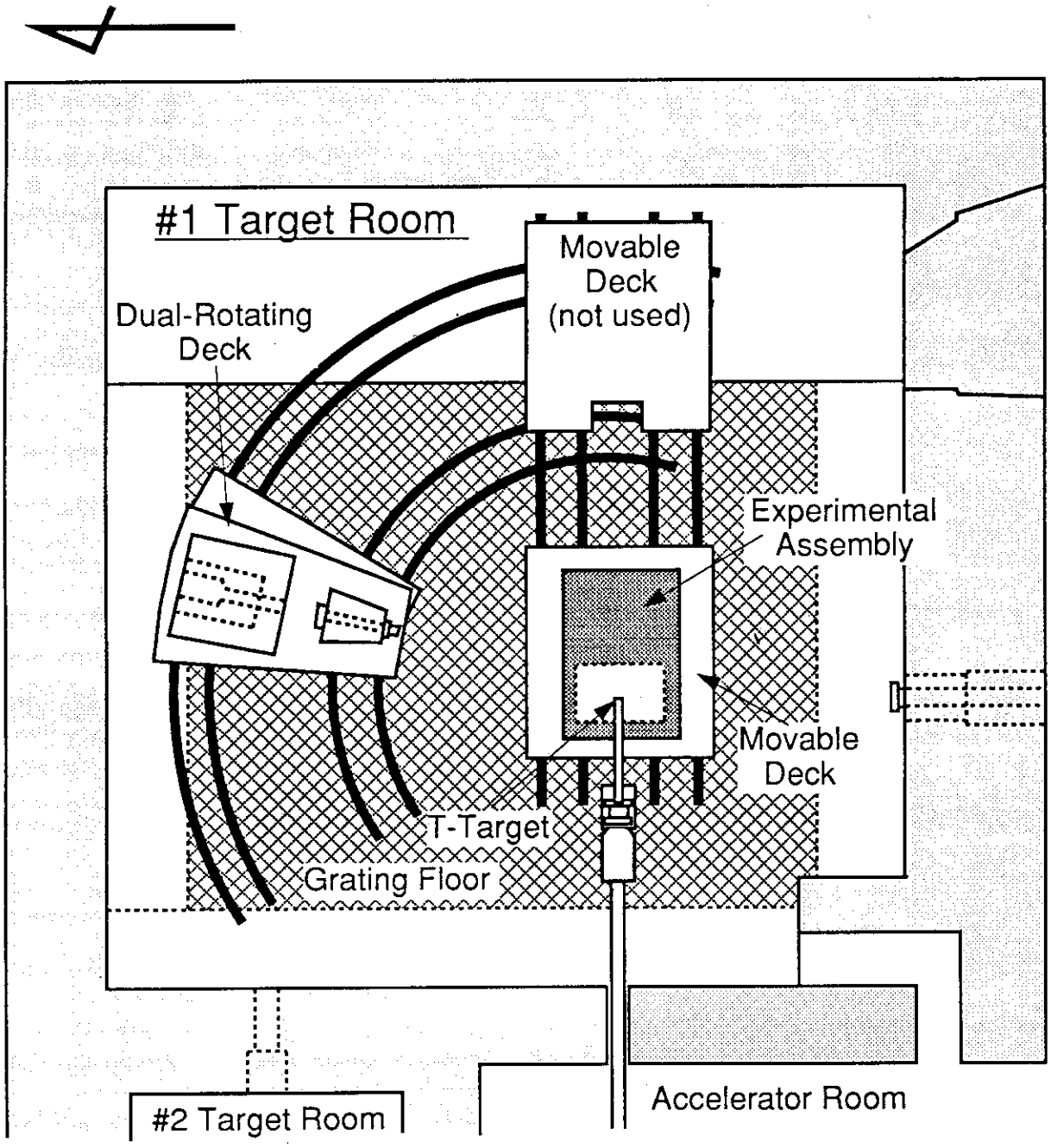

Fig. 2.1.1 Layout of the FNS first target room.

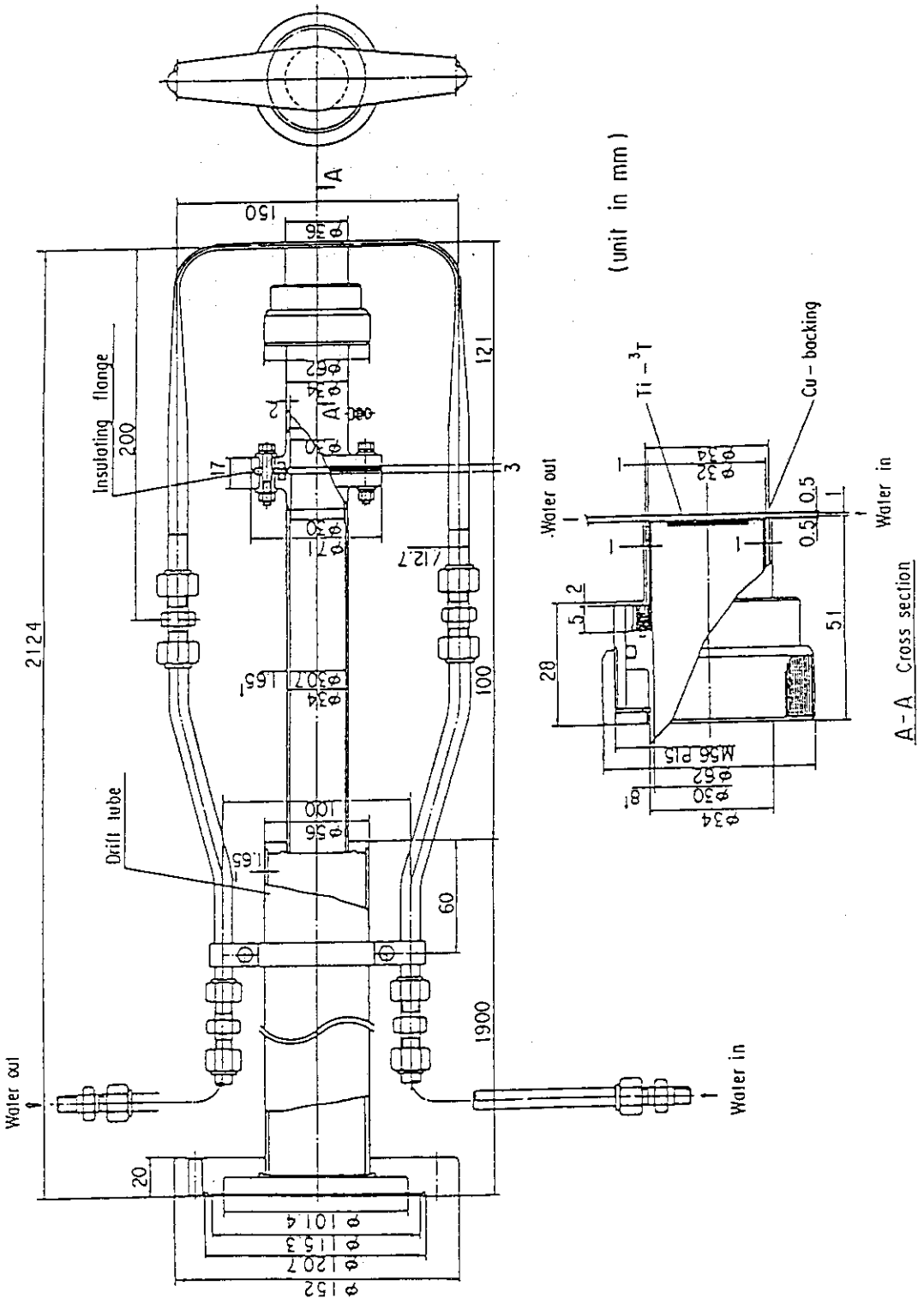

Fig. 2.1.2 Structure of the FNS fast water cooled tritium target for the 80° beam line.

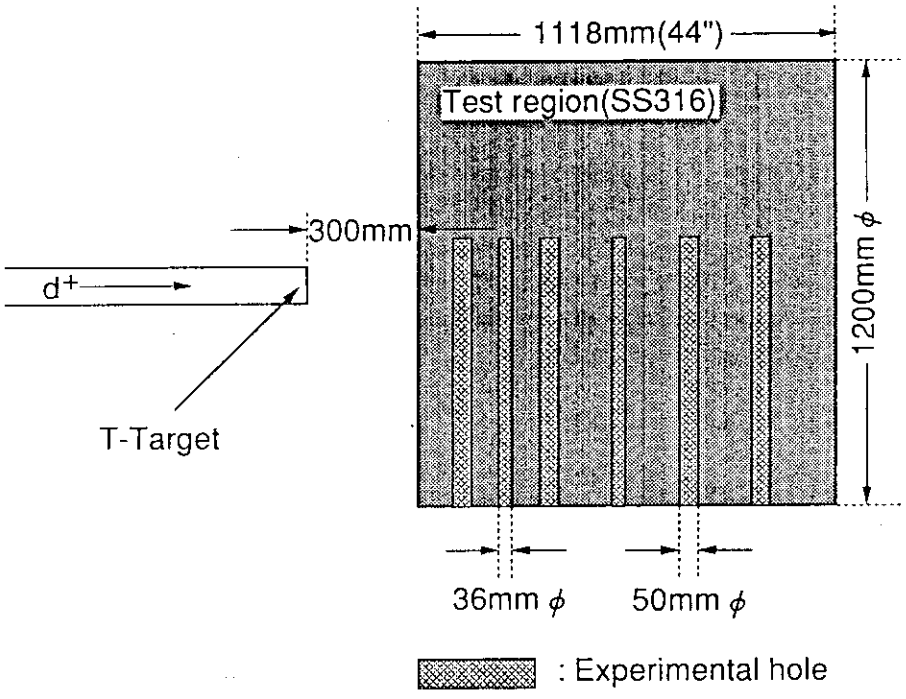

Fig. 2.2.1 Experimental assembly #1.

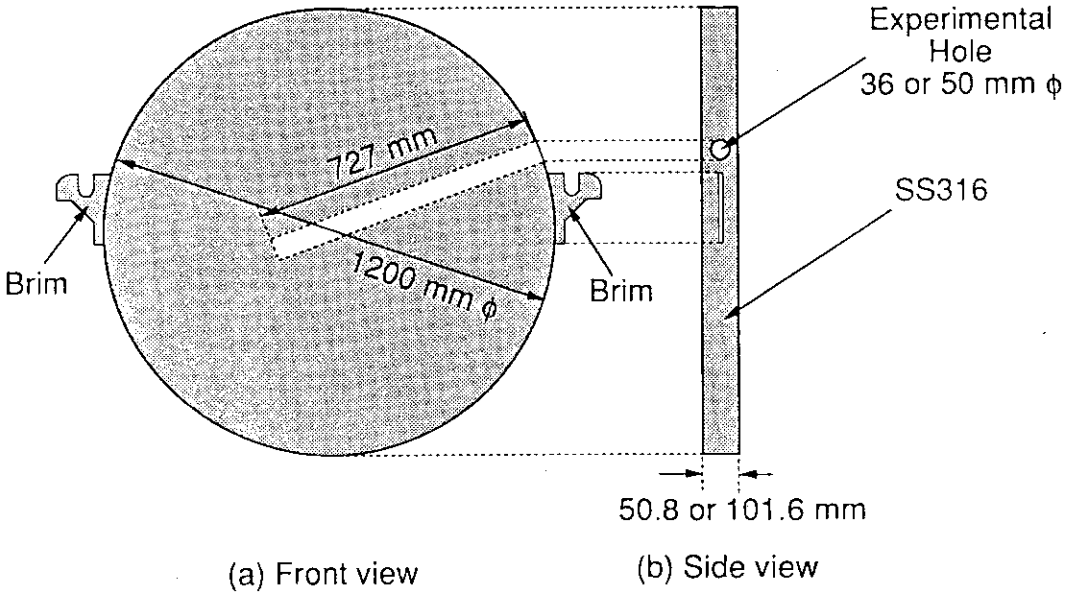

Fig. 2.2.2 Structure of SS316 disk with an experimental hole.

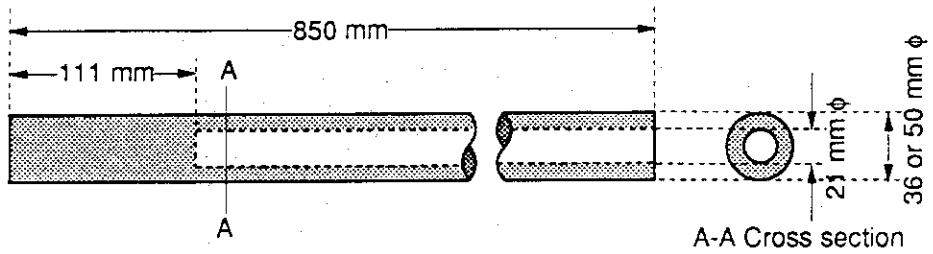

(a) for NE213 Scintillation Detector

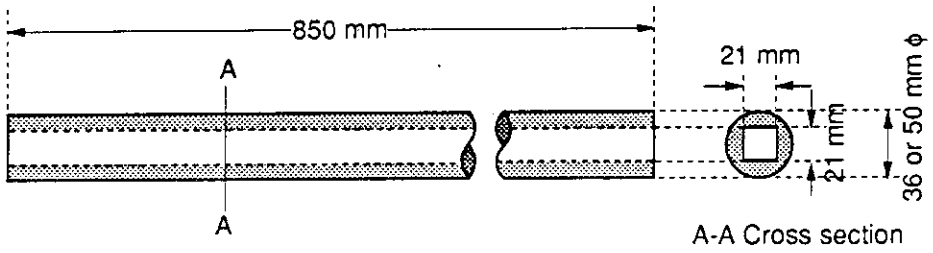

(b) for Proton Recoil Gas Proportional Counter

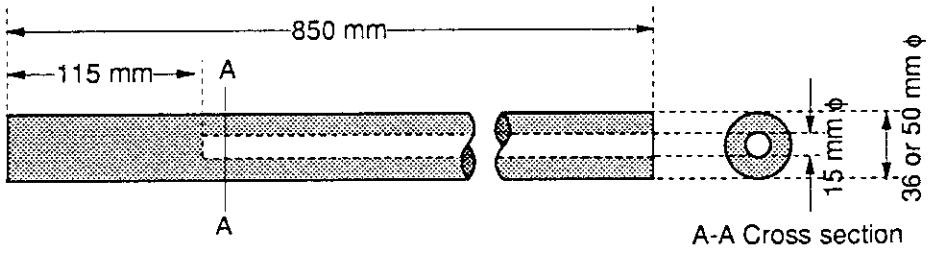

(c) for BF_3 Gas Proportional Counter

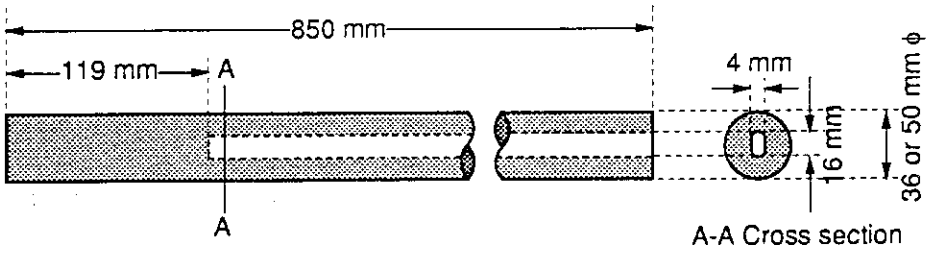

(d) for Micro Fission Chamber

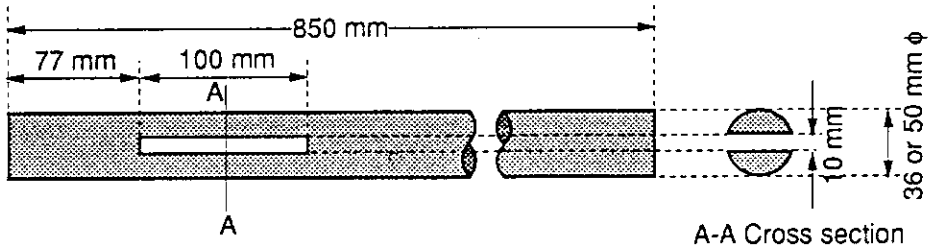

(e) for Activation Foil and TLD

Fig. 2.2.3 Structure of detector adapters.

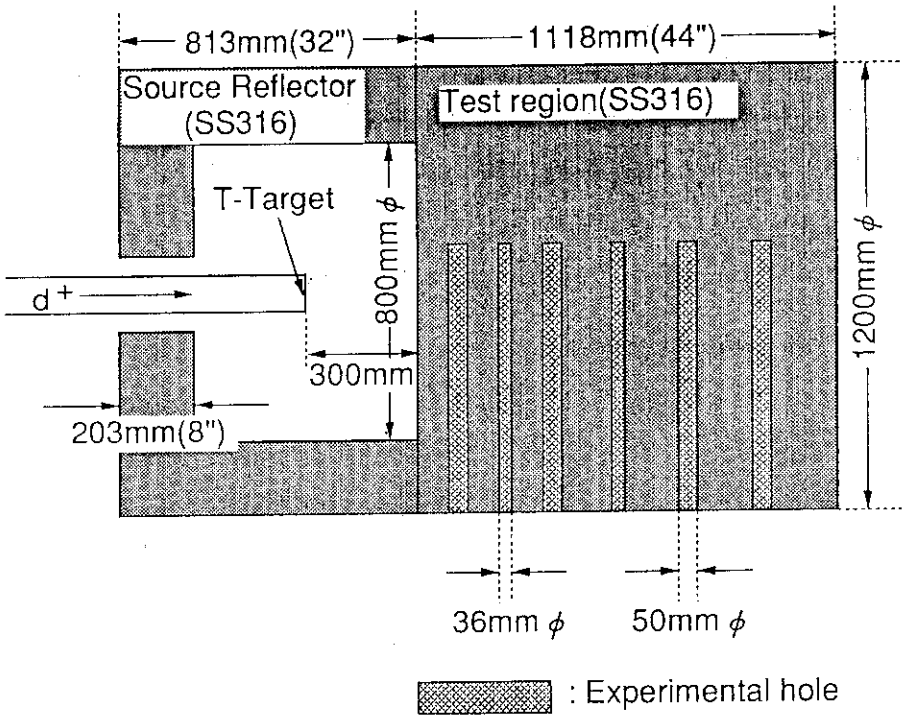

Fig. 2.2.4 Experimental assembly #2.

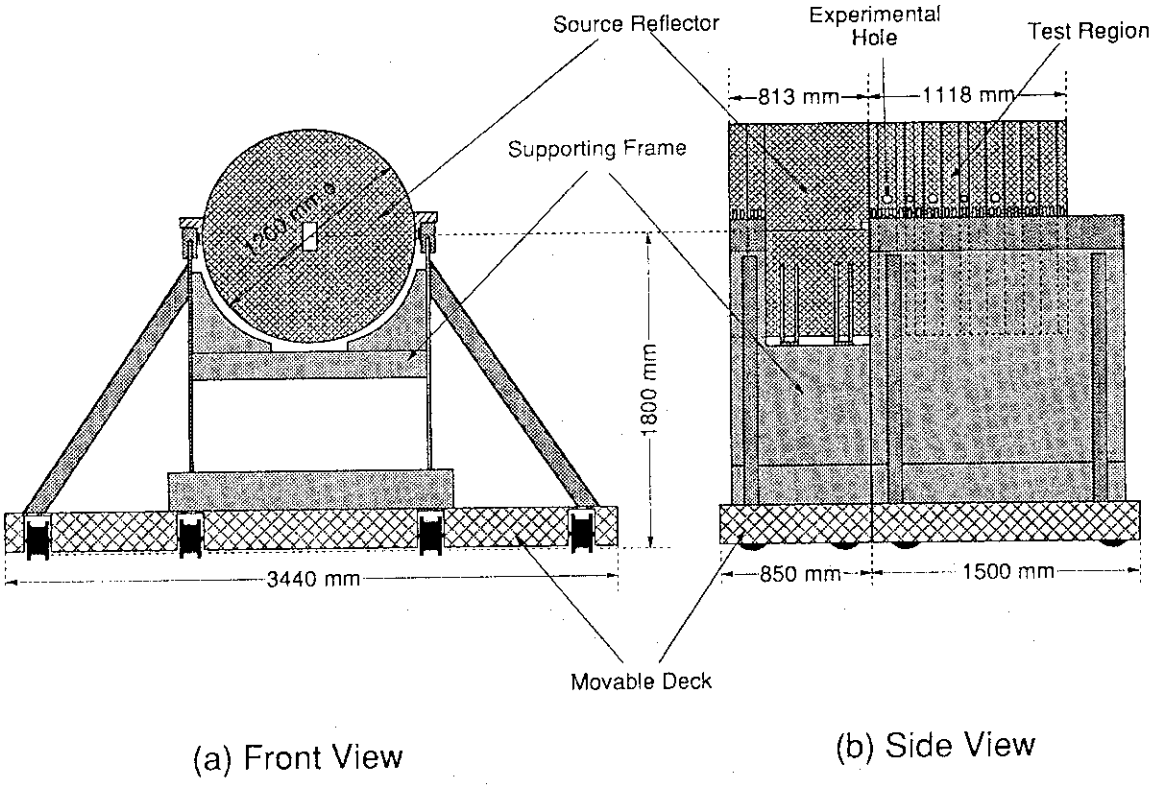

Fig. 2.2.5 Overview of the experimental assembly #2, supporting frame and movable deck.

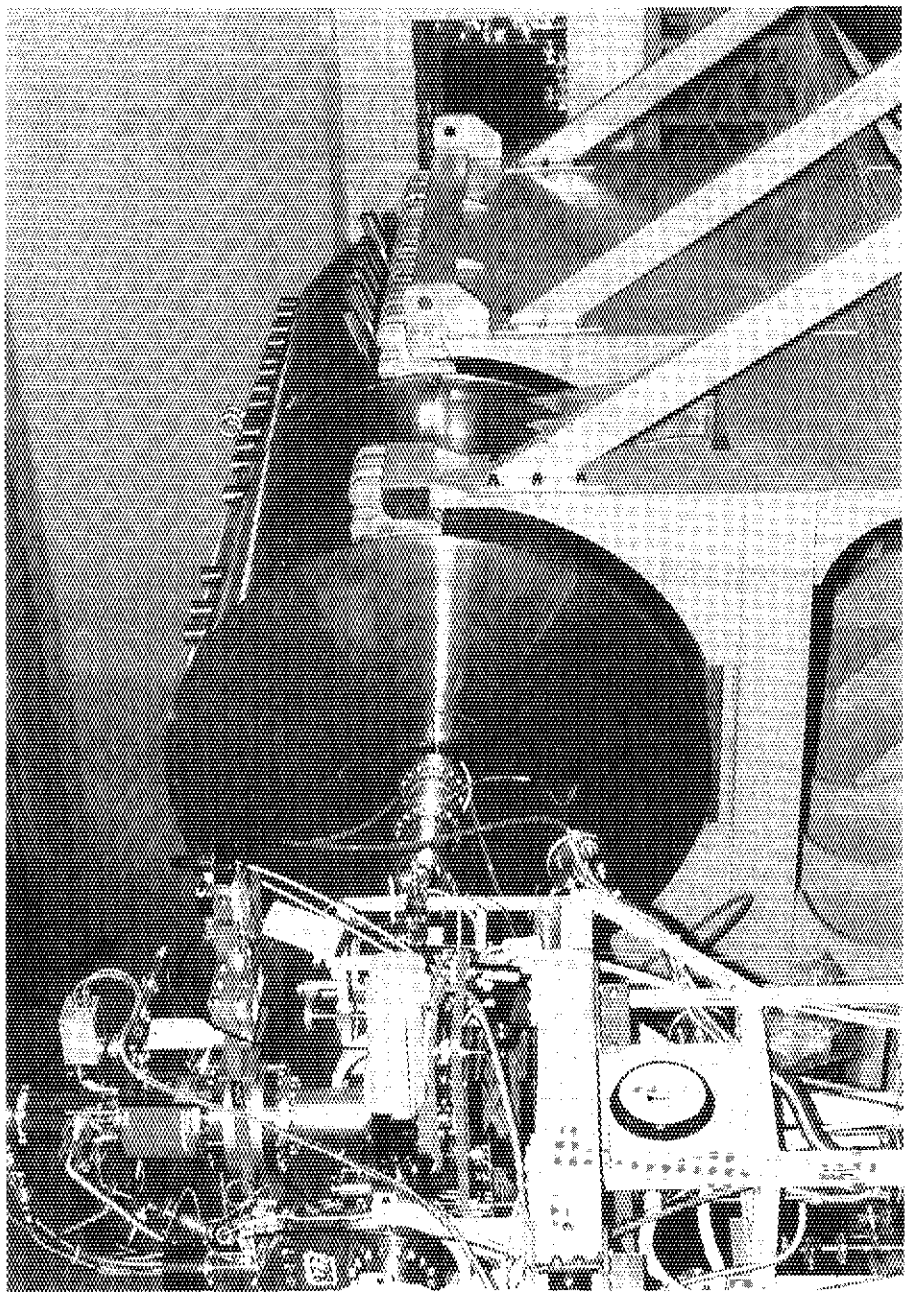

Fig. 2.2.6 Photograph of the experimental assembly #2 and supporting frame.

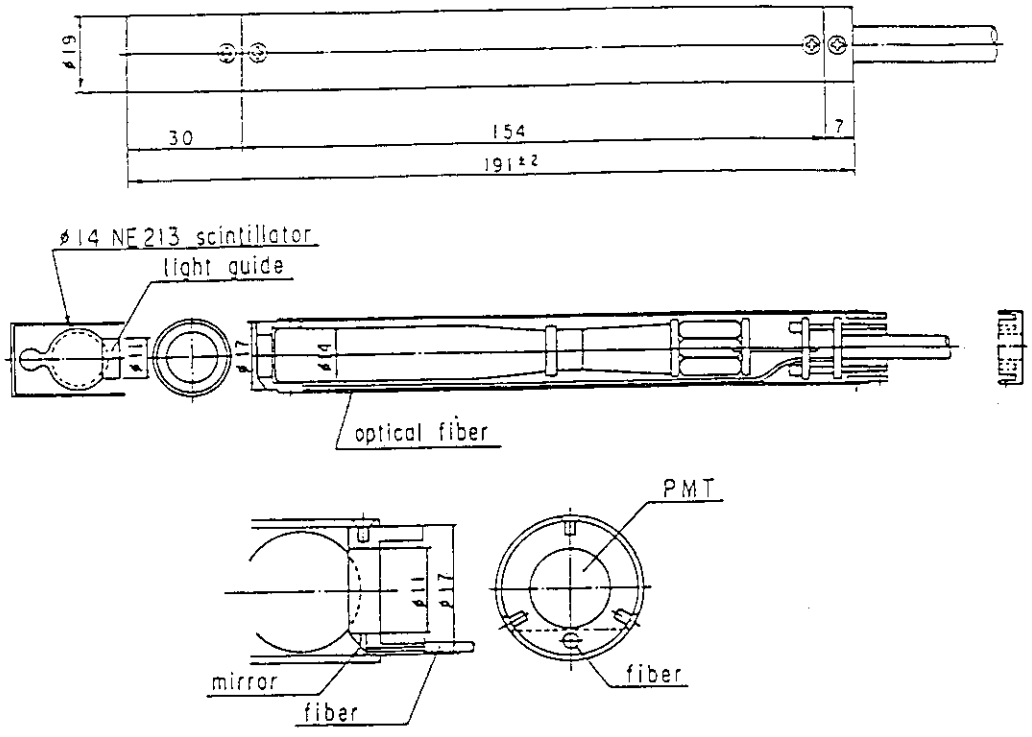

Fig. 3.1.1.1 Cross sectional view of small sphere NE213 scintillation detector.

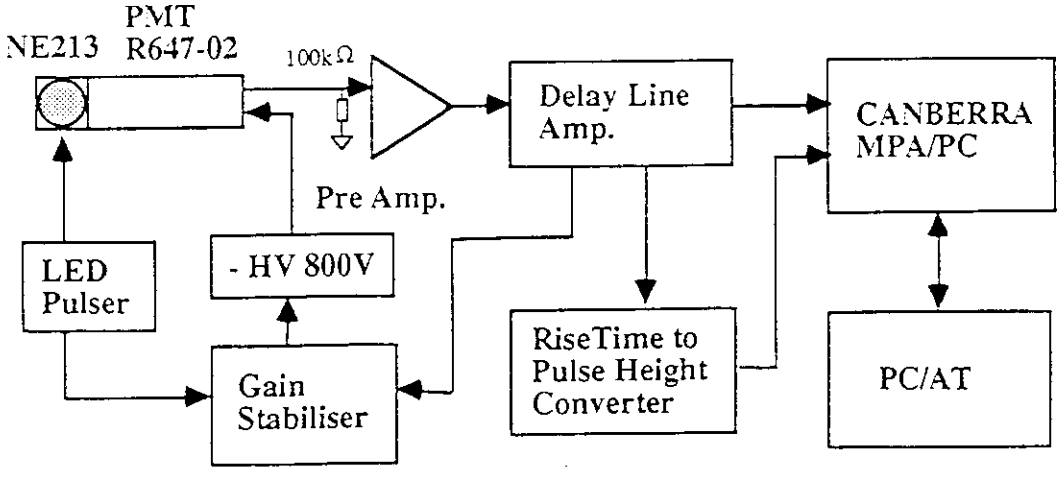

Fig. 3.1.1.2 Block diagram of electronic circuit for small sphere NE213 scintillation detector.

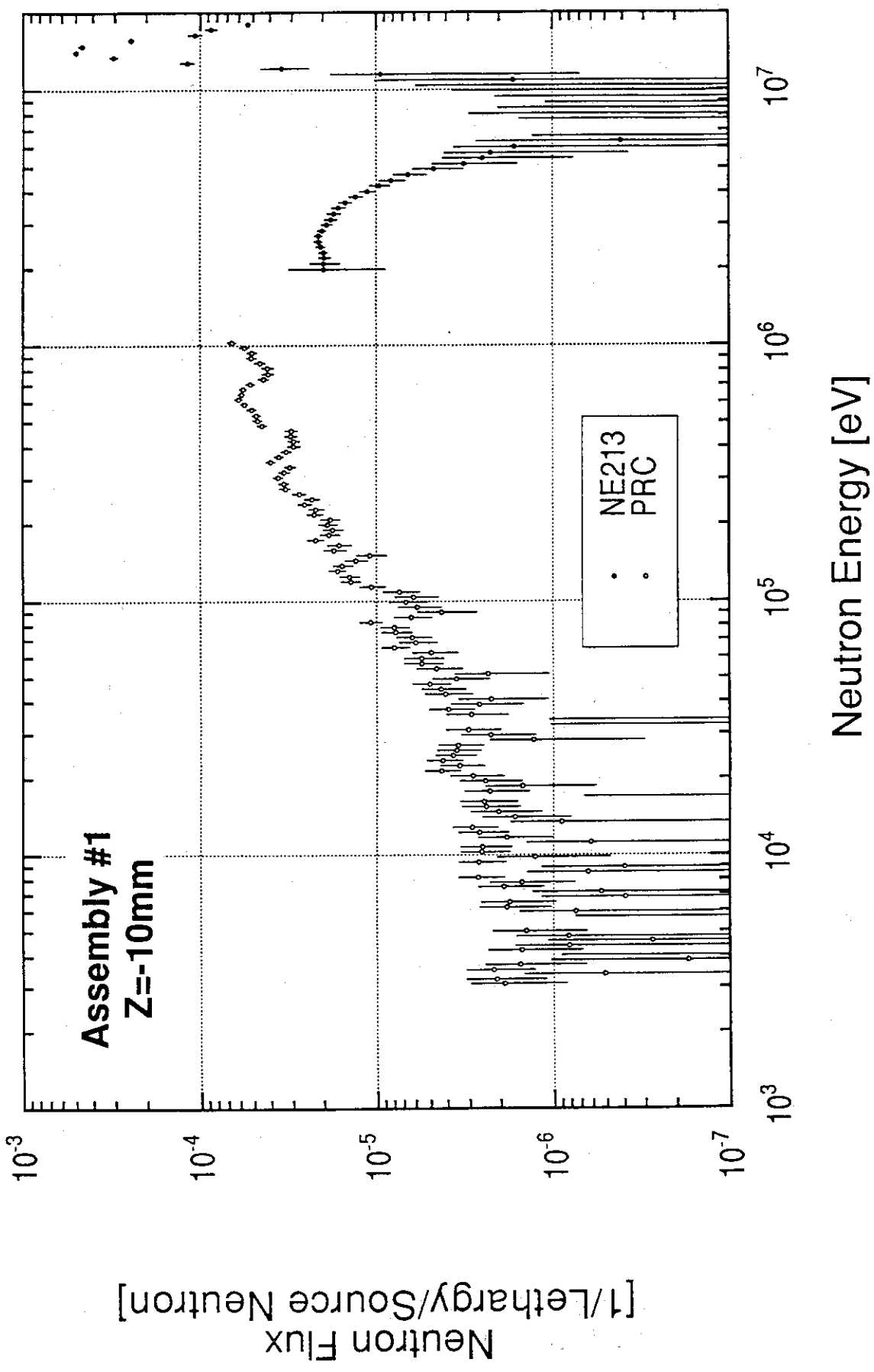

Fig. 3.1.1.3 The measured neutron spectrum at the front surface of the test region in the assembly #1.

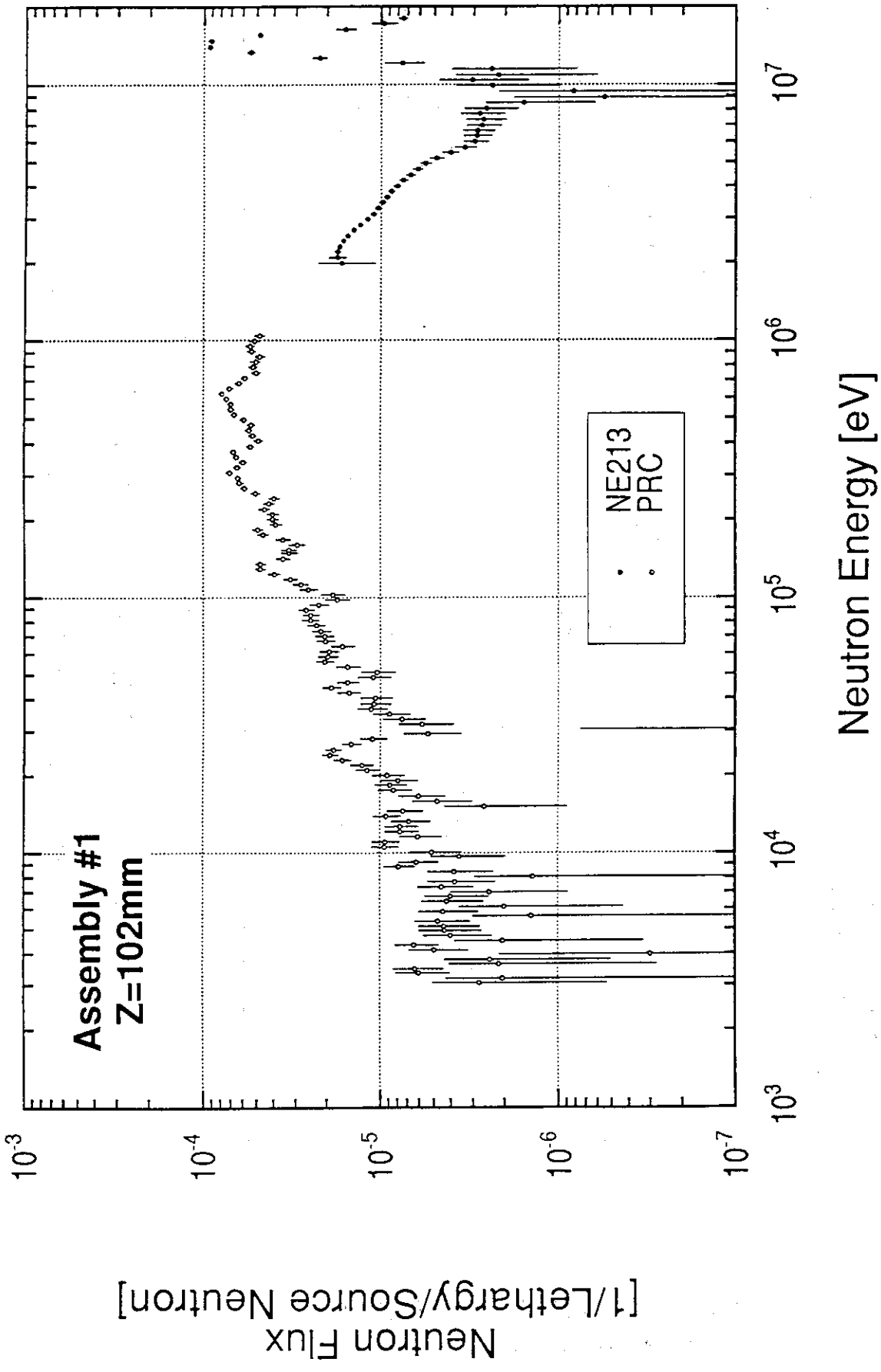

Fig. 3.1.1.4 The measured neutron spectrum at 102 mm from the front surface of the test region in the assembly #1.

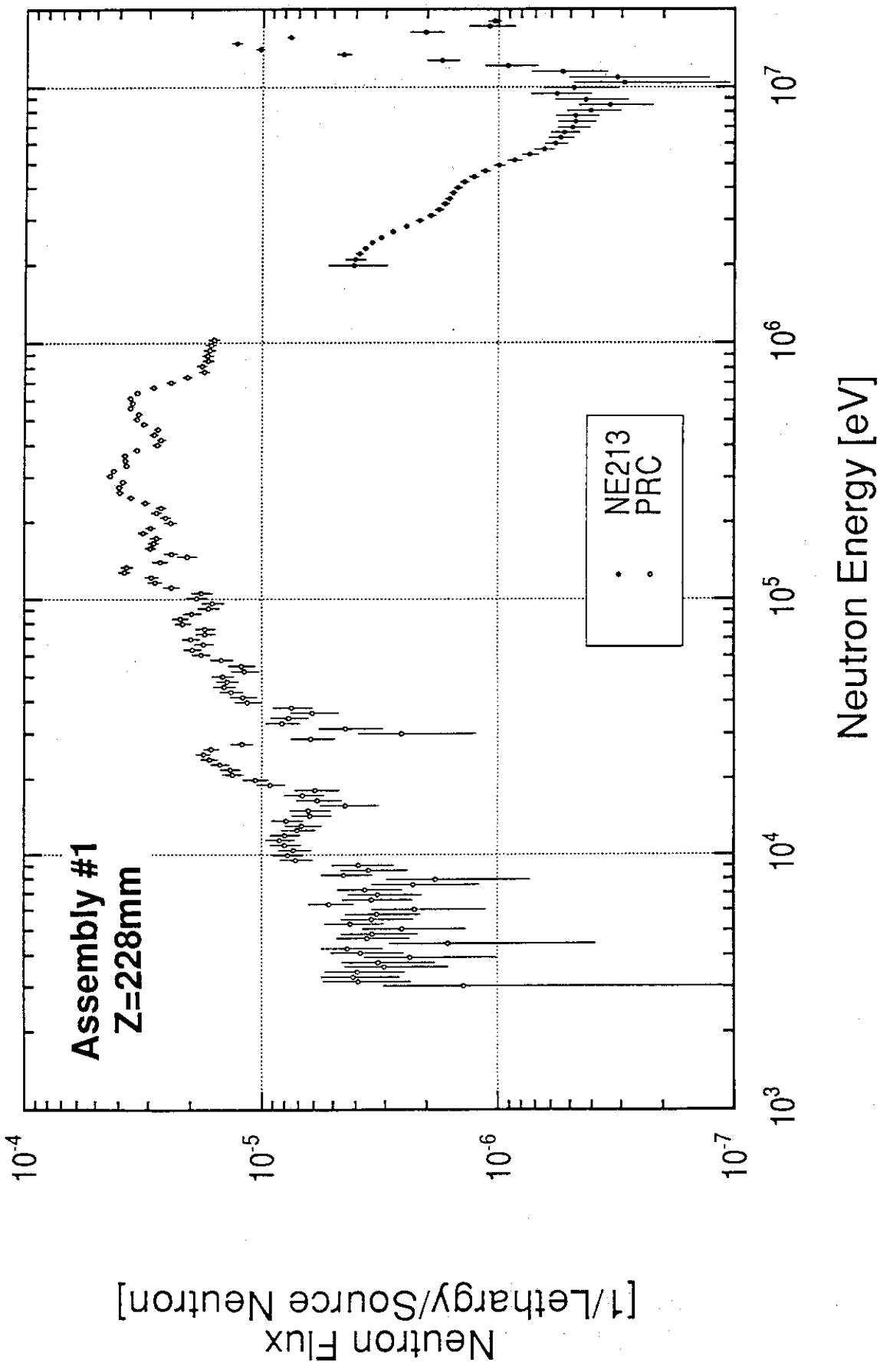

Fig. 3.1.1.5 The measured neutron spectrum at 228 mm from the front surface of the test region in the assembly #1.

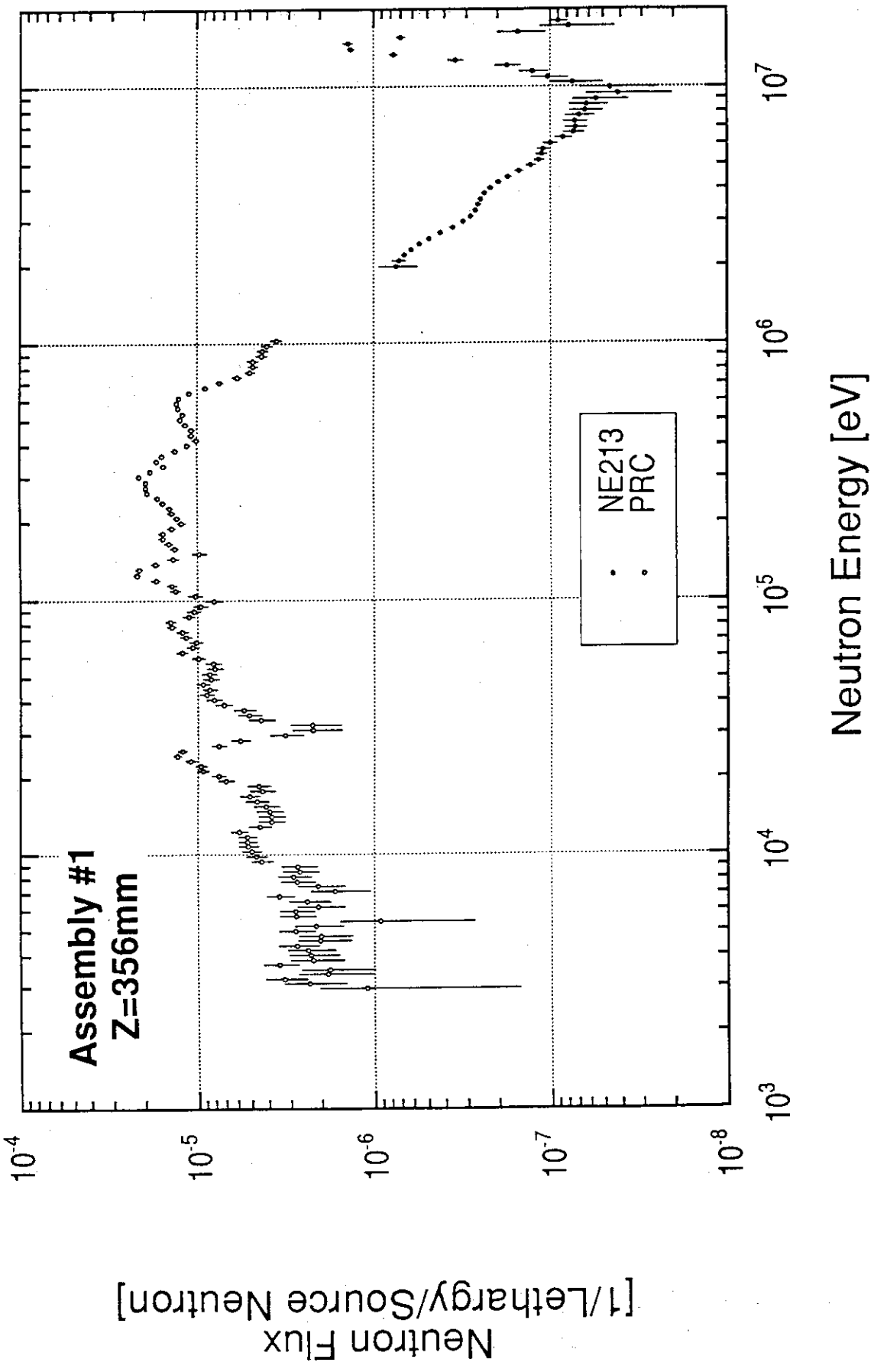

Fig. 3.1.1.6 The measured neutron spectrum at 356 mm from the front surface of the test region in the assembly #1.

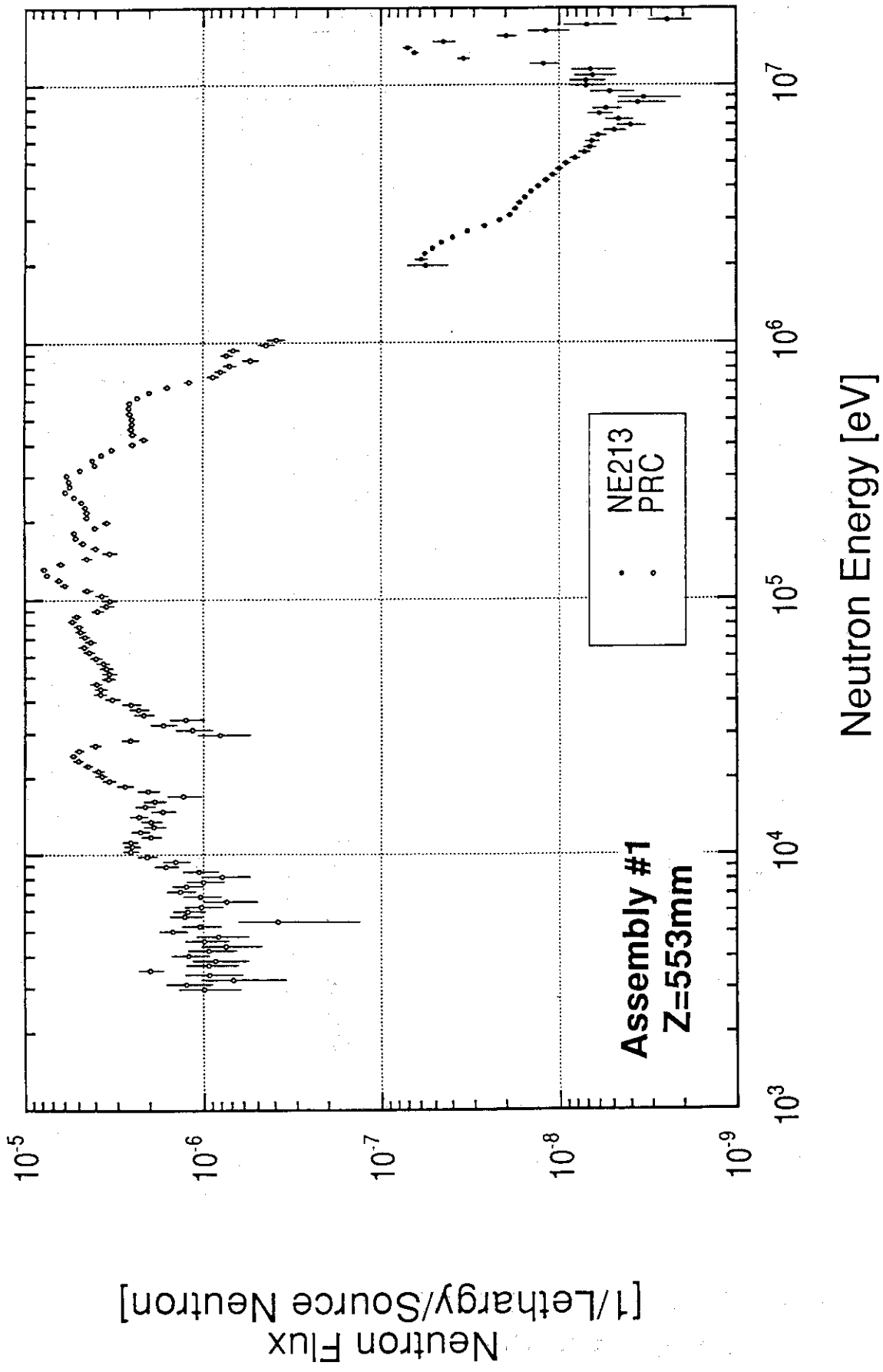

Fig. 3.1.1.7 The measured neutron spectrum at 553 mm from the front surface of the test region in the assembly #1.

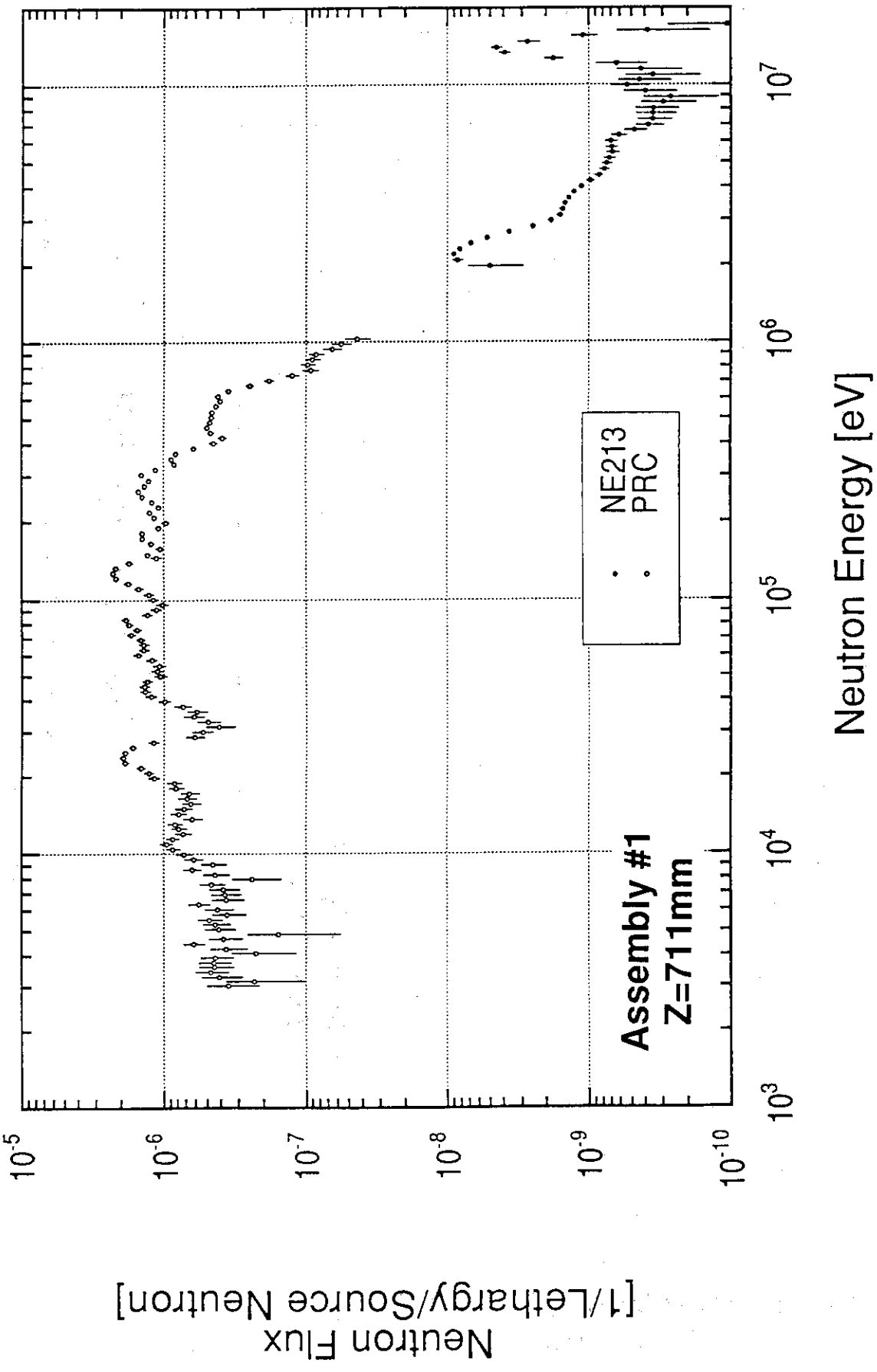

Fig. 3.1.1.8 The measured neutron spectrum at 711 mm from the front surface of the test region in the assembly #1.

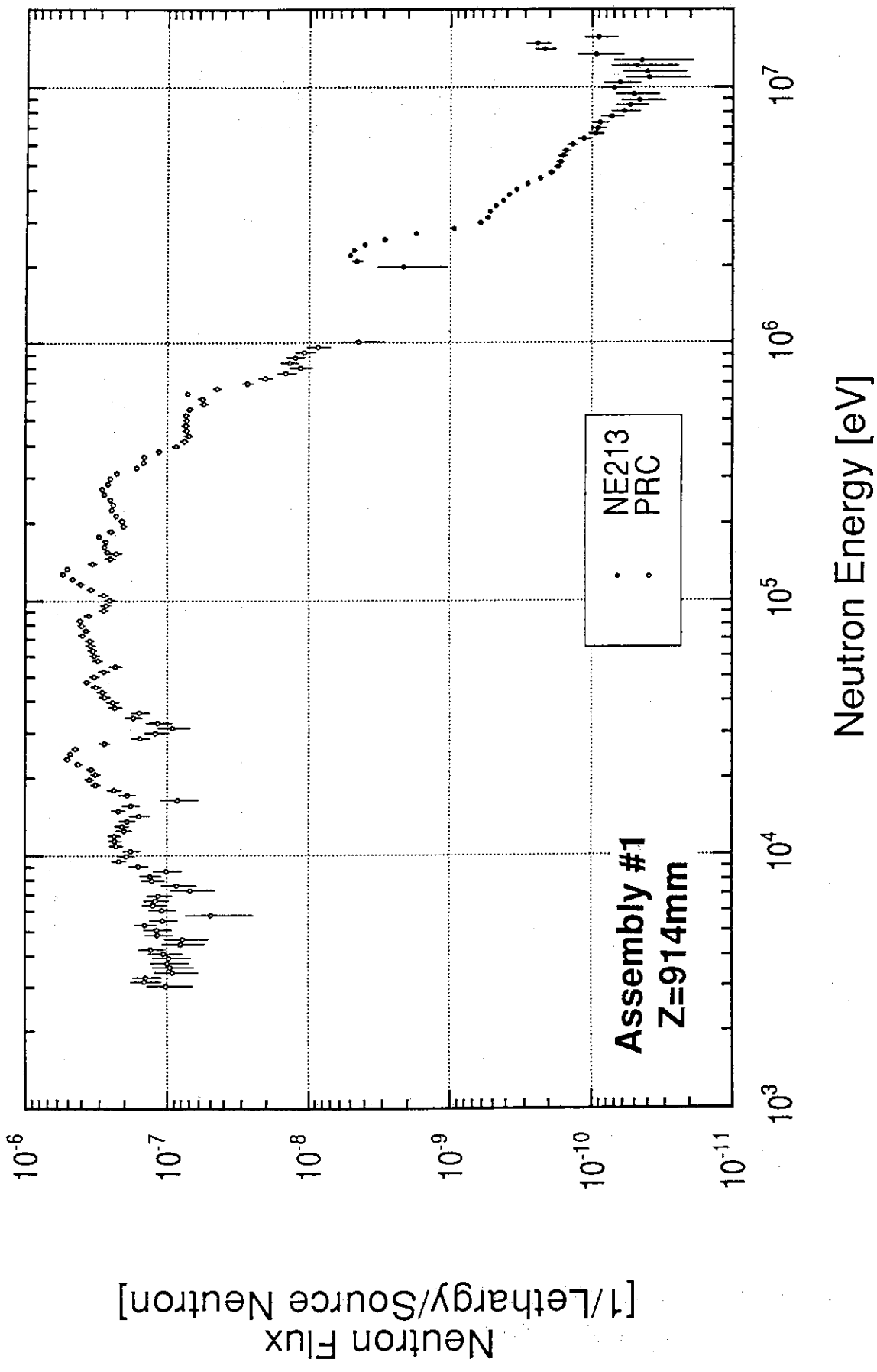

Fig. 3.1.1.9 The measured neutron spectrum at 914 mm from the front surface of the test region in the assembly #1.

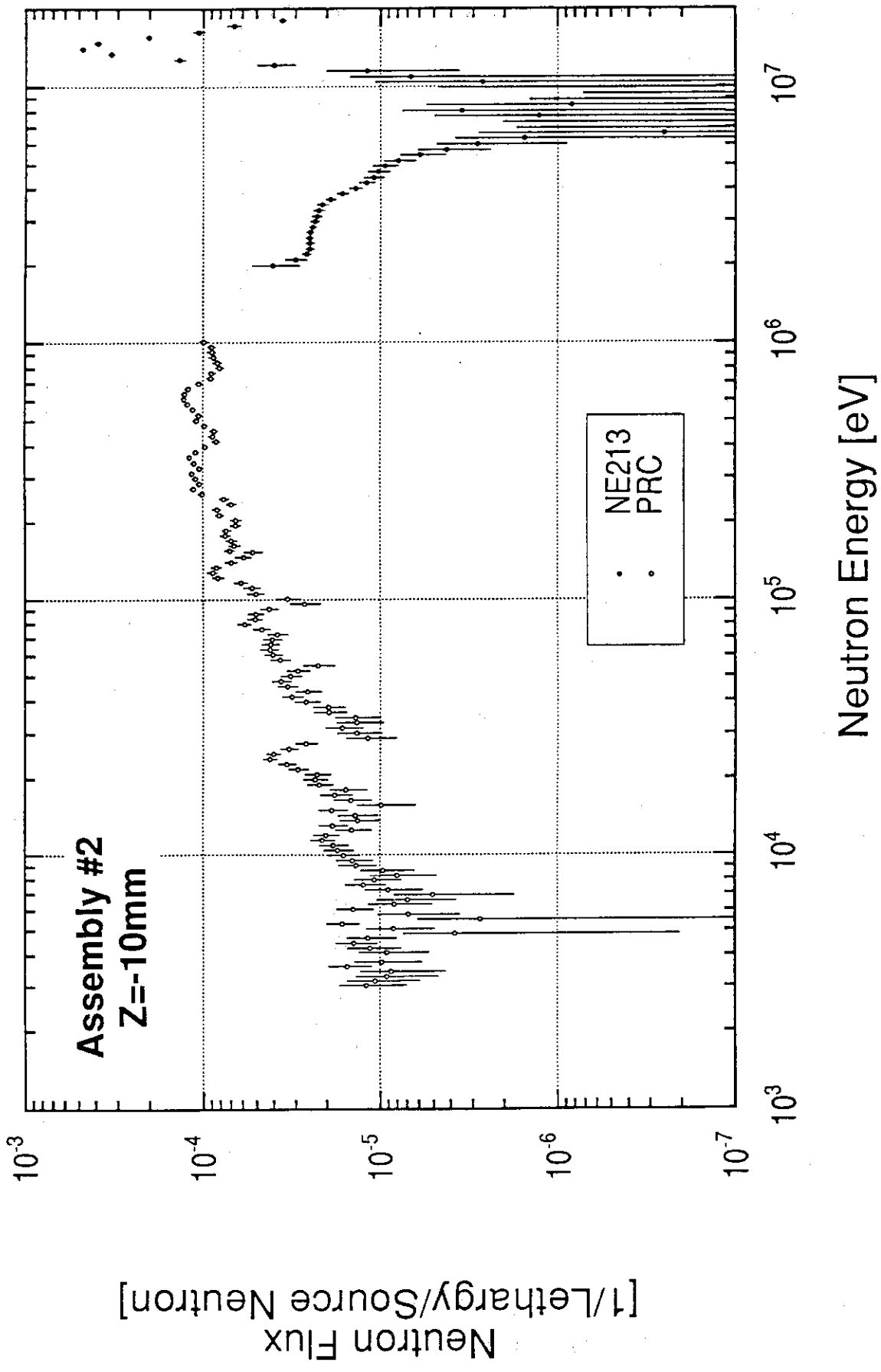

Fig. 3.1.1.10 The measured neutron spectrum at the front surface of the test region in the assembly #2.

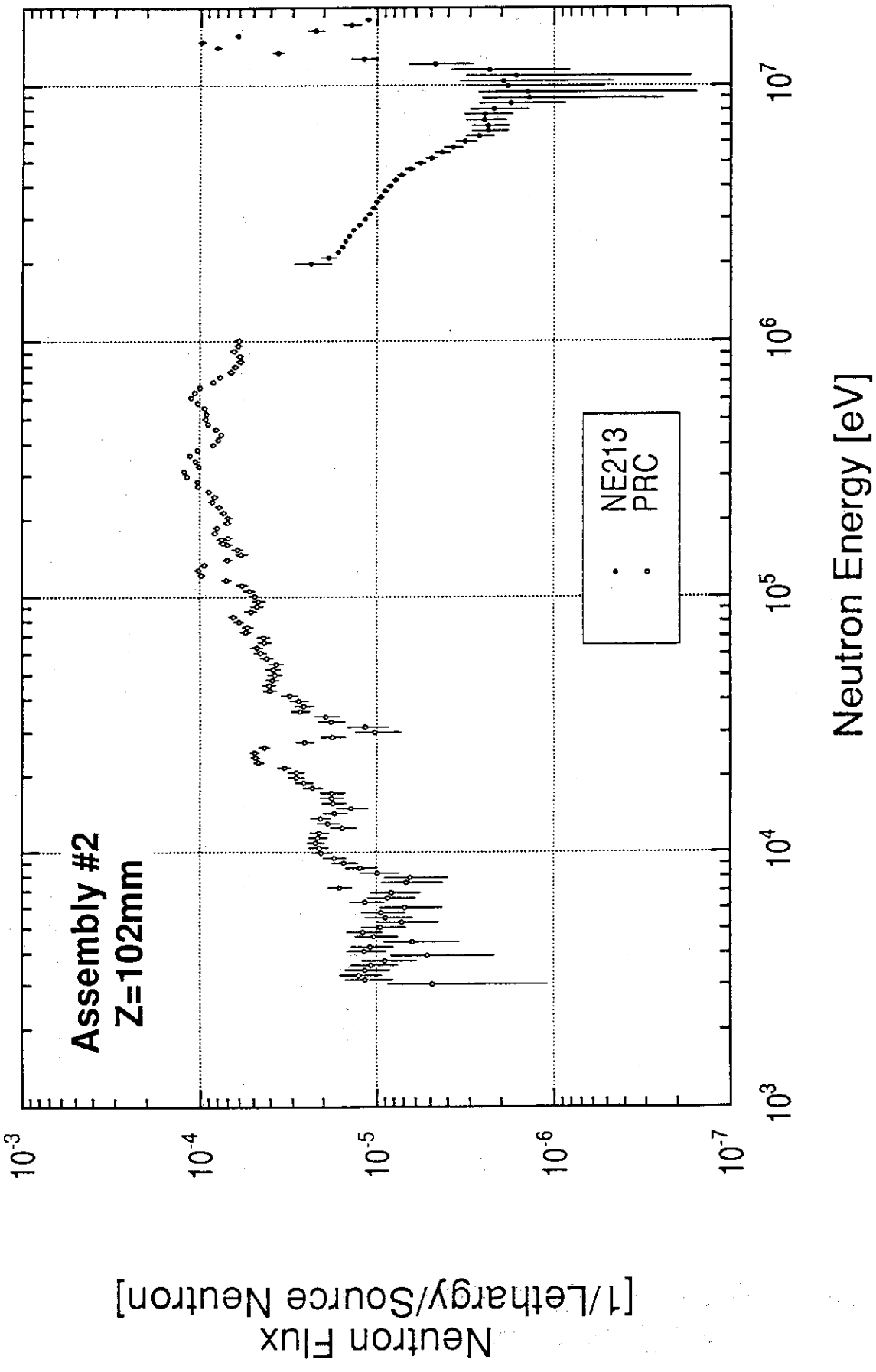

Fig. 3.1.1.11 The measured neutron spectrum at 102 mm from the front surface of the test region in the assembly #2.

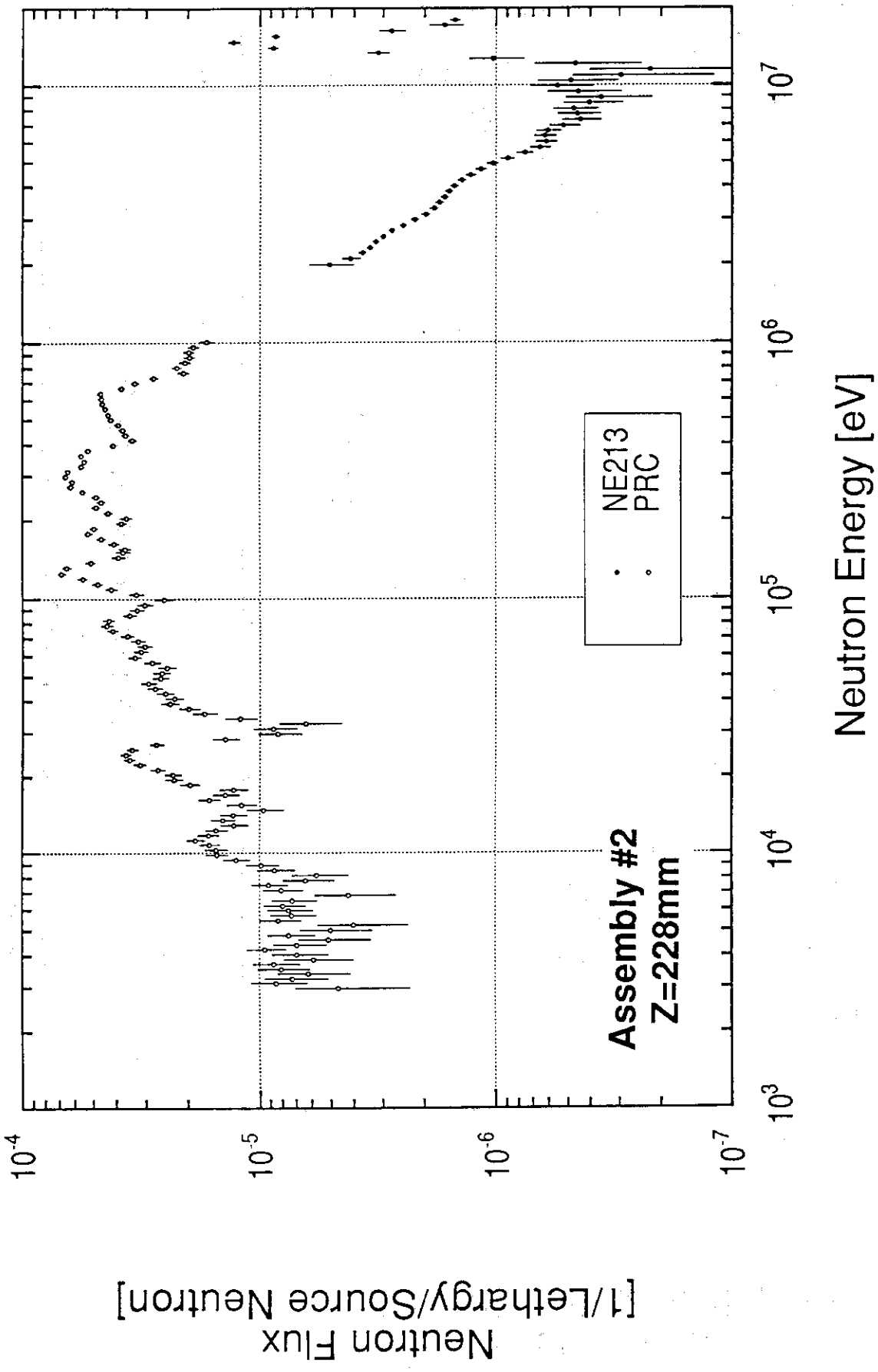

Fig. 3.1.1.12 The measured neutron spectrum at 228 mm from the front surface of the test region in the assembly #2.

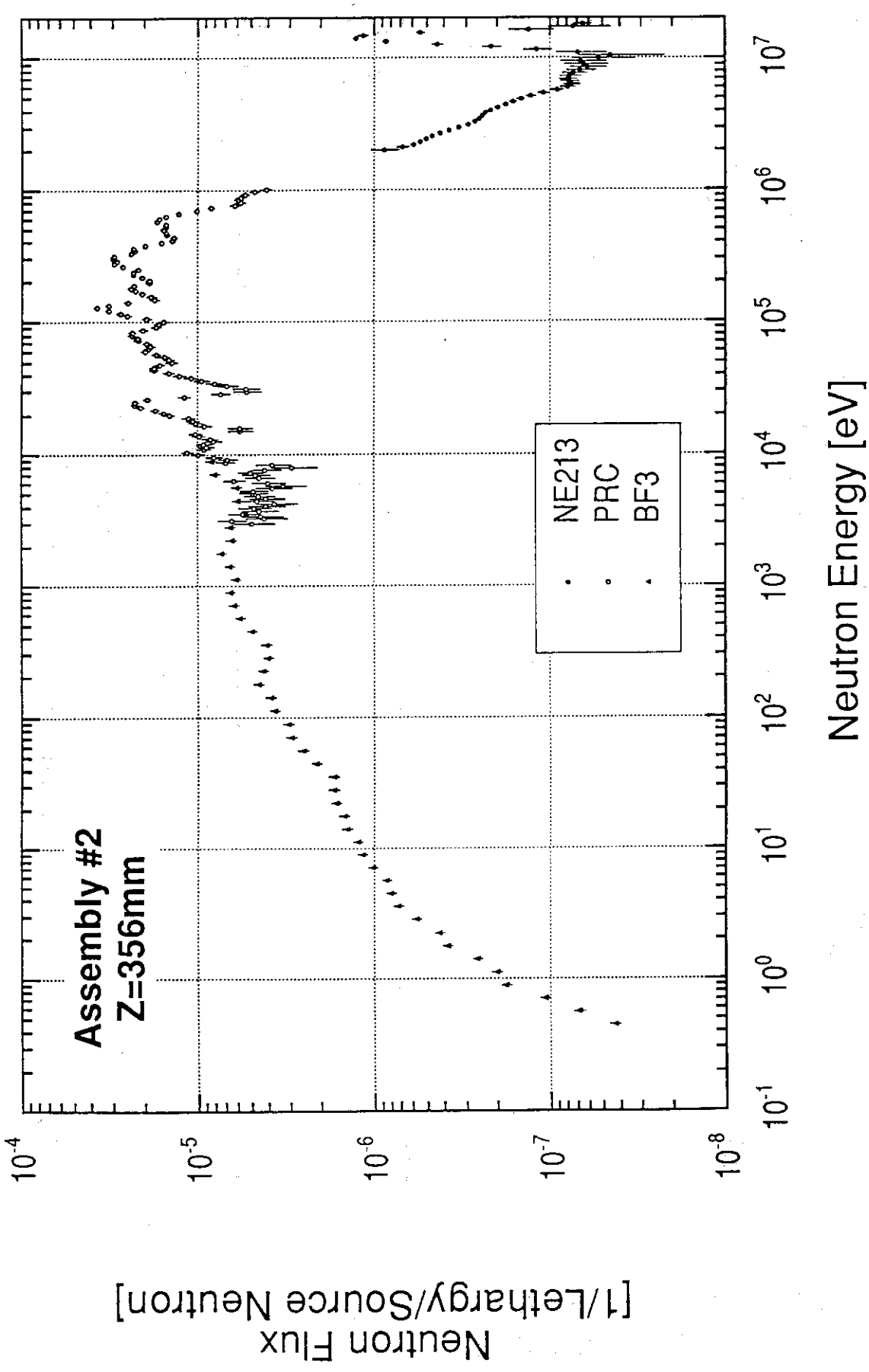

Fig. 3.1.1.13 The measured neutron spectrum at 356 mm from the front surface of the test region in the assembly #2.

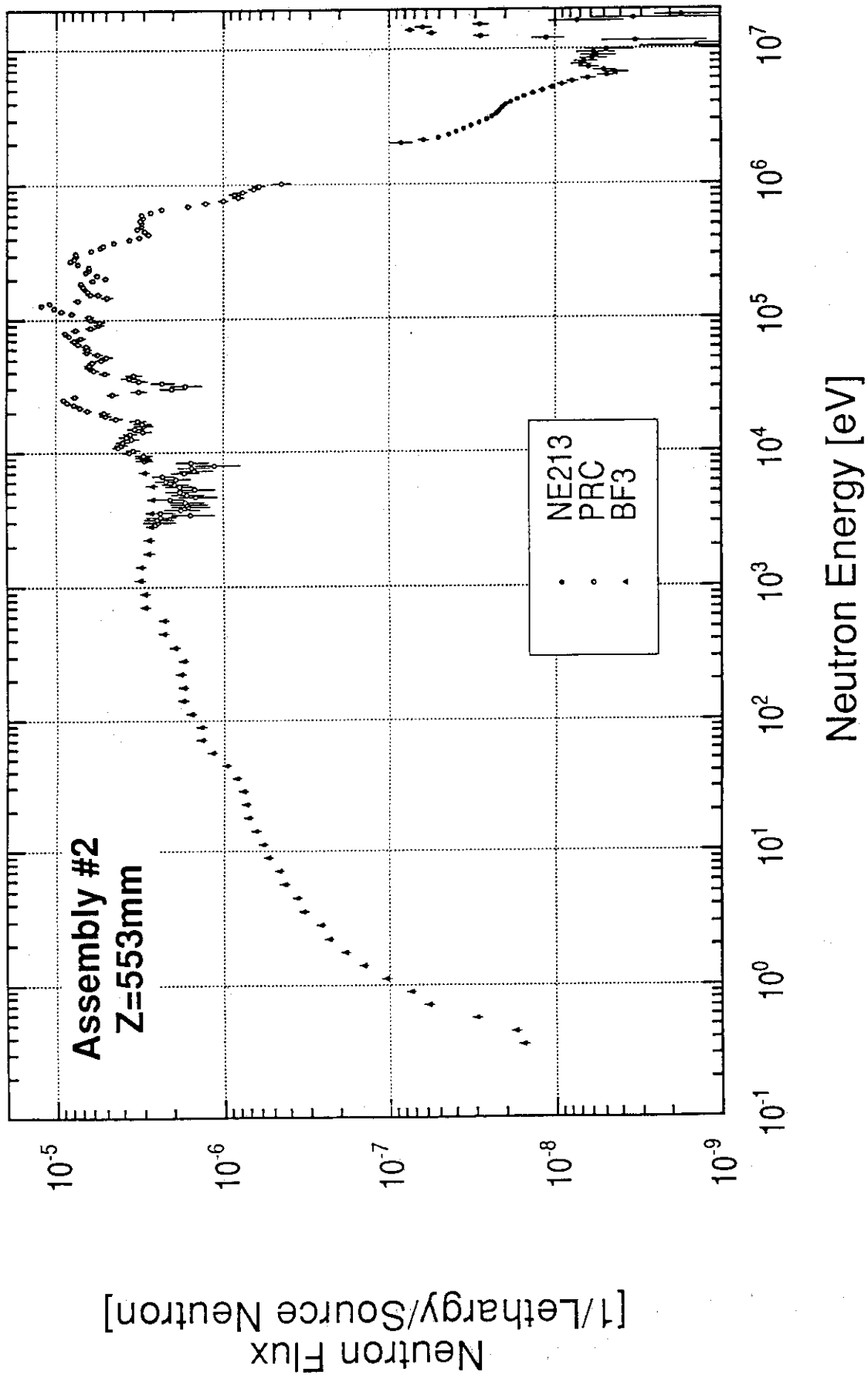

Fig. 3.1.1.14 The measured neutron spectrum at 553 mm from the front surface of the test region in the assembly #2.

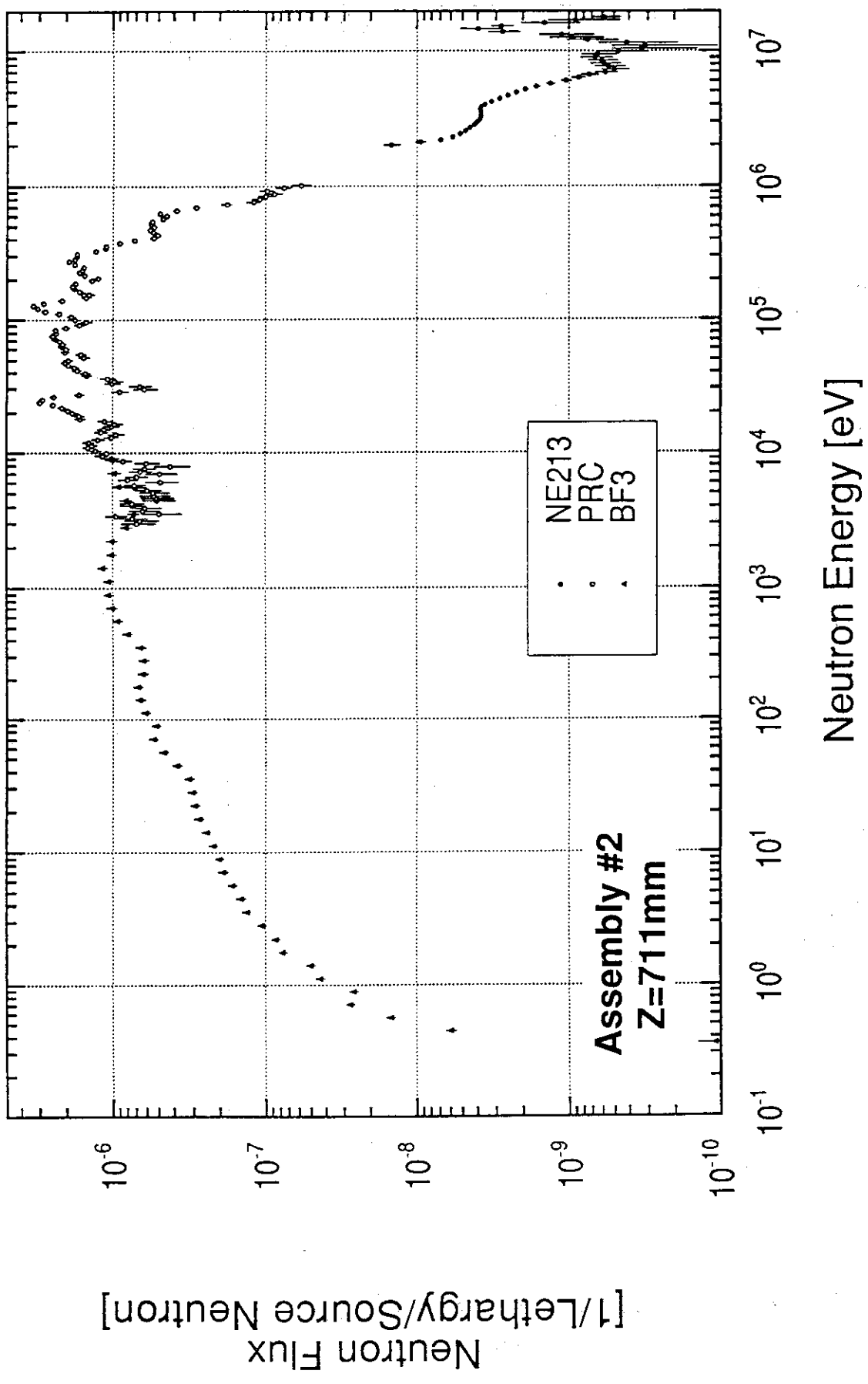

Fig. 3.1.1.15 The measured neutron spectrum at 711 mm from the front surface of the test region in the assembly #2.

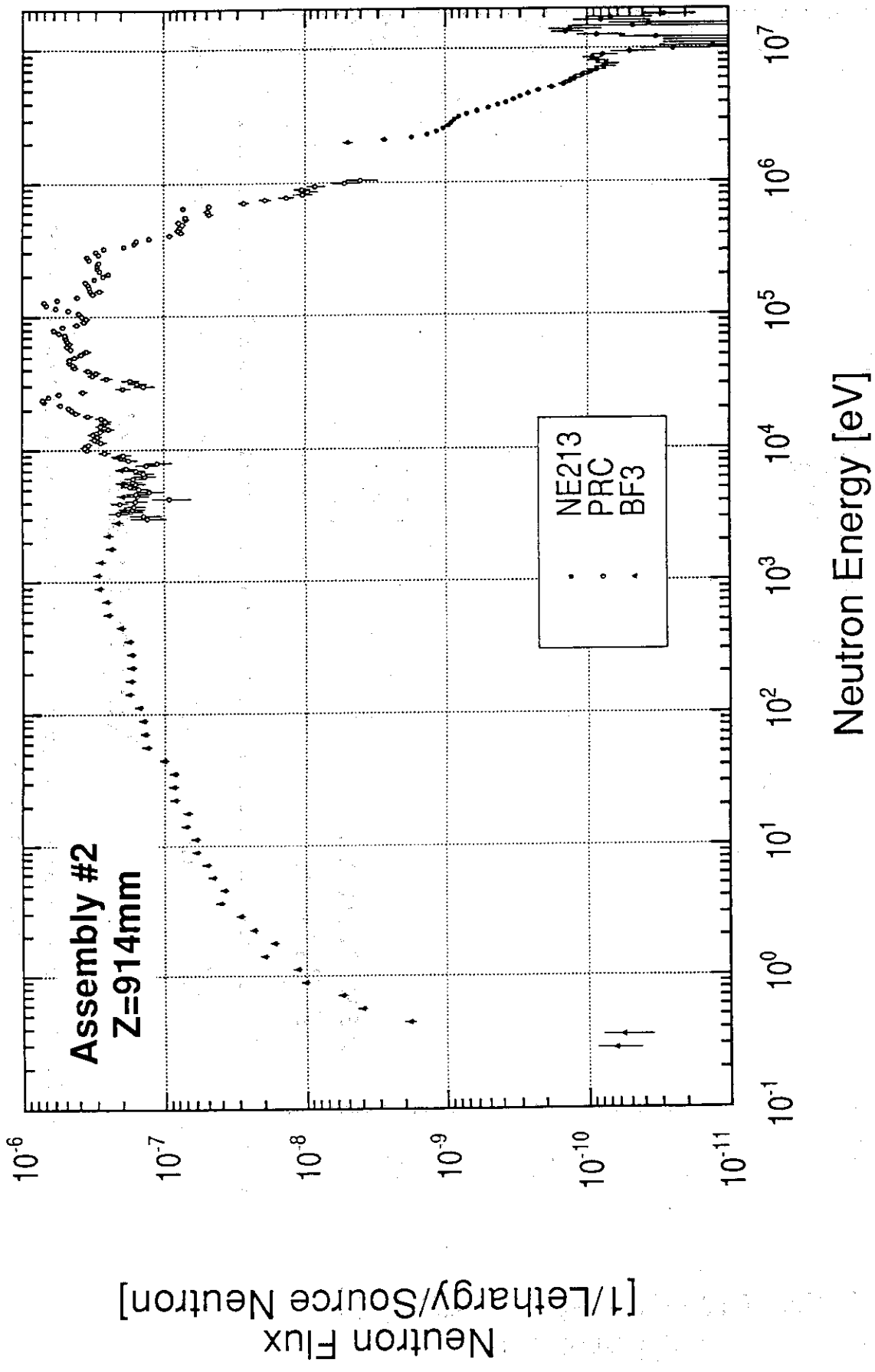

Fig. 3.1.1.16 The measured neutron spectrum at 914 mm from the front surface of the test region in the assembly #2.

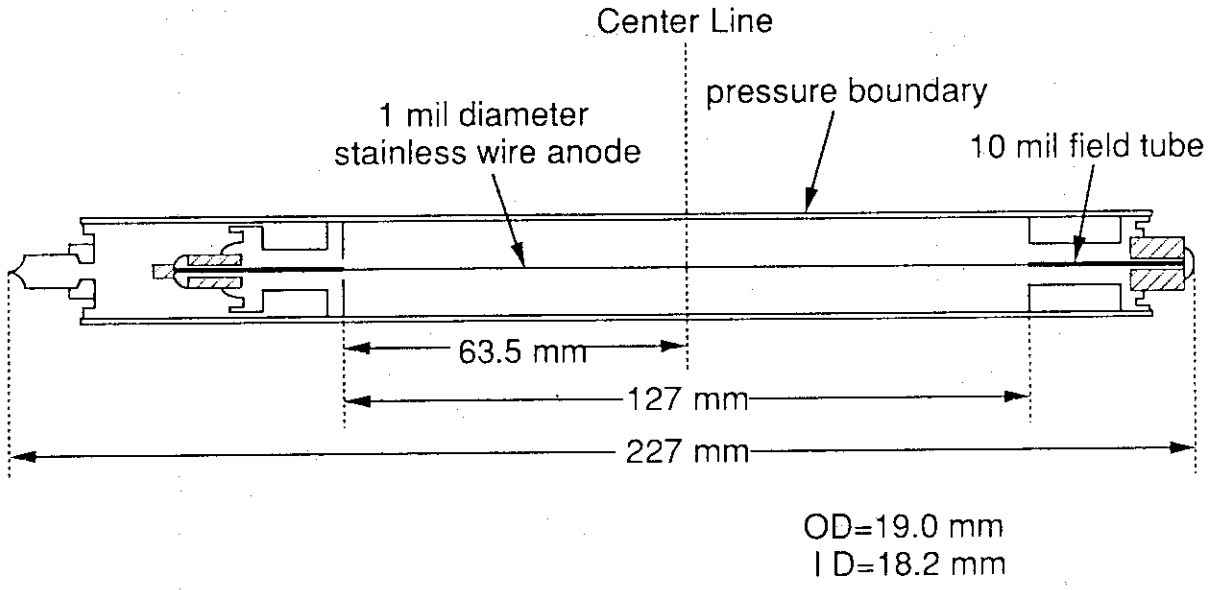

Fig. 3.1.2.1 Cross sectional view of the proton recoil gas proportional counter.

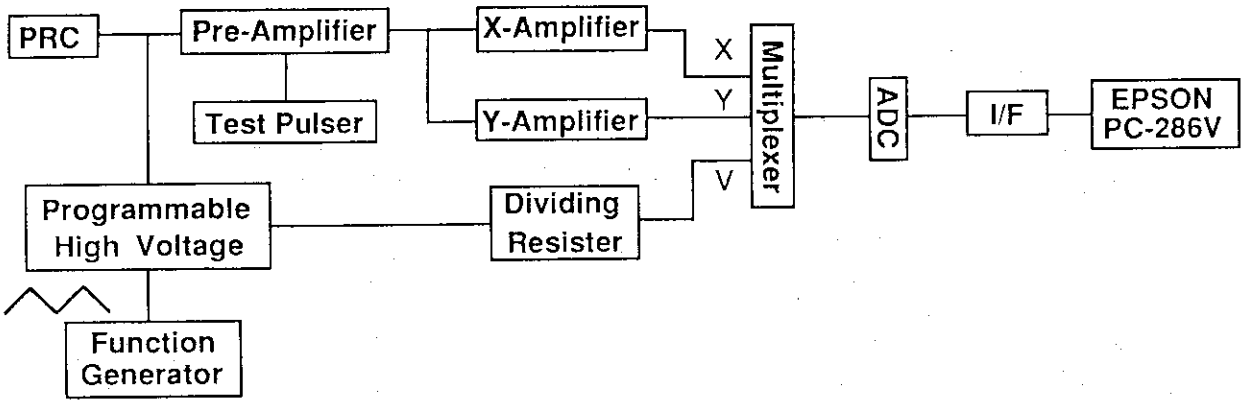

Fig. 3.1.2.2 Block diagram of electronic circuit for the PRC.

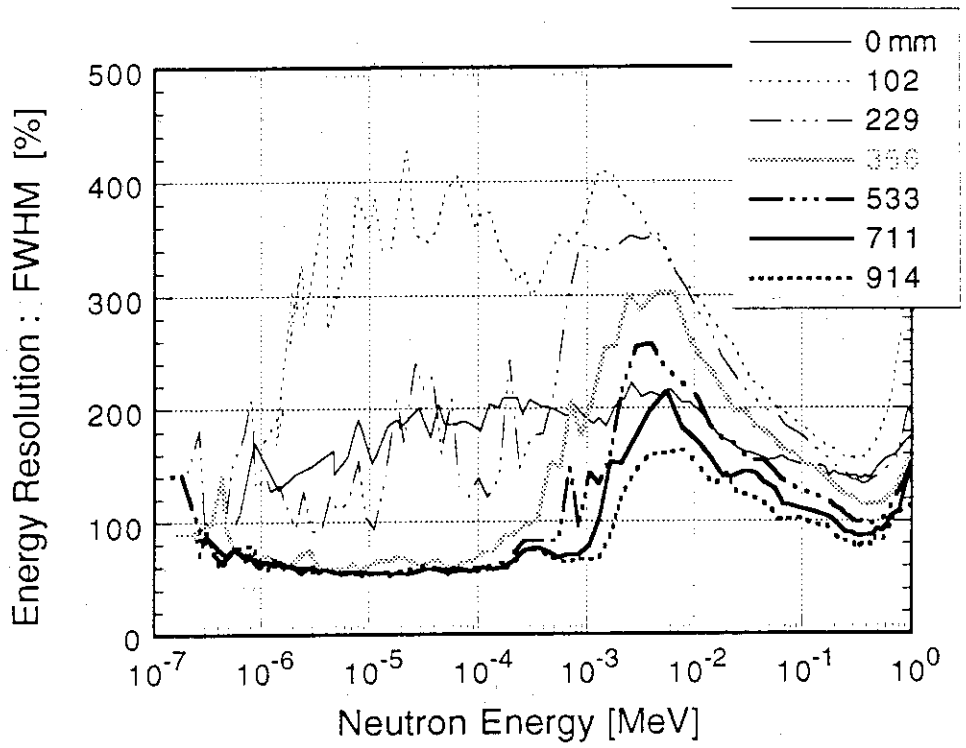

Fig. 3.1.3.1 Expected energy resolution of neutron spectra calculated by MCNP. Fluctuations seen in the resolution curves are due to statistical error in the Monte Carlo calculation.

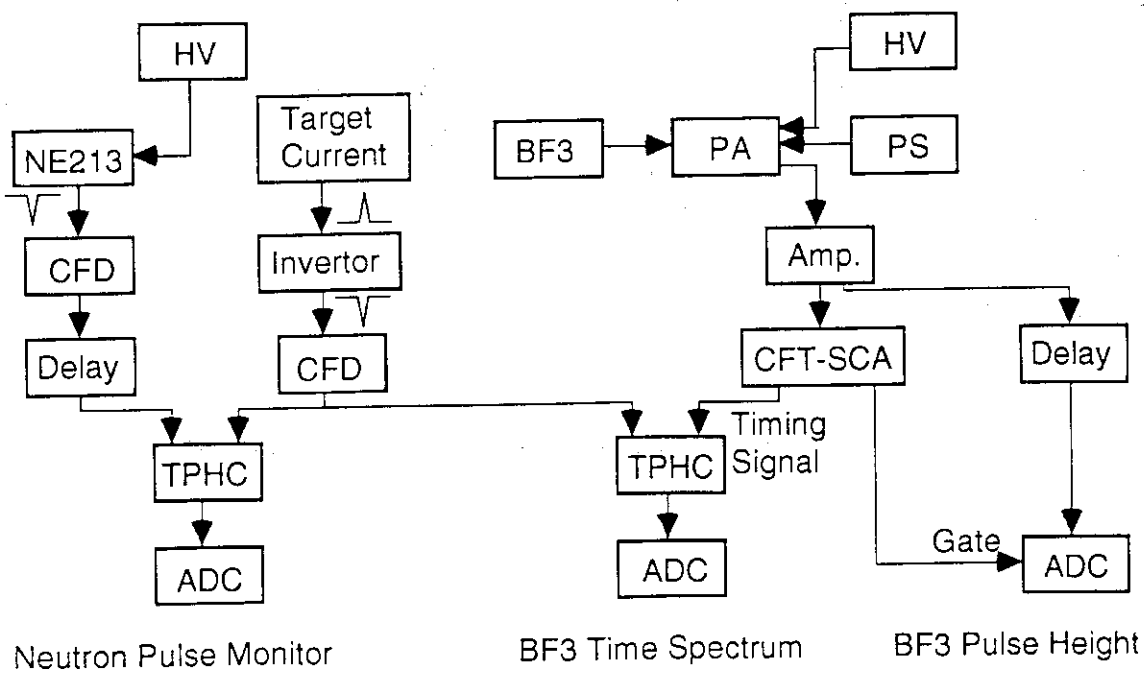

Fig. 3.1.3.2 Electronic circuit used in the eV neutron spectrum measurement.

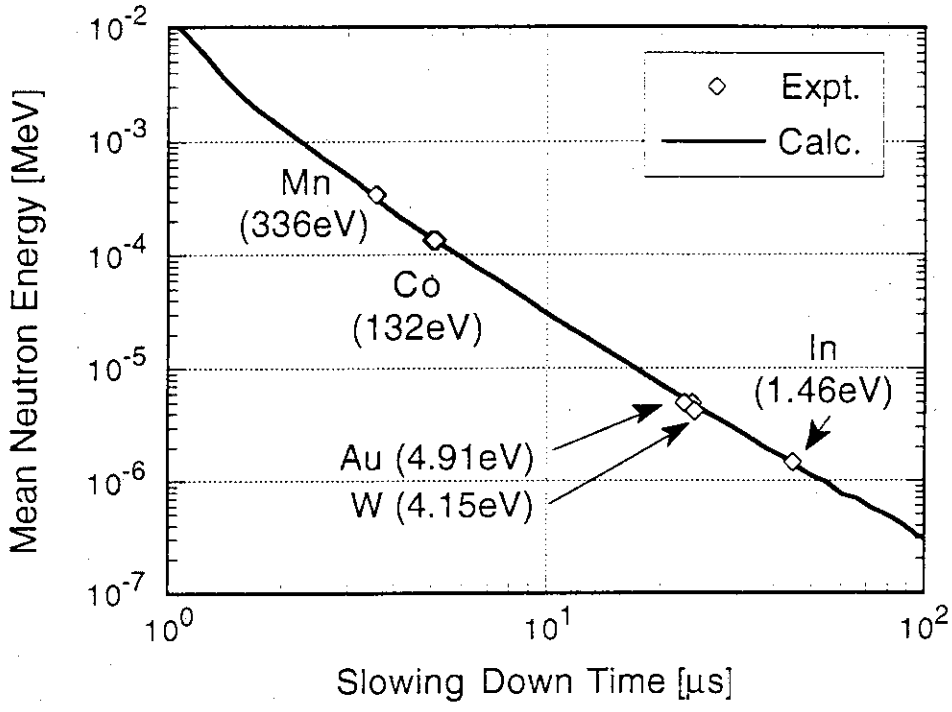

Fig. 3.1.3.3 The relation between slowing down time and neutron mean energy measured (white squares) and that calculated by MCNP (solid line).

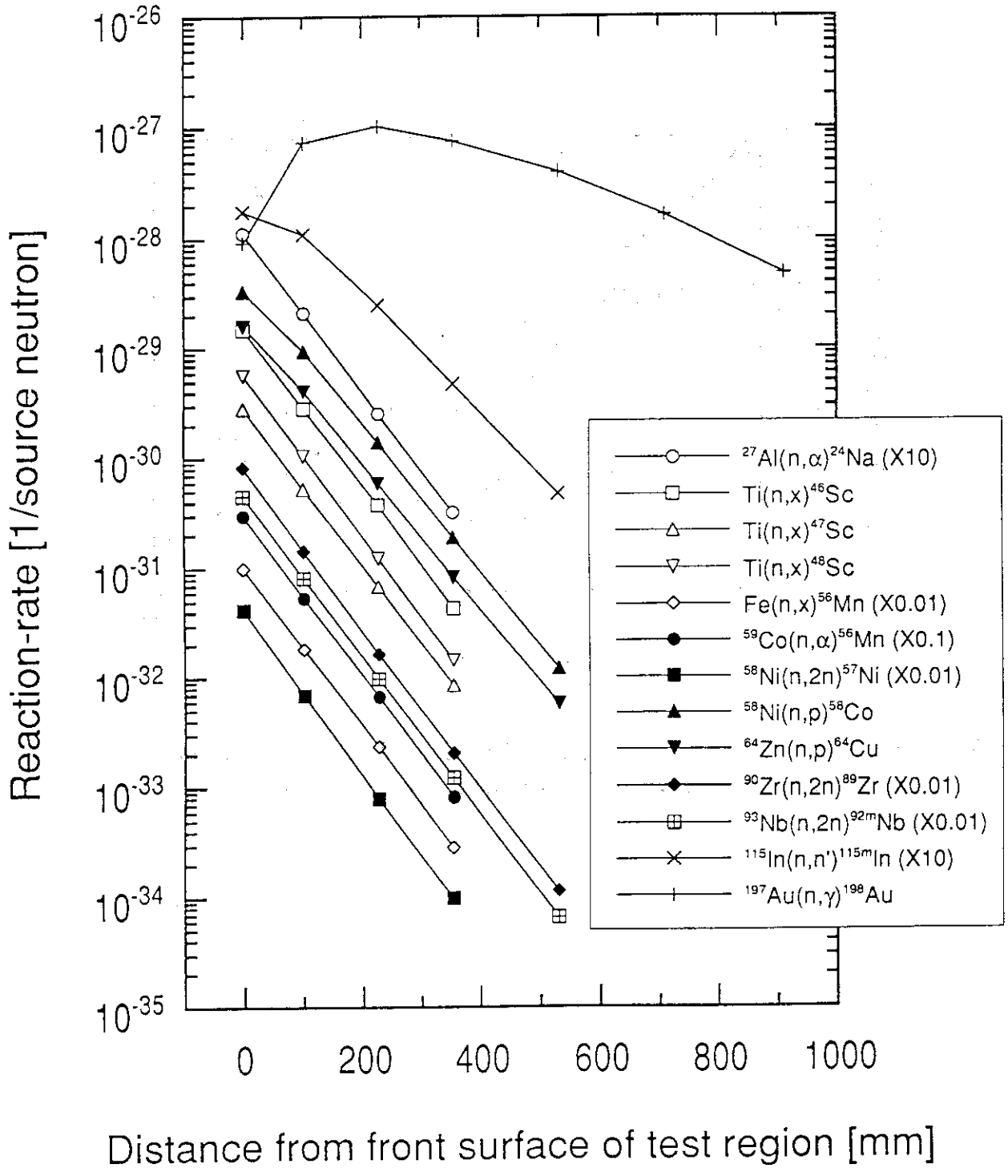

Fig. 3.2.1.1 Measured neutron activation reaction rates in the assembly #1.

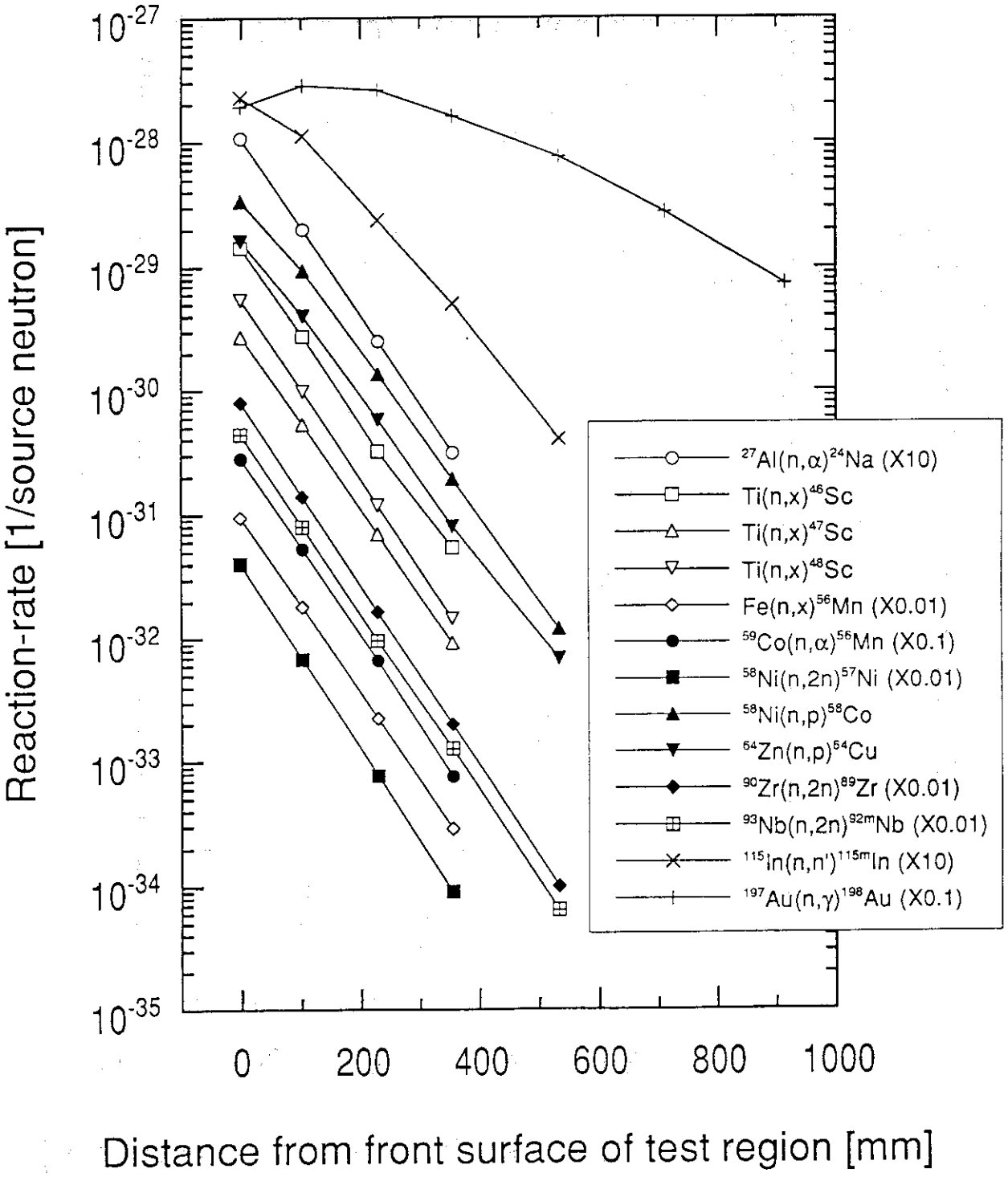

Fig. 3.2.1.2 Measured neutron activation reaction rates in the assembly #2.

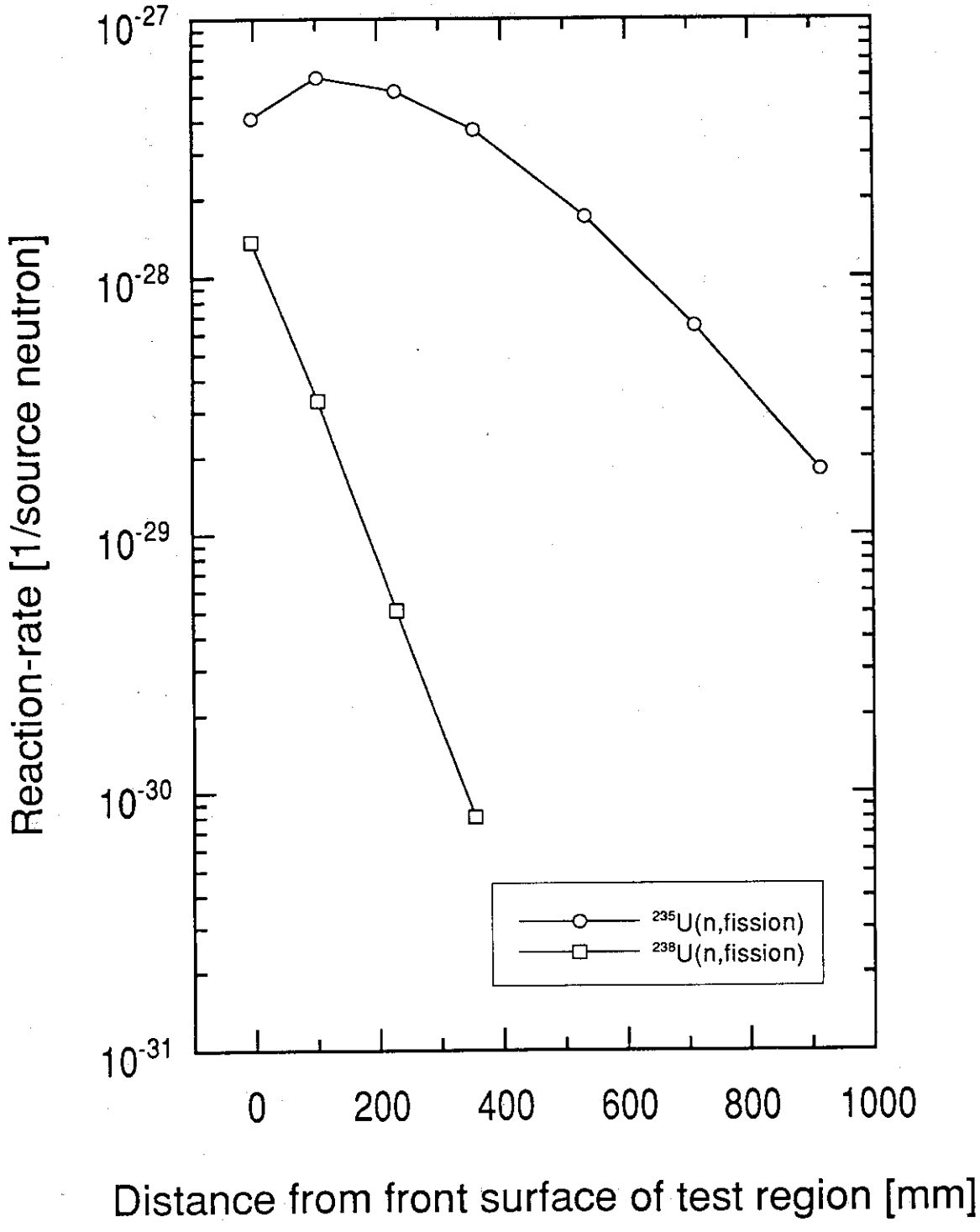

Fig. 3.2.2.1 Measured fission rates in the assembly #1.

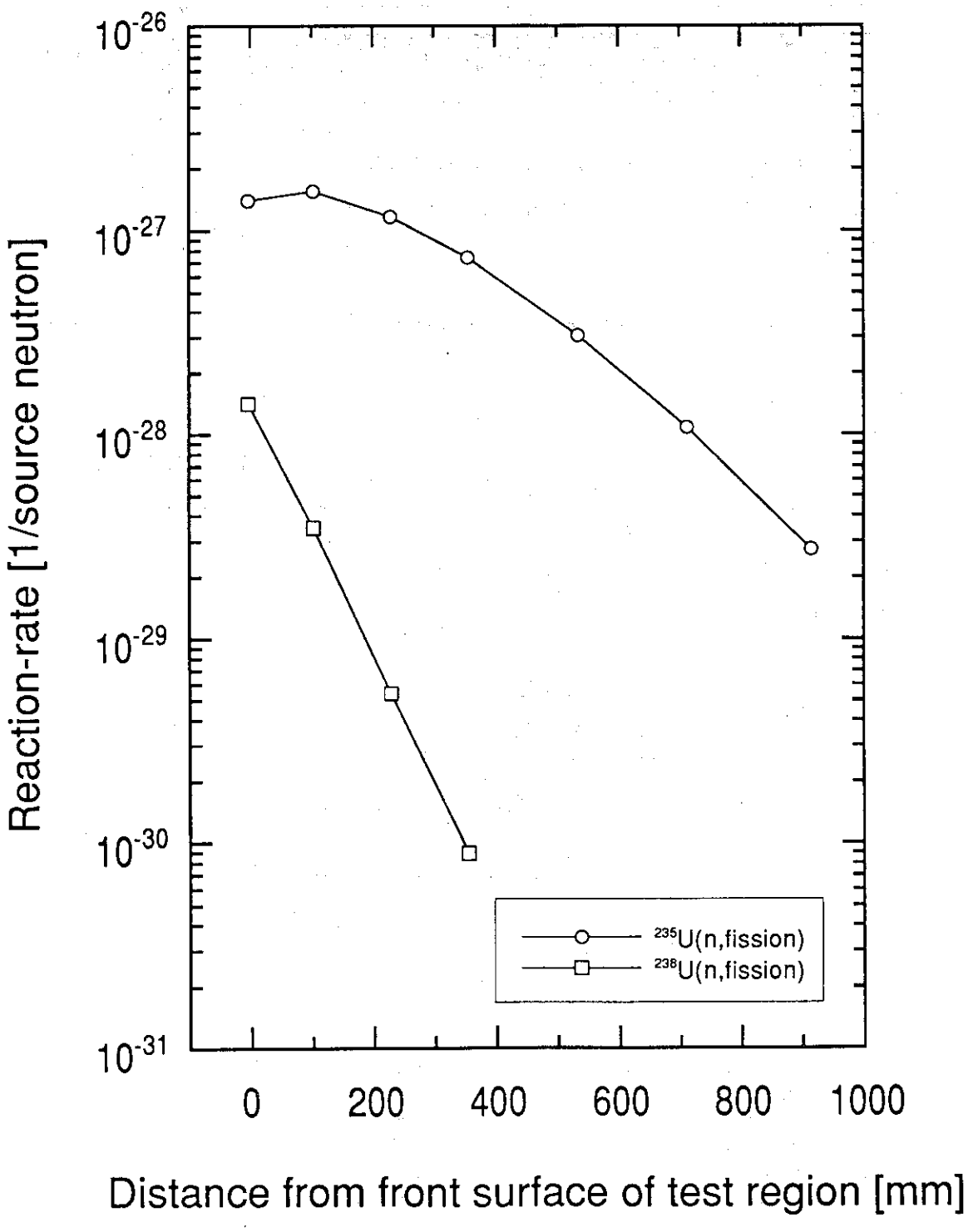

Fig. 3.2.2.2 Measured fission rates in the assembly #2.

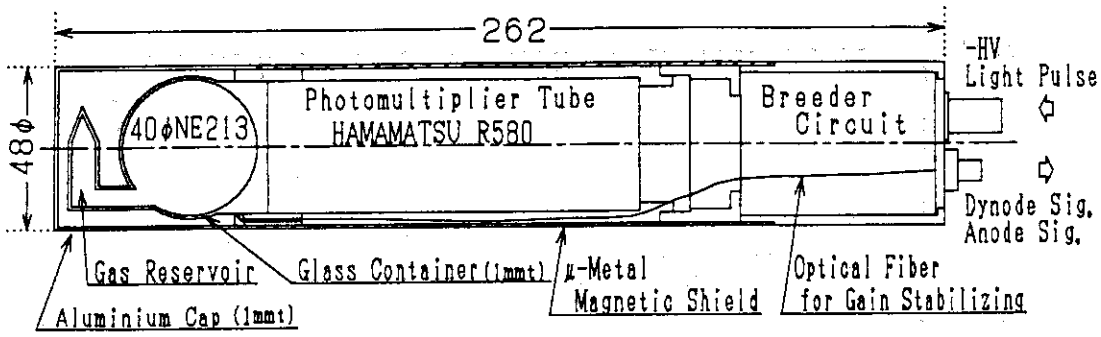

Fig. 3.3.1 Sectional view of the 40 mm diameter NE213 gamma-ray spectrometer.

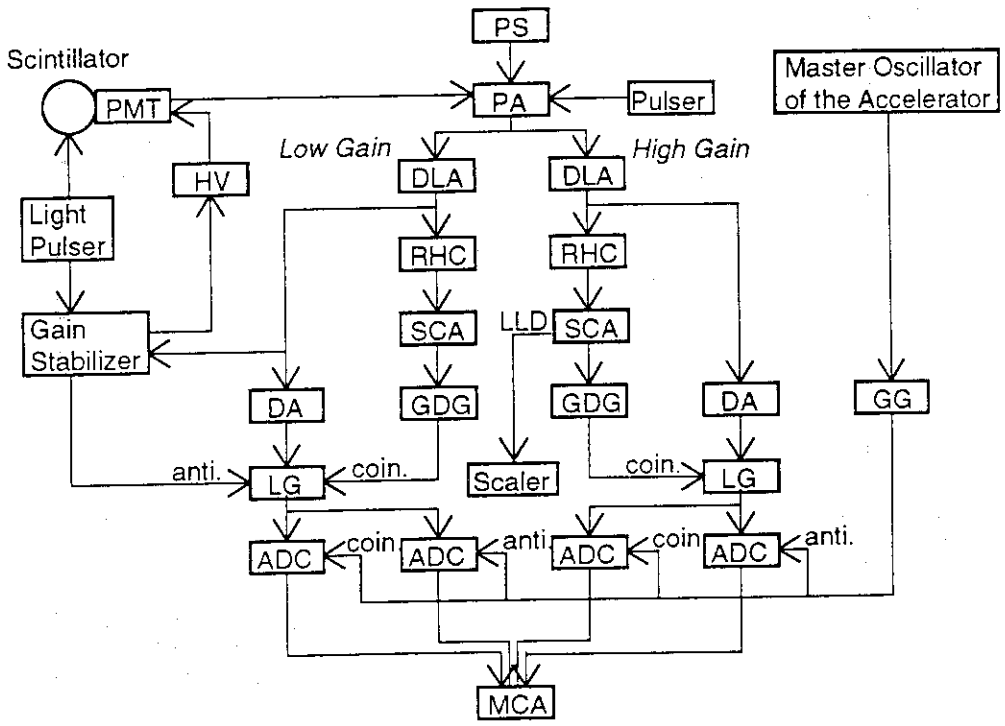

PMT	:	Photomultiplier Tube	Hamamatsu	R580
HV	:	High Voltage Power Supply	ORTEC	456H
PS	:	Power Supply	ORTEC	114
PA	:	Preamplifier	ORTEC	113
Pulser	:	Research Pulser	ORTEC	448
DLA	:	Delay Line Amplifier	ORTEC	460
RHC	:	Risetime to Height Convertor	OKEN	723-1
SCA	:	Single Channel Analyzer	CANBERRA	2035A
GDG	:	Gate & Delay Generator	ORTEC	416A
Scaler	:	Timer & Scaler	JAERI	178RA
DA	:	Delay Amplifier	CANBERRA	1457
LG	:	Linear Gate & Slow Coincidence	OKEN	721-1
GG	:	Dual Gate Generator	Le Croy	222
ADC	:	Analog to Digital Convertor	CANBERRA	6075
MCA	:	Multichannel Analyzer	CANBERRA	MPA/LBB

Fig. 3.3.2 Electronic circuit used in the gamma-ray spectrum measurement.

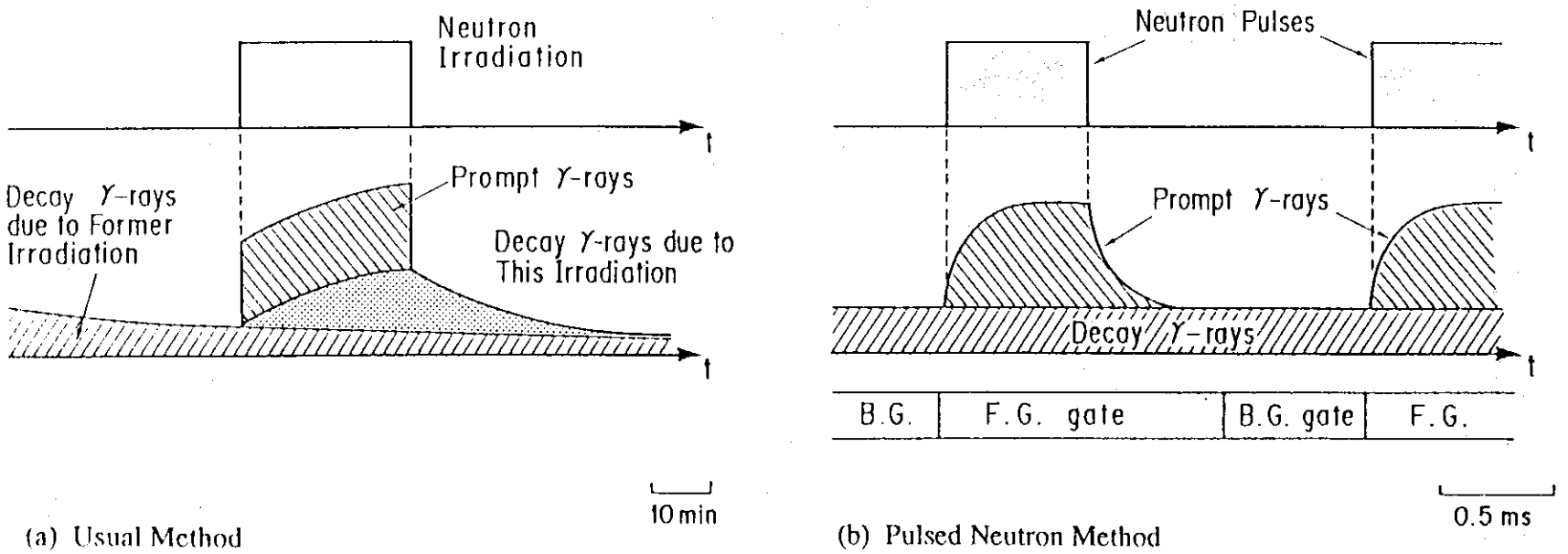

Fig. 3.3.3 Figure of explanation of rejection of decay gamma-rays. Amount of decay gamma-rays can not be determined accurately with (a) usual method but with (b) pulsed neutron method.

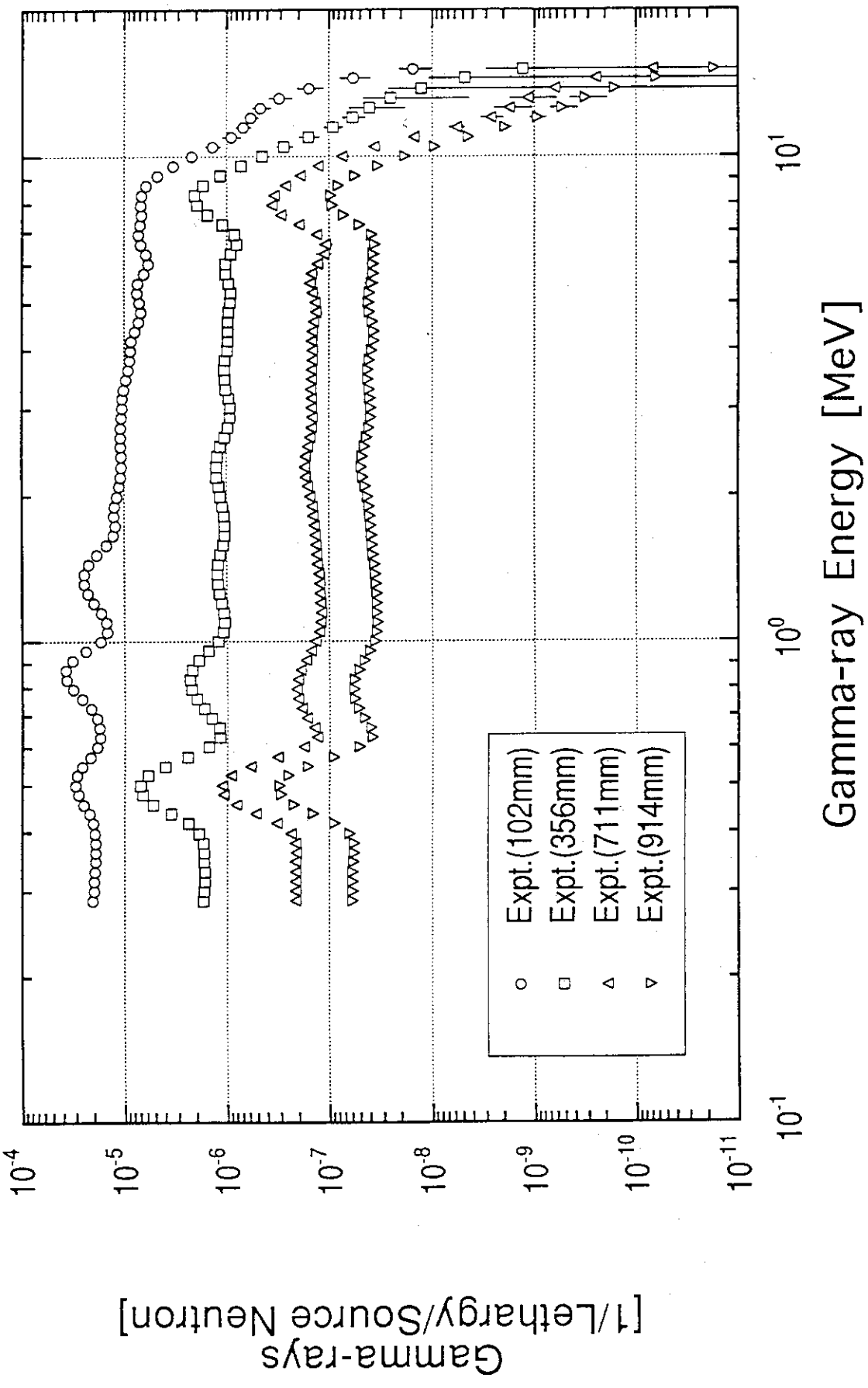

Fig. 3.3.4 Measured gamma-ray spectra in the assembly #1 by the NE213.

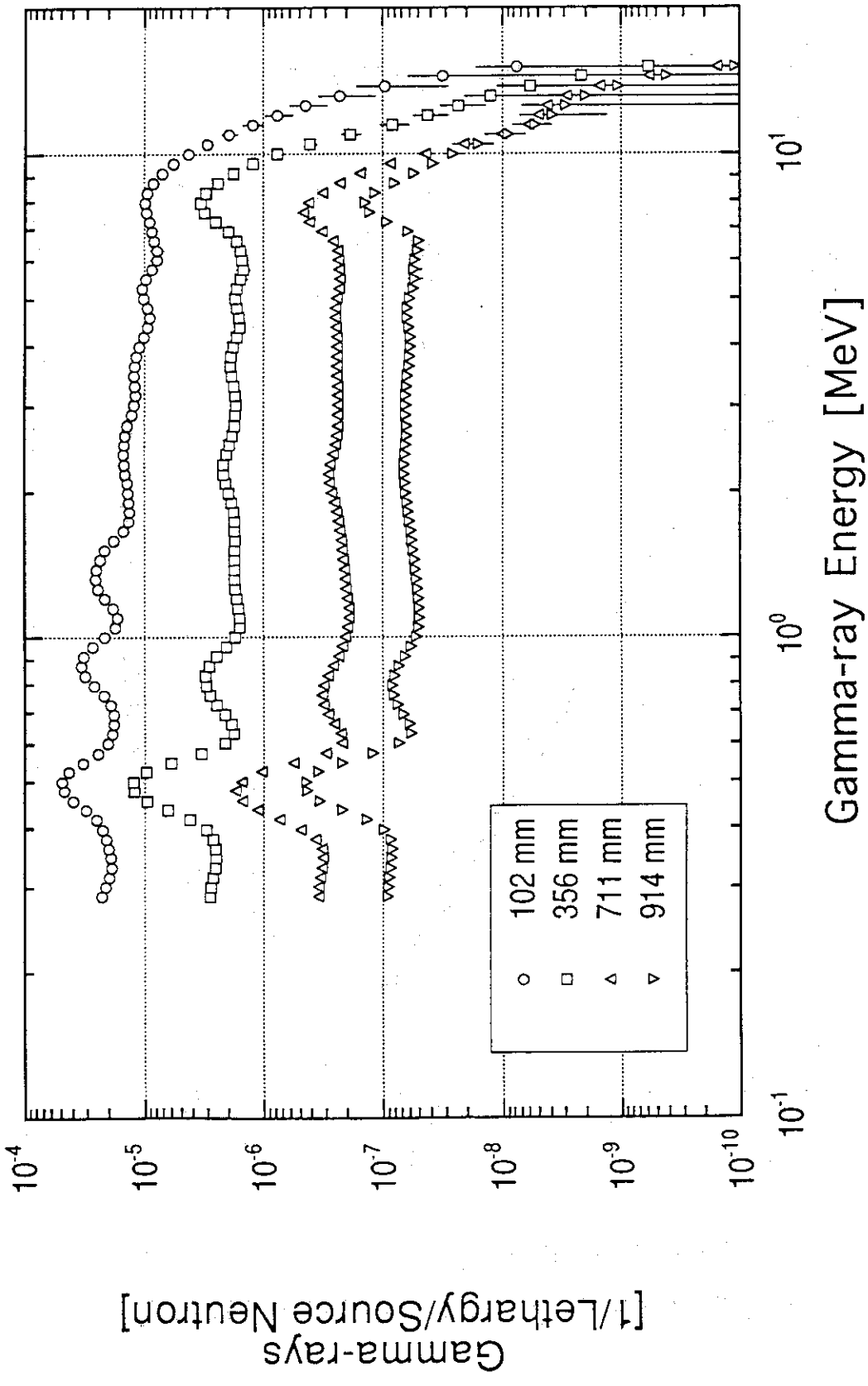

Fig. 3.3.5 Measured gamma-ray spectra in the assembly #2 by the BC537.

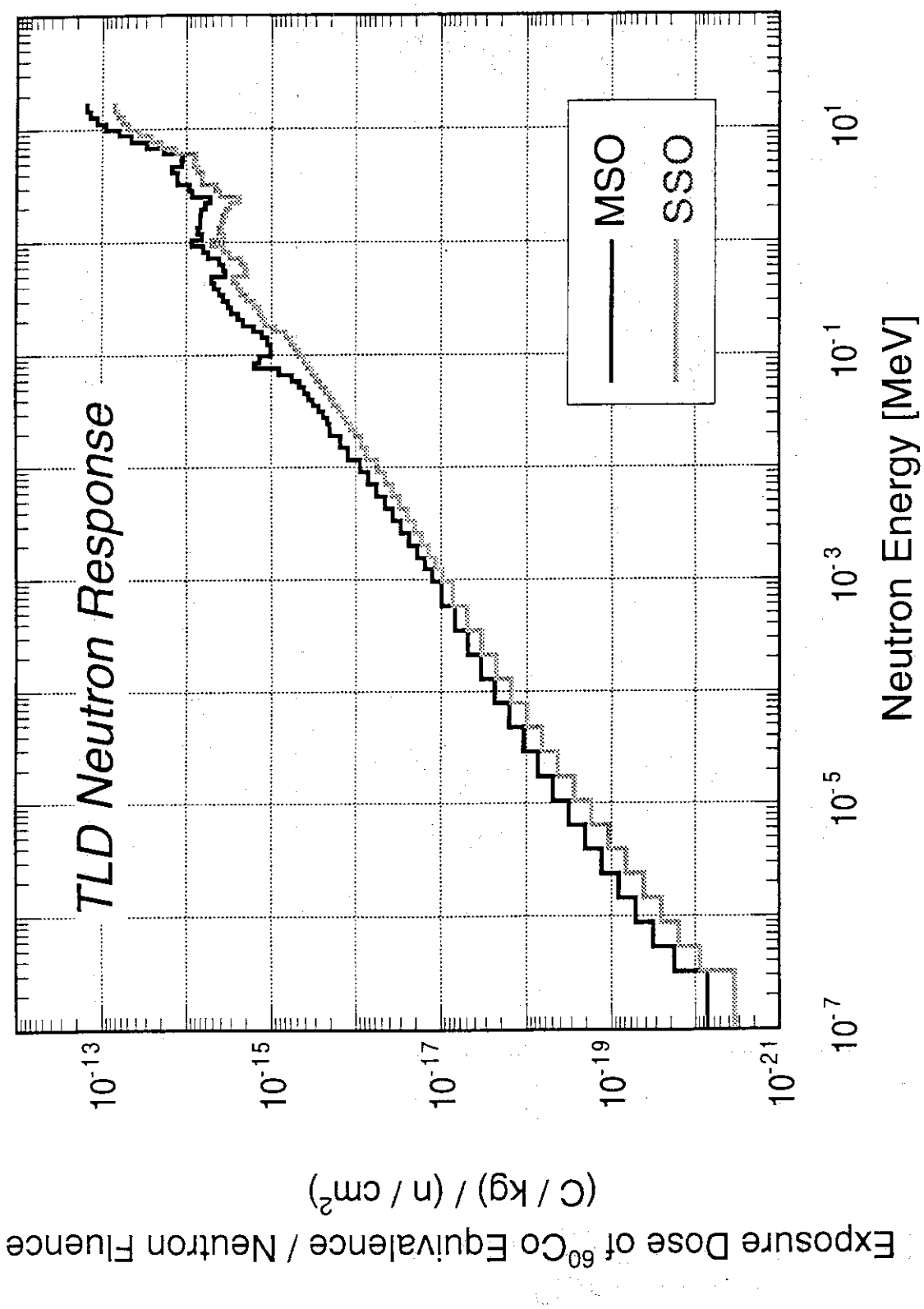

Fig. 3.4.1 Energy dependent neutron responses of Mg_2SiO_4 (MSO) and Sr_2SiO_4 (SSO).

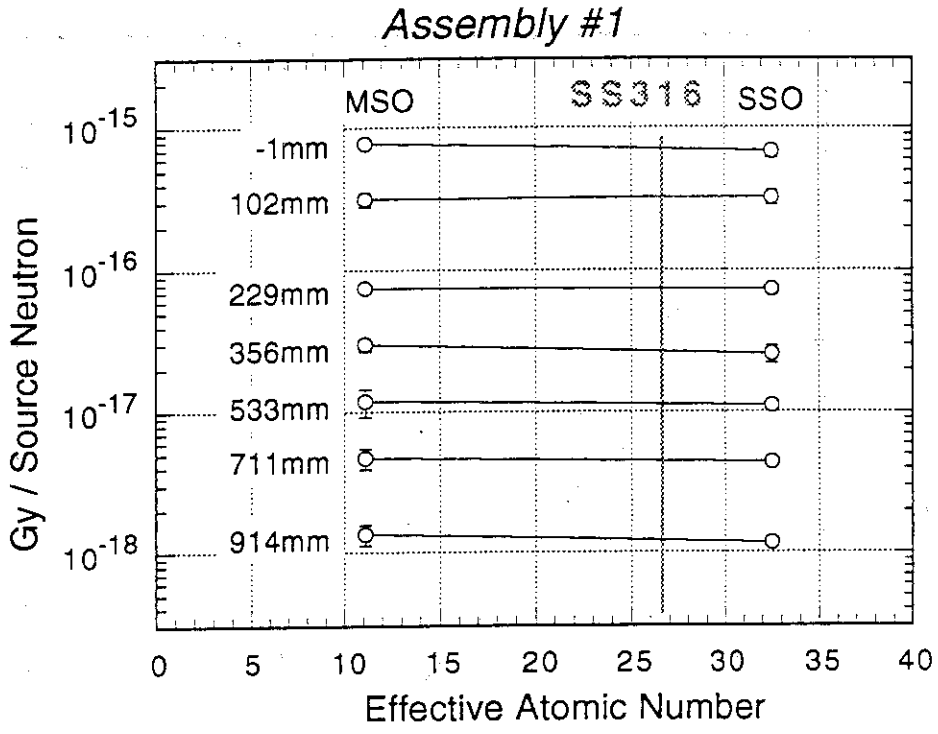

Fig. 3.4.2 Interpolation scheme to derive gamma-ray heating rates of SS316 in the assembly #1 from those of MSO and SSO.

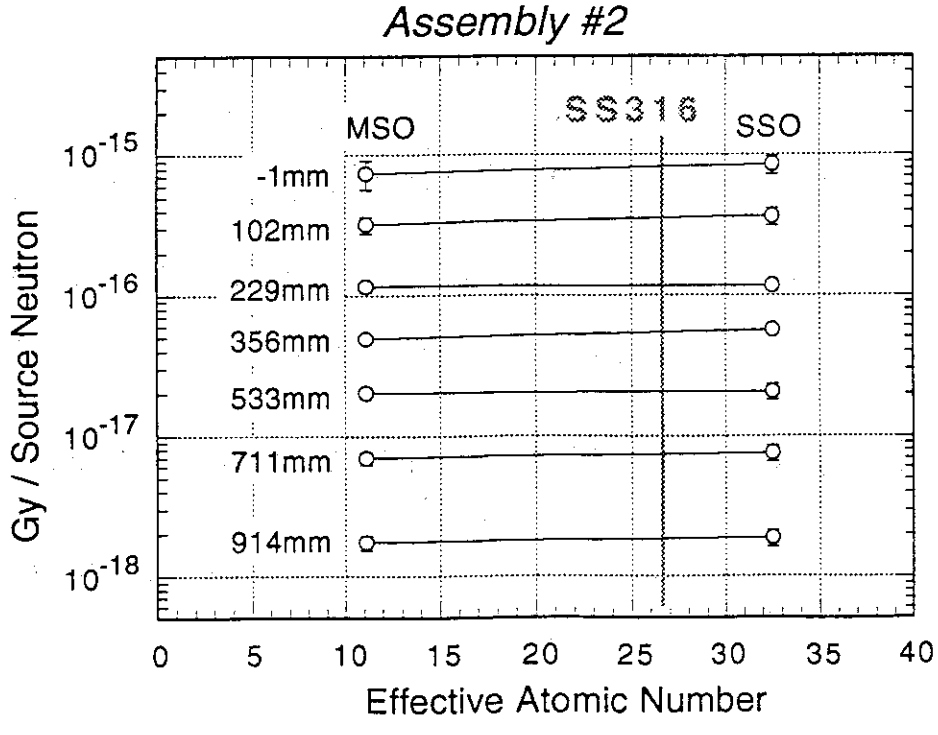

Fig. 3.4.3 Interpolation scheme to derive gamma-ray heating rates of SS316 in the assembly #2 from those of MSO and SSO.

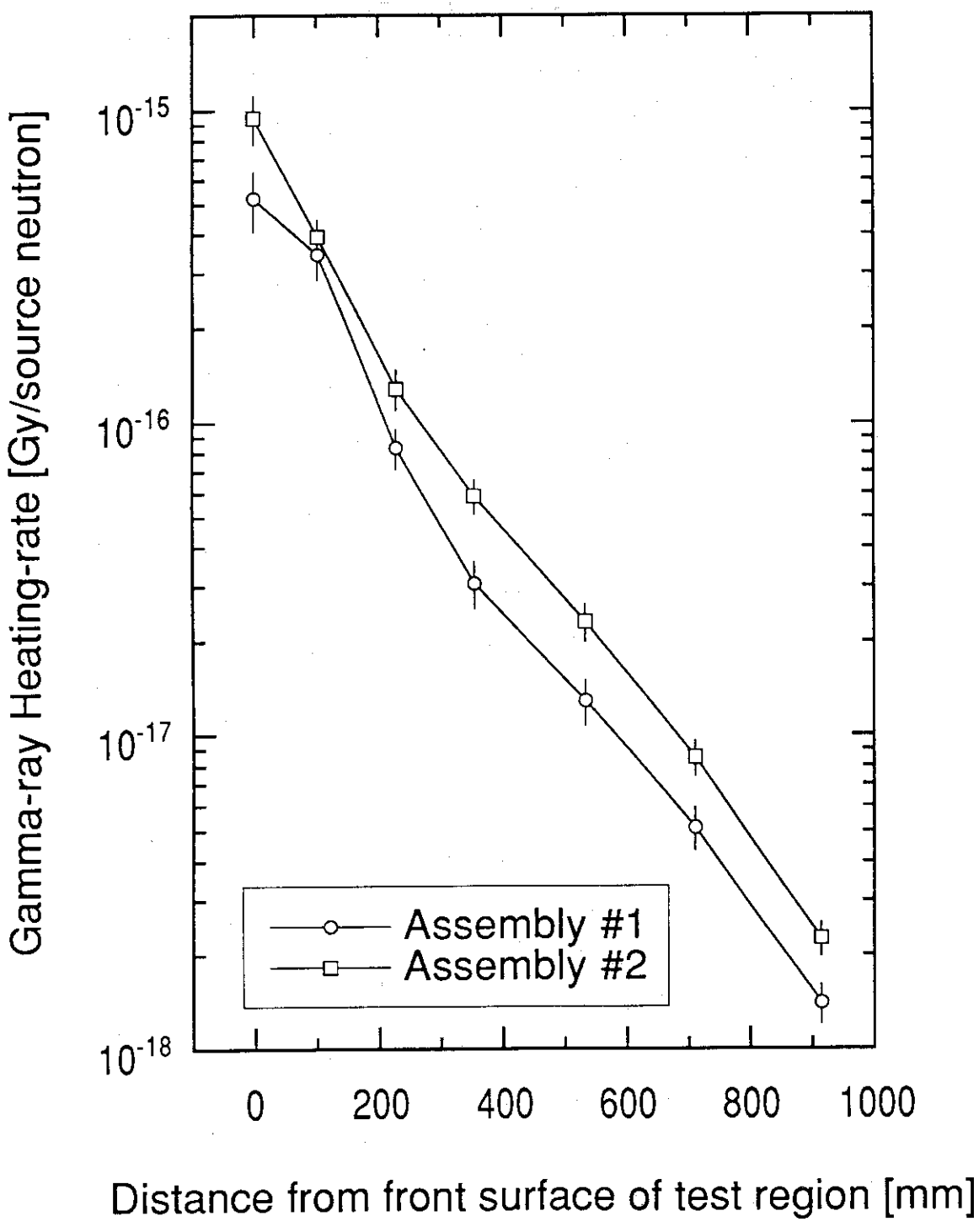

Fig. 3.4.4 Measured gamma-ray heating rates of SS316 in the assemblies #1 and #2 by the TLD.

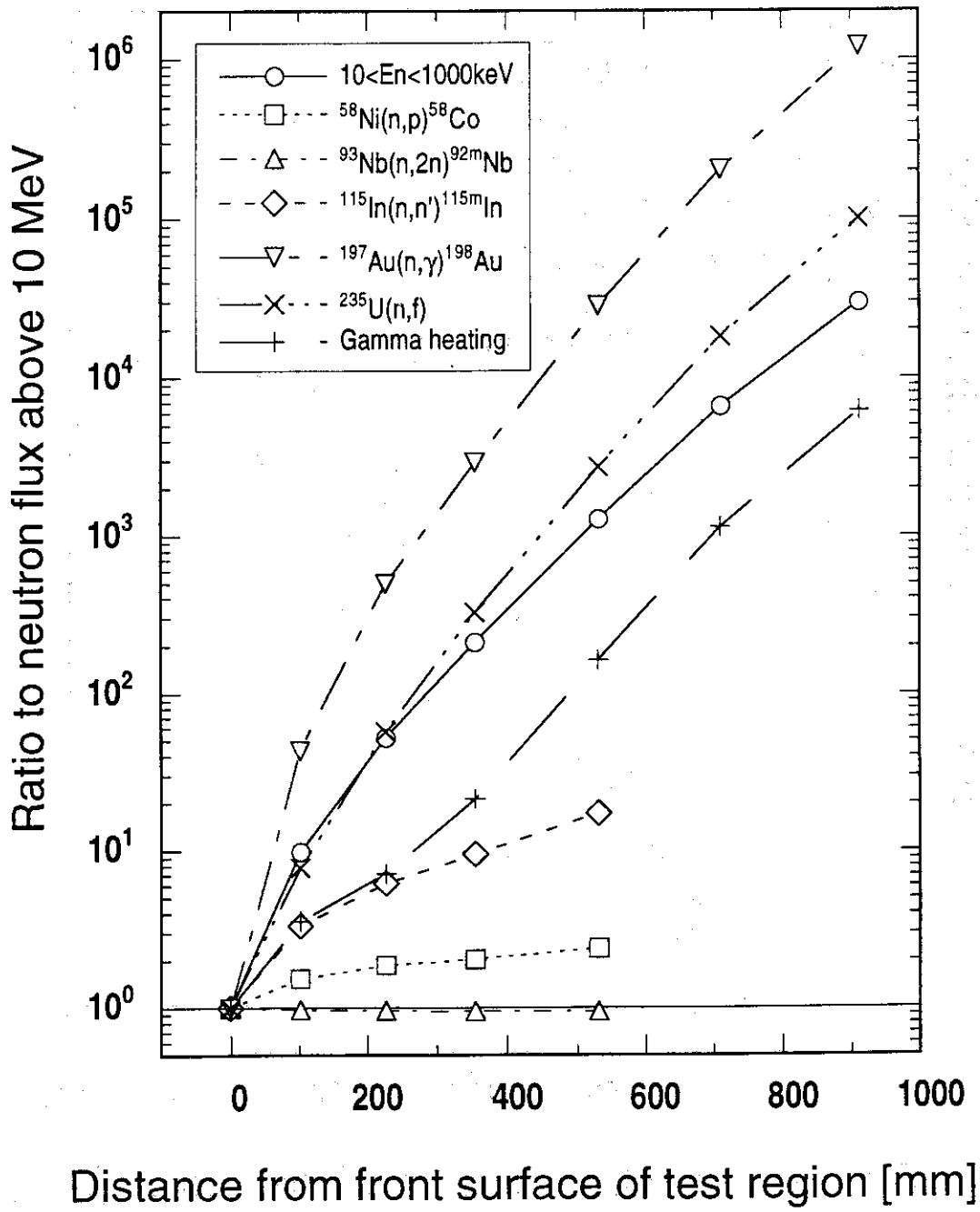

Fig. 4.1.1 Ratios of the integrated neutron fluxes from 10 keV to 1000 keV, reaction-rates of $^{115}In(n,n')^{115m}In$ and $^{197}Au(n,\gamma)^{198}Au$, fission-rate of ^{235}U and gamma-ray heating rate to neutron flux above 10 MeV in the assembly #1.

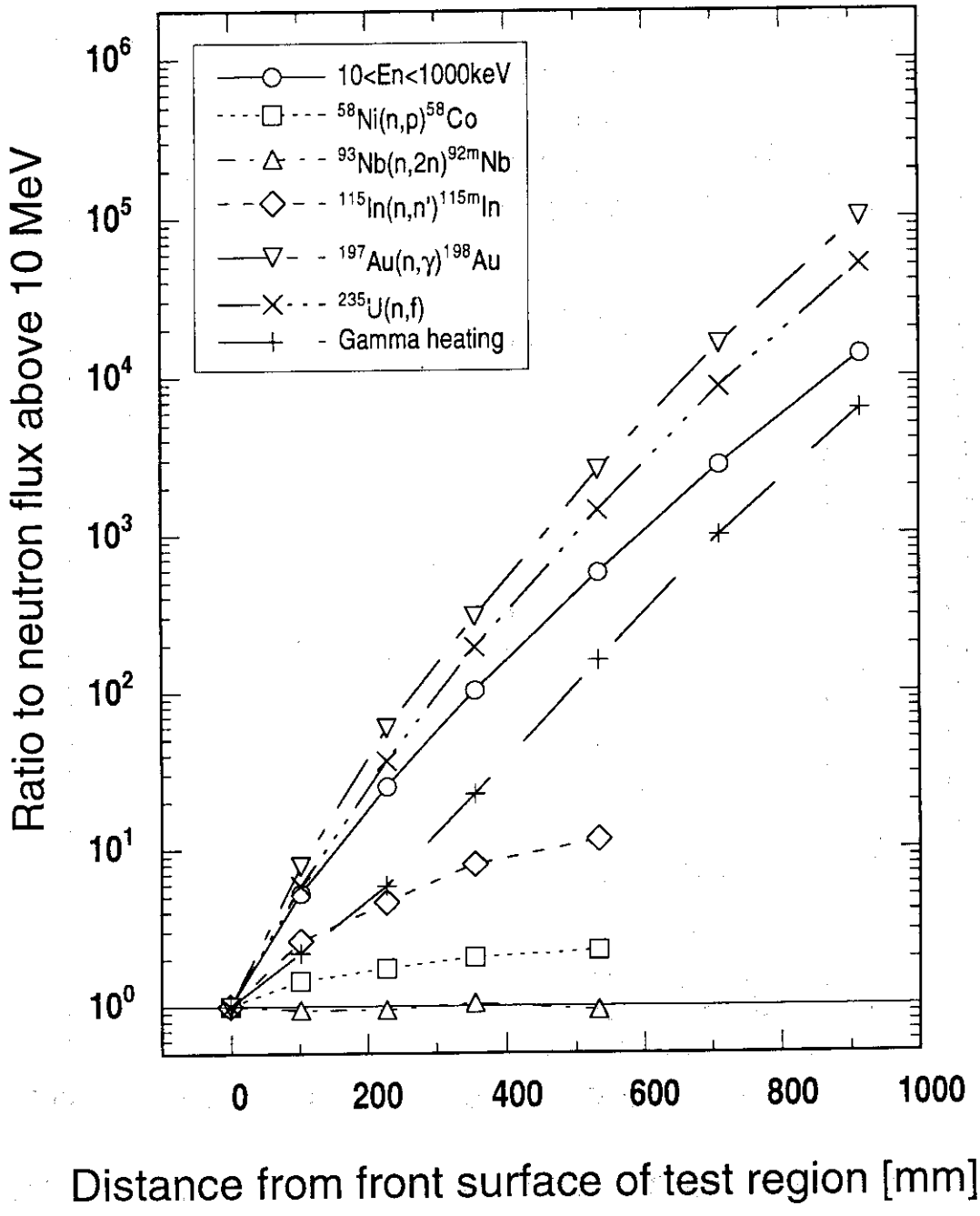

Fig. 4.1.2 Ratios of the integrated neutron fluxes from 10 keV to 1000 keV, reaction-rates of $^{115}In(n,n')^{115m}In$ and $^{197}Au(n,\gamma)^{198}Au$, fission-rate of ^{235}U and gamma-ray heating rate to neutron flux above 10 MeV in the assembly #2.

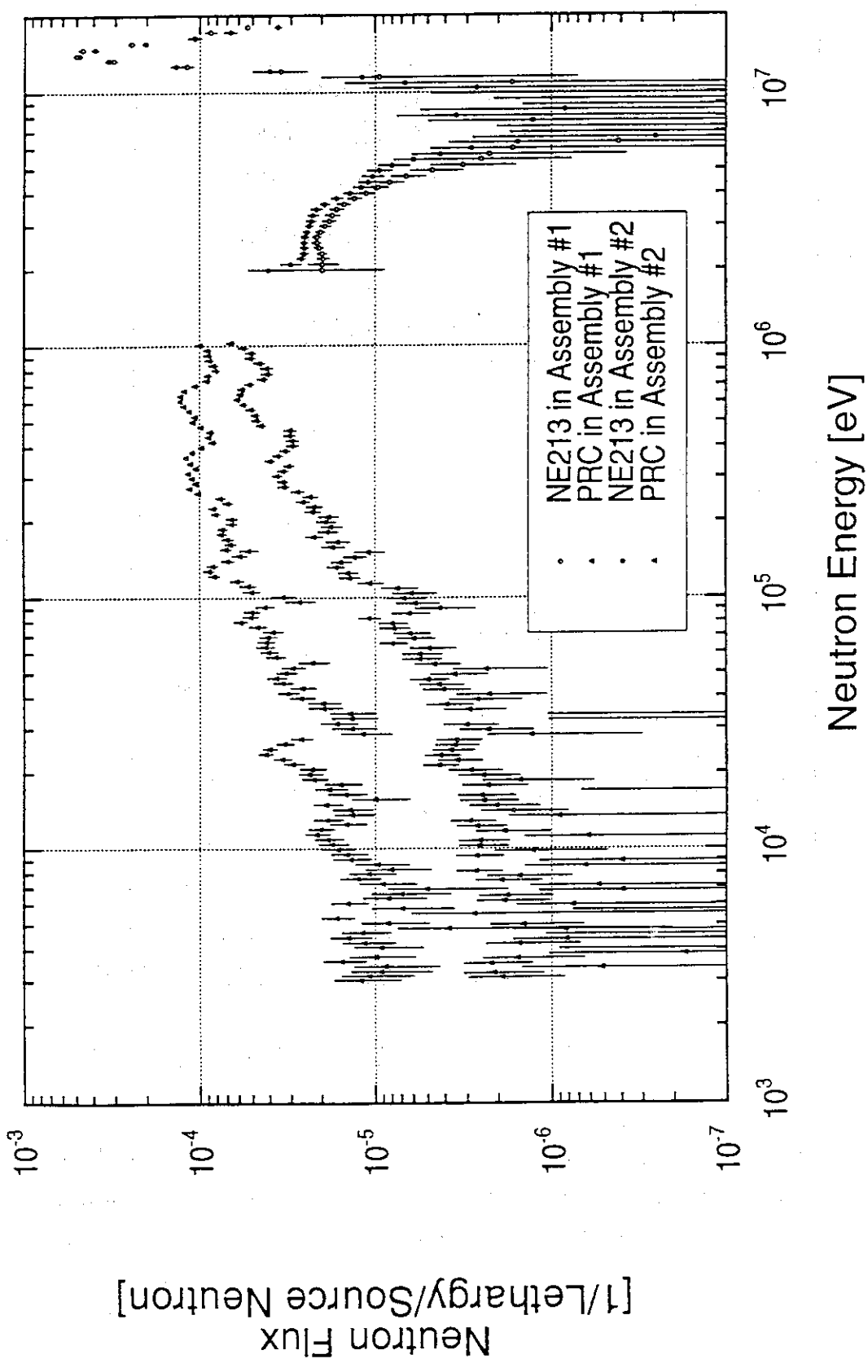

Fig. 4.2.1 Neutron spectra at the front surface of the test region in the assemblies #1 and #2.

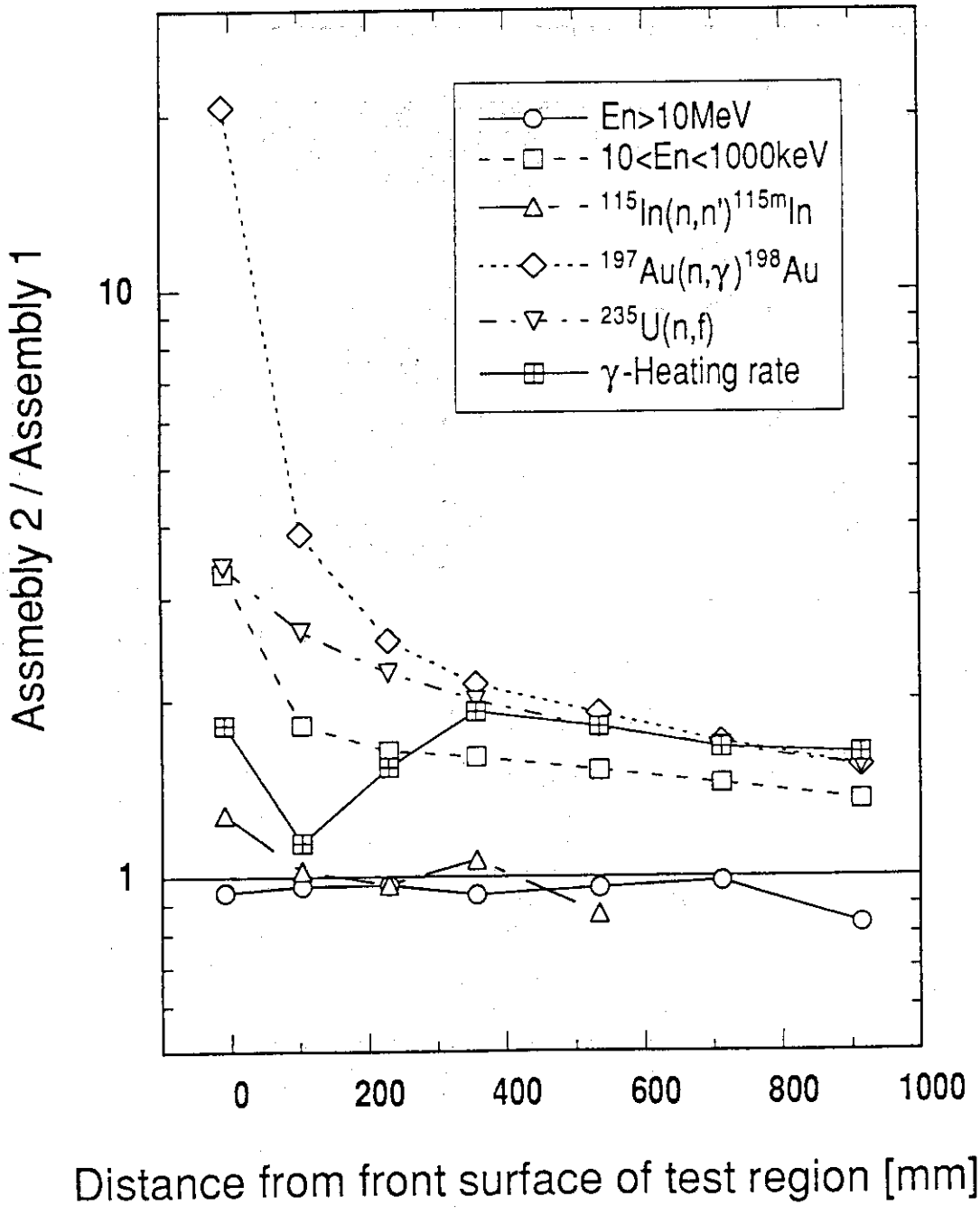

Fig. 4.2.2 Ratios of the integrated neutron fluxes above 10 MeV and from 10 keV to 1000 keV, reaction-rates of $^{115}In(n,n')^{115m}In$ and $^{197}Au(n,\gamma)^{198}Au$, fission-rate of ^{235}U and gamma-ray heating rate in the assembly #2 to those in the assembly #1.